University of St Andrews

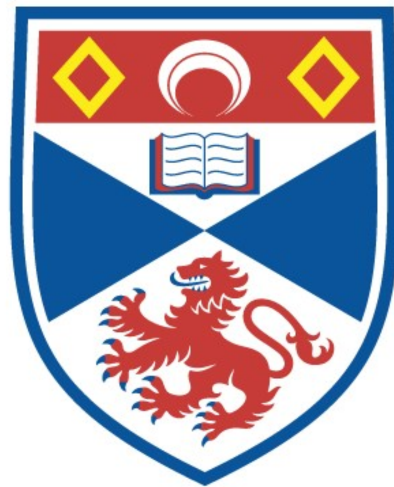

Full metadata for this thesis is available in
St Andrews Research Repository
at:
http://research-repository.st-andrews.ac.uk/

This thesis is protected by original copyright

ELECTROLUMINESCENCE AND SWITCHING PHENOMENA IN ZnSe SCHOTTKY DIODES

A Thesis

presented by

Alec Livingstone, B.Sc.

to the

University of St. Andrews

in application for the Degree

of Doctor of Philosophy.

Th 7063

DECLARATION

I hereby certify that this thesis has been composed by me, and is a record of work done by me, and has not previously been presented for a Higher Degree.

The research was carried out in the Wolfson Institute of Luminescence, within the School of Physical Sciences in the University of St. Andrews, under the supervision of Mr. J.W. Allen.

A.W. Livingstone

CERTIFICATE

I certify that Alec W. Livingstone, B.Sc., has spent nine terms at research work in the Wolfson Institute of Luminescence, within the School of Physical Sciences in the University of St. Andrews under my direction, that he has fulfilled the conditions of the Resolution of the University Court, 1967, No. 1, and that he is qualified to submit the accompanying thesis in application for the Degree of Doctor of Philosophy.

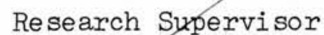

Research Supervisor

CAREER

I first matriculated in the University of St. Andrews in October 1965. Having studied Mathematics and Physics I obtained First Class Honours in Physics in 1969.

In October 1969, following the award of an S.R.C. Research Studentship, I was enrolled as a research student under Resolution of the University Court, 1967, No. 1, as a candidate for the degree of Ph.D.

ACKNOWLEDGEMENTS

I should firstly like to express my sincere thanks to Mr. J.W. Allen for his patient and stimulating guidance throughout this work.

I am indebted to Professor J.F. Allen, F.R.S., for the provision of the excellent facilities and funds.

Dr. J.M. Wilson of the Surface Physics Group in the Cavendish Laboratory kindly provided the Auger spectra for analysis of the surface composition. Dr. D.R. Wight of SERL provided a calibrated GaP light source and measurements of photoluminescent efficiency.

Spectra were measured in this laboratory by Mr. K. Turvey and Mr. M.D. Ryall.

My wife's encouragement and typing ability also helped considerably in the production of the thesis.

CONTENTS

SECTION PAGE

1. INTRODUCTION 1

2. THE M-I-S STRUCTURE

2.1 Introduction 6

2.2 Device Fabrication 7

2.3 Theoretical Considerations - Capacitance in Absence of Surface States 8

2.4 Theoretical Considerations - Capacitance in Presence of Surface States 10

2.5 Capacitance Results 13

2.6 I-V Characteristics 15

2.7 Discussion 17

3. LIGHT EMISSION FROM FORWARD BIASSED DIODES

3.1 Introduction 18

3.2 Model for Light Emission 18

3.3 Effect of Oxide Layer - Variation of η_h 20

3.4 Nature of the Emitted Light - Variation of η_r 22

3.5 Discussion 25

4. MEMORY AND SWITCHING

4.1 Introduction 27

4.2 Device Characteristics 28

4.3 Experimental Results 30

4.4 Switching Mechanism 32

4.5 Charge Transport in Insulators 34

4.6 Discussion 37

5. IMPACT IONIZATION

5.1 Introduction 38

5.2 Theoretical Considerations - Band to Band Transitions 39

5.3 Experimental Results - Band to Band Transitions 42

5.4 Discussion - Band to Band Transitions 44

5.5 Conclusions - Band to Band Transitions 44

5.6 Theoretical Considerations - Luminescent Centres 45

5.7 Experimental Results - Luminescent Centres 49

5.8 Discussion - Luminescent Centres 53

5.9 Conclusions - Luminescent Centres 53

6. CONCLUSIONS

6.1 Device Applications 55

6.2 Future Research 56

REFERENCES

CHAPTER 1

INTRODUCTION

Injection luminescence in solids has made considerable progress since it was first reported in 1907. In the ensuing 65 years the rate of progress has been rather more than exponential, and it is estimated that the total European market for light emitting devices in 1980 will be worth £10M per annum. In a field in which new materials and technologies appear every day this work will examine the potential of another contender - zinc selenide.

The 1907 observation of light emission was made by ROUND[1] in SiC to which he had made a point contact. The same phenomenon was observed 16 years later by LOSSEV[2], but its significance was not to be appreciated for many years. Useful luminous efficiency was first achieved by DESTRIAU[3] in 1936. He discovered that light could be generated by applying an alternating voltage to a block of insulator in which had been embedded a luminescent material, usually zinc sulphide doped with copper. The emission process was understood at least qualitatively, and some progress was made toward better efficiencies. The operation of the device relied on the inhomogeneity of the material. An applied voltage created high local fields which produced electron-hole pairs. These separated and recombined on successive cycles of the applied voltage. With this limited understanding of the device's operation there were several parameters, such as voltage and frequency, which could be varied in an attempt to increase the light emission. Beyond that, there was insufficient information available about the processes involved within the material to allow further improvement.

LEHOVEC[4] in 1955 also produced electroluminescence in SiC. He suggested that the point contact used in the earlier work had not been responsible for the emission, but merely made contact to local n-type regions in p-type bulk material. He also suggested that the light had been produced by the recombination of electron-hole pairs across the energy gap. This was a well known process of exciting a solid, namely the injection of carriers at a p-n junction.

An electroluminescent device relying on recombination of carriers in a p-n junction has most of the advantages associated with solid state structures. It will operate on DC of a few volts, of the order of the energy gap, and it should be robust and reliable. There are two principle criteria which must be satisfied by the material for such a device. The emission must be visible and the radiative recombination process must be efficient. It was obvious that the two semiconductors best known at the time, Si and Ge, were unsuitable. Both have small energy gaps, which means that the radiation of highest energy will occur in the infra-red, and both are indirect band gap materials. An indirect material is one in which the extrema of the conduction and valence bands do not occur for the same value of crystal momentum. Thus any recombination between carriers at these points requires the simultaneous co-operation of two or more phonons if momentum is to be conserved, and the process is unlikely. An alternative is to allow recombination at an impurity atom in the energy gap. In this case the impurity takes up the extra momentum. A suitable semiconductor is GaP, and WOLFF(5), in 1955, found electroluminescence in this material and suggested that this might be due to recombination at some impurity site. It was shown later that the emission in GaP could be either green or red depending on whether the material was doped with zinc or zinc plus oxygen(6).

To obtain a wider range of colours a material with a larger energy gap is required. Materials of the II-VI series have this property but there are problems of material preparation. It is especially difficult to prepare both n and p-type II-VI compounds. This was partly resolved when FISCHER(7), in 1964, reported electroluminescence as a result of majority carrier injection at a Schottky barrier on n-type zinc selenide. This meant that the problems associated with the production of p-type material need no longer hinder the use of the II-VI's as electroluminescent materials.

In the meantime, industry had decided that the development of light emitting panels of the Destriau type had reached a plateau, and began turning to GaP_xAs_{1-x}.

GaP_xAs_{1-x} is an alloy of GaP and GaAs. GaAs is a material with smaller band gap than GaP, and is direct. Near the beginning of the 1960's several manufacturers were marketing discrete GaP_xAs_{1-x} light emitting devices. Film markers and punched card readers were just two of the applications for the new compact light source. More important, these devices provided a replacement for the then current alphanumeric displays such as nixie tubes, and by 1968 the first integrated solid state displays were on the market. These took the form of either a 7x5 array of light emitting diodes capable of presenting all the alphanumerics, or 7 illuminated bars which could display numerals only. To avoid making connection to every diode an integrated circuit was incorporated in the device to translate the machine language input and drive the appropriate lamps. Since their introduction efficiencies have risen and prices have fallen, and such displays are now common in a wide range of digital instruments. The factor which is at present limiting their application is the material cost. The raw materials themselves are extremely expensive, as are the diffusion techniques used to prepare junctions, and at the present time the largest economic substrate size is 0.8 cm across, and it seems unlikely that GaP_xAs_{1-x} will ever find application in arrays capable of presenting characters of 2 or 3 cm in height.

Our interest in ZnSe Shottky diodes arose from the original report by FISCHER(7) and simultaneous work at SERL, Baldock. ZnSe is a much cheaper material than any of the gallium based compounds. Similarily, the formation of a Schottky barrier is less expensive than the process necessary to create a diffused junction. This renders the material suitable for use in large scale arrays. In this department we have manufactured electroluminescent Schottky diodes on ZnSe. My particular interest was originally the impact ionization processes which take place at the luminescent centres in the material. In chapter 5 measurements of carrier multiplication will be presented. This process occurs as carriers gain sufficient energy from the applied field to excite carriers across the band gap, or to ionize the luminescent centres. The former

process is well understood, and the theories of WOLFF[8], SHOCKLEY[9] and BARAFF[10] have been used by other workers to quantify experimental observations in many materials. The results obtained for ZnSe fit the existing theories for reasonable values of the adjustable parameters, and obey an empirical relationship with the results for other materials. A new model for generation and recombination of carriers at the luminescent centre is proposed. This fits the observed multiplication and predicts qualitatively the field dependence of the light emission.

Light emission has also been obtained from a metal-insulator-semiconductor structure in which ZnSe is the semiconductor. This structure now emits light in forward bias, a process which is not possible in an ideal Schottky diode. The preparation and general measurement techniques involved in the M-I-S structure are described in chapter 2. Chapter 3 presents a model for light emission in forward bias. Such a device is of interest, not only because it allows the possibility of obtaining the same luminous output at a lower applied voltage, but also because we observe a new radiation mechanism. In addition to recombination at luminescent centres we have, in material with no intentional deep levels, an excitonic transition with an emission energy near that of the band gap.

An additional property of the interfacial insulating layer is that it can store charge. By some means which is not clear, charge can be transferred from the deep centres in the semiconductor to charge storage sites in the insulator. This stored charge can modify considerably the rectifying characteristic of the device. Chapter 4 discusses these mechanisms in more detail. The resulting device has two distinct rectifying states which can be selected by current or voltage pulses. It will not change state without application of the correct bias and is capable of remembering its state even when all bias is removed. Our electroluminescent switching device, although in its early stages of development could have considerable application in large scale sequentially scanned arrays. This will be discussed in chapter 6.

Throughout the work, physical mechanisms have been proposed and, as far as possible, verified by experiment. Although the experimental device will bear little relation to any commercial successor the physical principles described here will still apply. Where certain experiments have been inconclusive future lines of research will be proposed in the concluding chapter.

CHAPTER 2

THE M-I-S STRUCTURE

2.1 Introduction. The metal-insulator-semiconductor structure, in which ZnSe is the semiconductor, has been successfully used as a light emitting diode, and also as a memory and switching device. The particular properties which are important in these applications will be discussed in later chapters. In this chapter the M-I-S structure is discussed in more general terms, describing the analytic tools which can give the information necessary for these later chapters. In particular the measured capacitance will be related to the film thickness and the depletion layer capacitance, and a conductance technique which can give information about the nature of the insulator will be discussed.

Both approaches used here have been developed and applied to the SiO_2-Si interface, and some parameters relating to this structure are relevant to the ZnO-ZnSe structure. However there are important differences between the systems, not the least of which is that the 'insulator' in this case is in fact slightly conducting, and these differences have to be appreciated before any calculations can be justified. In practice the oxide resistance has a sufficiently high value to be ignored when the capacitance is corrected to its high frequency value using the conductance technique.

If metal were evaporated directly on to the semiconductor, the small signal capacitance C_d would be related to the applied voltage V by the expression[11,12]

$$C_d^2(V + V_{do}) = (\text{const.})N_d \qquad (2.1.1)$$

where N_d is the donor density and V_{do} the diffusion potential. If the experimental results have this form then a graph of C_d^{-2} vs V will be a straight line with the intercept on the voltage axis equal to the diffusion potential. The donor density can be obtained from the slope of the line once the numerical factor has been evaluated. The following sections will show how both the intercept and slope of the C^{-2} vs V plot may be modified by the presence of an insulating layer, although the linearity of the plot may be preserved.

Current-voltage characteristics have been included in this chapter for the sake of completeness, although in the case of forward bias their form can not be explained except in the most general terms.

Throughout this work the terms 'oxide' and 'insulator' will be synonymous when referring to the interfacial layer of the M-I-S structure. Similarily, the charge storage sites in the insulator will be occasionally referred to as 'surface states'.

2.2 Device Fabrication. The manufacturing process described in this section also applies to the devices which have been used in later chapters. The ZnSe used throughout the work was prepared by a direct synthesis of the constituents and grown into a polycrystalline ingot by the vapour transport method. During the synthesis aluminium was added to make the material n-type, usually in a concentration of around 10^{16} - 10^{17} atoms cm^{-3}. At this stage manganese luminescent centres could be incorporated in similar concentrations. To increase the conductivity of the material slices of the grown ingots were boiled in zinc. This process removed any copper which might have unintentionally entered the ZnSe. The zinc will also fill any vacancies. It was also possible to dope the crystals with copper at this stage by adding it to the zinc melt. Since copper is an acceptor in ZnSe its maximum concentration is limited by the amount of aluminium present if the material is to remain n-type.

Dice, 2mm x 2mm x 1mm, were cut from the ingot either ultrasonically or by wire saw, and polished with rouge paper. The dice were mostly polycrystalline, the individual crystallite size being about 1mm. Single crystals were occasionally prepared.

Several chemical etches were used to remove surface mechanical damage. The most common was a 2-5% solution of bromine in methanol, although concentrated caustic soda and potassium dichromate in sulphuric acid(13) were also used. A characteristic of all these etches is that they leave zinc oxide and selenium on the crystal surface. The latter is readily dissolved in carbon disulphide, but

the ZnO is extremely difficult to remove despite rinsing in potassium or sodium hydroxide. This oxide was used as the insulating layer of the M-I-S structure.

Ohmic indium contacts were alloyed to one face of the sample and protected by Apiezon wax while the etch was repeated. The dice were transferred under methanol to the liquid nitrogen trapped, oil diffusion pumped vacuum chamber where a metal, usually gold, was deposited at a pressure below 10^{-5} torr. The typical spot size was 0.5 mm^2, and a schematic of the completed device is shown in figure 2.2.1. The devices were mounted under a spring contact on a substantial metal heat sink and the junction protected by a clear plastic. A solution of polystyrene in toluene was used for temporary encapsulation, and clear Araldite or Ward's Bio-Plastic was used for long term protection.

Although the chemical method of obtaining an oxide is simple to carry out, it is difficult to control. With a little perseverance it is possible to lay down a thick oxide with some degree of repeatability, however insulator thicknesses less than 100 Å are difficult to achieve. This is principally because no suitable agent has been found which will remove ZnO reliably without attacking the ZnSe substrate. The problem of obtaining clean surfaces free from mechanical damage has still to be solved.

Auger spectroscopy carried out by Dr. J.M. Wilson of the Surface Physics Group in the Cavendish Laboratory has verified that ZnO is present on the surface of our crystals after a chemical etch.

2.3 Theoretical Considerations - Capacitance in Absence of Surface States.

Many methods have been proposed to relate the measured capacitance of the M-I-S structure to the depletion layer capacitance while, at the same time, giving some information about the nature of the insulator. The particular analysis discussed here was proposed first by GOODMAN[14] and has been modified by COWLEY[15] and CARD and RHODERICK[16]. In this analysis a DC field is applied to the device, deforming the charge distribution in the depletion region of the semiconductor.

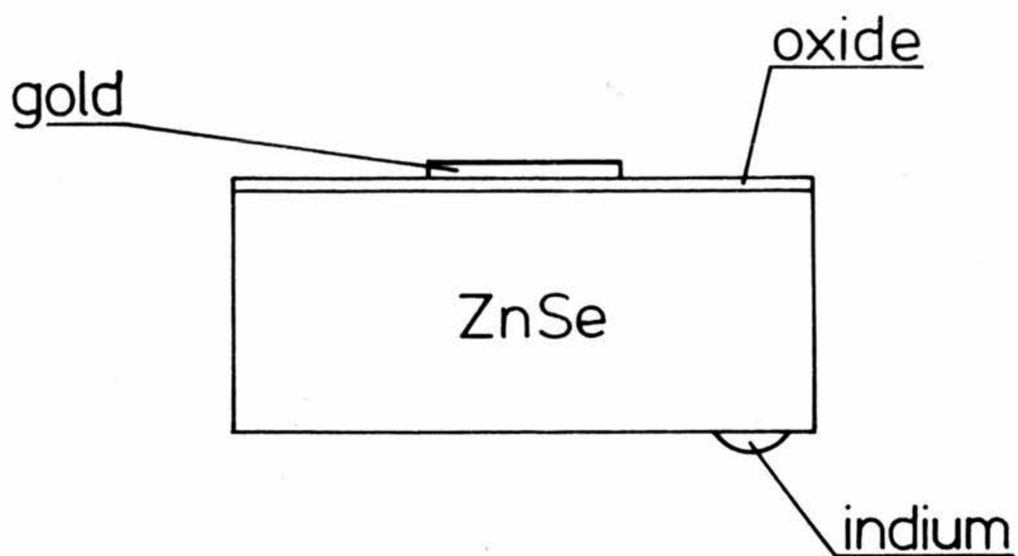

Figure 2.2.1. Typical device construction.

Since in this simple case the oxide capacitance is independent of bias, an applied high frequency field will measure a change in the charge in the depletion region alone. This can be related to the capacitance by the simple analysis which led to equation 2.1.1. If the frequency of the measuring signal is sufficiently high

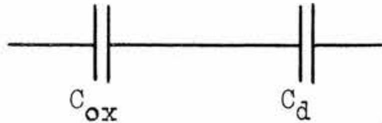

Figure 2.3.1

the equivalent circuit of the device reduces to the form shown in figure 2.3.1, where C_{ox} and C_d represent the oxide and depletion region capacitances respectively. Thus, by evaluating the voltage dependent part of the capacitance, and knowing the diffusion potential of the junction, the oxide capacitance, and hence the film thickness, can be evaluated.

Under zero bias the energy levels at the interface are as shown in figure 2.3.2. Here d is the film thickness, V_{do} the diffusion potential, Δ_o the volt drop across the insulator, and ε_i and ε_{sc} the dielectric constants of the insulator and semiconductor respectively. Using Gauss' law to relate the space charge to the volt drop across the insulator

$$\Delta_o = \frac{d}{\varepsilon_i}(2\ e\ \varepsilon_{sc}\ N_d\ V_{do})^{1/2}. \qquad (2.3.1)$$

Relating the energies shown in figure 2.3.2 the quantity ϕ_{ms} can be defined by the expression

$$\phi_{ms} = V_{do} + \Delta_o = \phi_m - (\chi_s + \phi_n). \qquad (2.3.2)$$

The diffusion potential V_{do} can be written

$$V_{do} = \phi_{ms} + \frac{V_1}{2} - V_1^{\ 1/2}(\phi_{ms} + V_1/4)^{1/2} \qquad (2.3.3)$$

where

$$V_1 = 2\ e\ \varepsilon_{sc}\ N_d\ \frac{d^2}{\varepsilon_i^{\ 2}}. \qquad (2.3.4)$$

Now equation 2.3.1 becomes

$$\Delta_o = V_1^{\ 1/2} V_{do}^{\ 1/2}. \qquad (2.3.5)$$

If a reverse bias voltage is applied to the device (figure 2.3.3), V_d and Δ are not, in general, equal to their zero bias values. Equations 2.3.2 and 5 now become

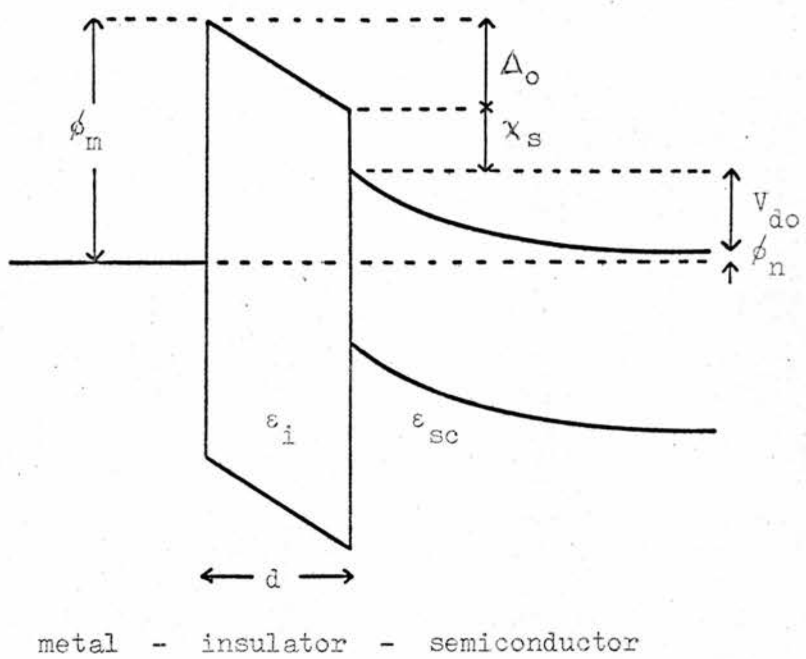

Figure 2.3.2. Energy levels at the junction of an M-I-S structure under zero bias.

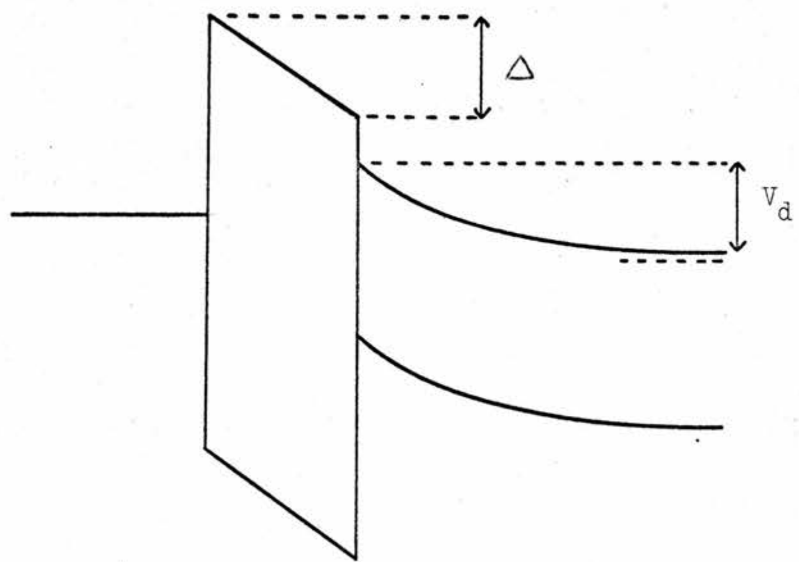

Figure 2.3.3. The M-I-S structure modified by bias.

$$\phi_{ms} + V = V_d + \Delta \qquad (2.3.6)$$

$$\Delta = V_1^{1/2} V_d^{1/2}. \qquad (2.3.7)$$

The space charge in the semiconductor is, of course, related to the donor density and so the capacitance of the junction can be written

$$C = \frac{\delta Q_{sc}}{\delta V} = (2\ e\ \varepsilon_{sc}\ N_d)^{1/2} \frac{\delta V_d^{1/2}}{\delta V}$$

$$= (e\ \varepsilon_{sc}\ N_d/2)^{1/2} (\phi_{ms} + V + V_1/4)^{-1/2}. \qquad (2.3.8)$$

That is, the slope of the C^{-2}-V plot has not been altered by the presence of the insulator, but the intercept is now

$$V_o = \phi_{ms} + V_1/4$$

$$= V_{do} + V_1/4 + (V_1\ V_{do})^{1/2} \qquad (2.3.9)$$

using equations 2.3.2 and 5. The thickness of the oxide can be found from 2.3.3 if V_{do} can be obtained from an independent observation such as the photoresponse of the junction.

2.4 Theoretical Considerations - Capacitance in Presence of Surface States.

One of the problems encountered when making measurements on a device whose insulator contains some density of charged centres, is that the time constant of these centres causes dispersion of the observed capacitance. Before the results of section 2.3 can be broadened to include the effect of the charge centres it is necessary to understand what the frequency dependence of the capacitance will be. This can be done using a conductance technique described by NICOLLIAN and GOETZBERGER(17). This method relies on the fact that a trap time constant τ will give rise to a conductance G_s as the distribution of charge at the interface lags behind the measuring signal. Measurements of conductance can give sufficient information about the surface states to allow the measured capacitance to be corrected to the high frequency limit necessary before an extension of section 2.3 can be applied.

The total charge density in the junction must be(17)

$$Q_t = Q_d + Q_s + Q_{ox} \qquad (2.4.1)$$

where Q_d is the depletion region charge density, Q_s the moveable charge density in the insulator, and Q_{ox} the fixed charge in the insulator. The total AC current density $i_t(t)$, is, at time t

$$i_t(t) = i_d(t) + i_s(t) \qquad (2.4.2)$$

where $i_d(t)$ is the displacement current charging the space charge region, and $i_s(t)$ is the current charging the surface states. In any experimental procedure there must be a relationship between the applied bias and time, and $i_d(t)$ can be related to the variation of charge in the depletion region with applied bias and time. This is essentially the experiment carried out in obtaining a C^{-2}-V plot for a simple structure, and it can be shown that the slope of this plot, yielding the donor density, is related to $i_d(t)$. However this will only give the slope of the C^{-2}-V plot, not the intercept.

SHOCKLEY and READ(18) have shown $i_s(t)$ to have the form

$$i_s(t) = e\, N_s\, c_n(1 - f(t))n_s - e\, N_s\, e_n\, f(t) \qquad (2.4.3)$$

where N_s is the surface state density, c_n and e_n the electron capture and emission probabilities, $n_s(t)$ the electron density and $f(t)$ the Fermi function, both at time t. This current can be shown to result in an admittance(17)

$$Y_s = \frac{e^2}{kT}\,\frac{N_s\, f_o(1 - f_o)}{1 + jf_o/c_n n_{so}} \qquad (2.4.4)$$

where the subscript o denotes values modified by bias. This is the admittance of an RC network which can be separated into its real and imaginary parts such that the equivalent parallel capacitance is

$$C = \frac{C_s}{1 + \omega^2\tau^2} \qquad (2.4.5)$$

with a conductance

$$G_p = \frac{C_s^{\ 2}}{1 + \omega^2\tau^2} \qquad (2.4.6)$$

where

$$C_s = e^2\, N_s\, f_o(1 - f_o)/kT \qquad (2.4.7)$$

and

$$\tau = \frac{f_o}{c_n\, n_{so}}\,. \qquad (2.4.8)$$

Equation 2.4.5 has to be modified to include the depletion term, so that the total parallel capacitance, ie the measured value, is

$$C_p = C_d + \frac{C_s}{1 + \omega^2\tau^2}. \qquad (2.4.9)$$

The model should really be extended from this simple, single trap picture to include some continuum of surface states. It can be shown(17) that this will make no difference to the calculated value of C_d, but, depending on the approximation used, the time constant and density of surface states may be wrong by a factor near 3.

The above analysis leads to an equivalent circuit for the M-I-S structure as in figure 2.4.1. Using 2.4.6 all the surface state parameters necessary to

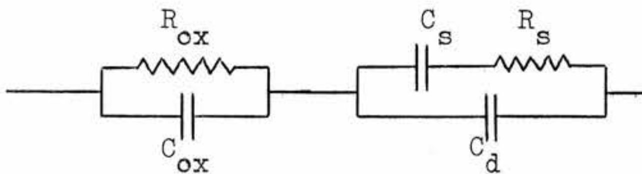

Figure 2.4.1

correct C_p to its high frequency form can now be calculated. In the high frequency limit the equivalent circuit will reduce to that shown in figure 2.3.1. The principles outlined in section 2.3 can now be applied after modification to include the effect of the surface states.

Most of the alterations to section 2.3 require little explanation. Gauss' law applied to the potential across the insulator, with and without bias, modifies equations 2.3.5 and 7 as follows

$$\Delta = V_1^{1/2} V_d^{1/2} + \frac{d}{\varepsilon_i} Q_s(V) \qquad (2.4.10)$$

$$\Delta_o = V_1^{1/2} V_{do}^{1/2} + \frac{d}{\varepsilon_i} Q_s(V) \qquad (2.4.11)$$

so that

$$\Delta - \Delta_o = V_1^{1/2}(V_d^{1/2} + V_{do}^{1/2}) + \frac{d}{\varepsilon_i} \Delta Q_s. \qquad (2.4.12)$$

It is necessary at this stage to consider how Q_s varies with applied bias. CARD and RHODERICK(16) have discussed this variation with reference to two special cases. These are when the occupancy of the surface states is governed by the Fermi level of either the metal or the semiconductor. These cases have also been

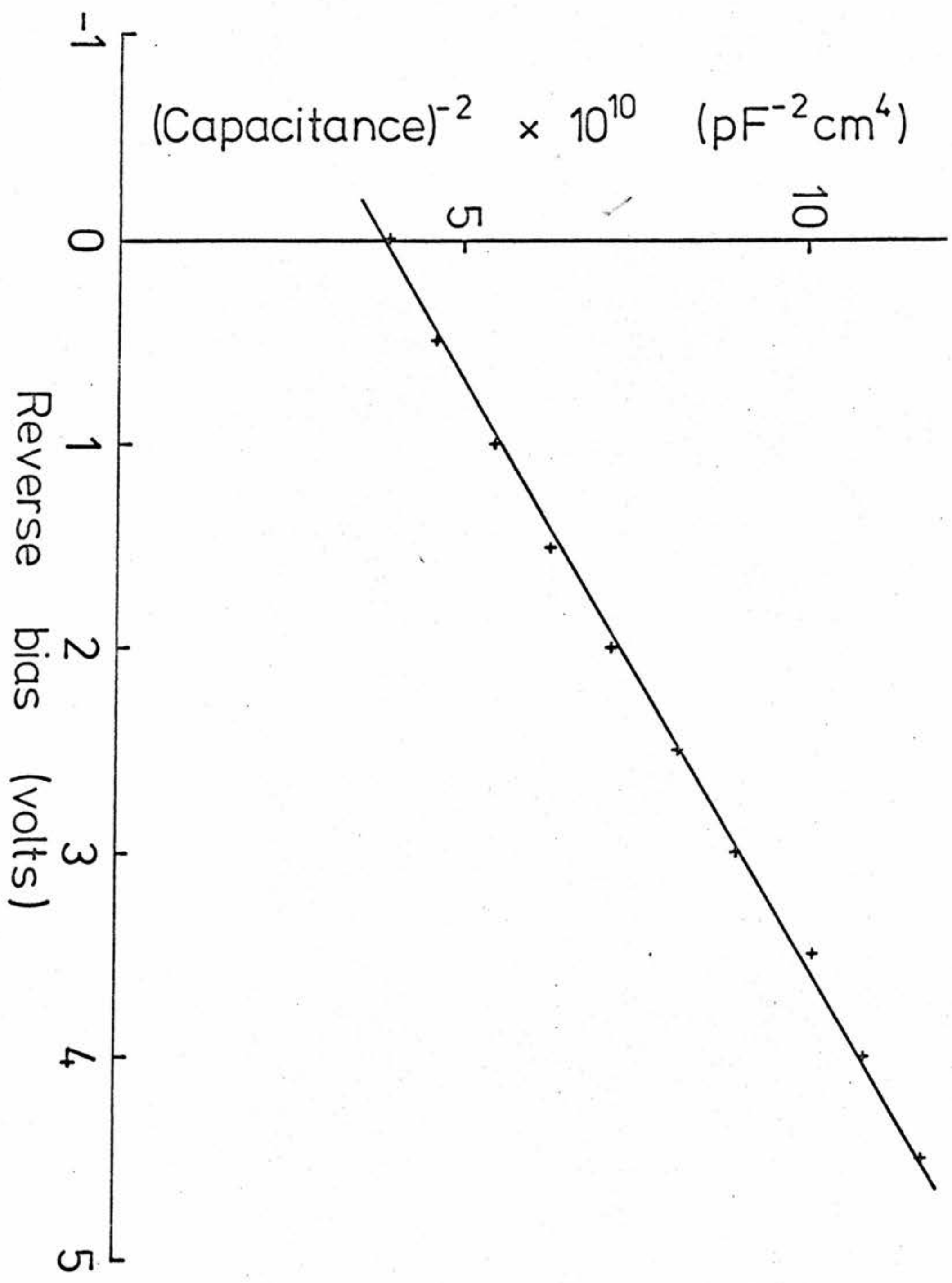

Figure 2.5.1. Typical C^{-2}-V plot for a device which does not have a significant density of charged centres in the oxide.

discussed by COWLEY[15] in terms of thin and thick oxides respectively. In the case of the Au-ZnO-ZnSe structure it is not immediately apparent which of these two forms should apply. In practice, only the approximations associated with the former give meaningful results. In this case the charge stored in the insulator varies with the voltage which is maintained across it, so that

$$Q_s = -e\ N_s(\Delta - \Delta_o). \qquad (2.4.13)$$

In the absence of any evidence to the contrary this form has been used without further justification. The modified diffusion potential V_d now has a form

$$V_d^{1/2} = -\frac{V_1^{1/2}}{2(1+\alpha)} + \frac{V}{4(1+\alpha)^2} + V + V_{do} + \frac{V_1^{1/2} V_{do}^{1/2}}{(1+\alpha)} \qquad (2.4.14)$$

where

$$\alpha = e\ N_s\ d/\varepsilon_i. \qquad (2.4.15)$$

Substitution into 2.3.8 now leads to an expression for the capacitance which implies that, in this case also, the slope of the C^{-2}-V plot is unaltered, whereas the intercept is modified as follows

$$V_o = V_{do} + \frac{(V_1 V_{do})^{1/2}}{(1+\alpha)} + \frac{V_1}{4(1+\alpha)^2} \qquad (2.4.16)$$

where V_1 and α yield values of the film thickness and surface state density respectively. This represents a useful check on the results obtained from the conductance technique which also gave a value for N_s.

2.5 Capacitance Results. All the capacitance results reported in this section were made using a transformer unity ratio bridge, constructed in this laboratory, capable of satisfactory operation from 10 kHz to 2 MHz. Generally the parallel resistance and capacitance network was measured. If it was necessary to make measurements at high current levels the series resistance of the device was first obtained from the forward biassed I-V characteristic and included in the equivalent circuit on the bridge.

The simplest form of capacity plot is one for a device whose AC conductivity indicates a very small surface state density. Figure 2.5.1 shows such a plot with an intercept V_o equal to 2.13 volts and a donor density of $1.66 \times 10^{17}\ cm^{-3}$. The

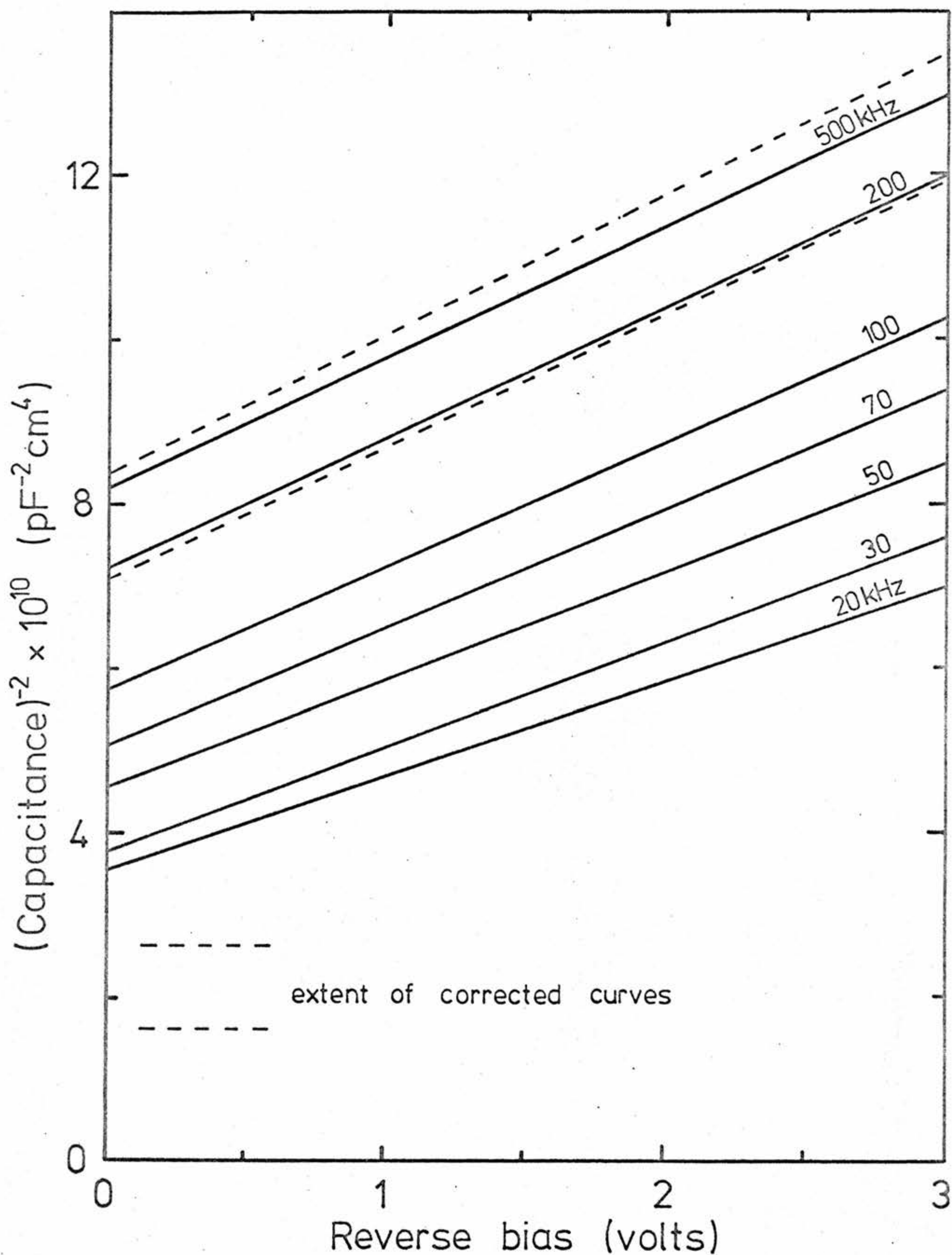

Figure 2.5.2. C^{-2}-V plot for a device with a large density of charged centres in the insulator. Shows the correction predicted by the conductance technique.

equivalent parallel conductance and capacitance have to be obtained from the measured values, taking into account the oxide capacitance. This correction is small; generally less than 5-10% of the total value. An estimate of the oxide capacity can be obtained from a consideration of the value of C^{-2} at the diffusion potential, ie when $C_d^{-2}=0$. This agrees well with the capacitance which can subsequently be calculated from the film thickness. The thickness can be obtained from equations 2.3.3 and 9 if the relevant dielectric constants and the diffusion potential are known. The dielectric constant has been taken as 9.1 for ZnSe and 8.5 for ZnO[19]. Photoresponse measurements by BRAUN et al[20] indicate that V_{do} = 1.4 eV. Using these values the sample of figure 2.5.1 has an oxide 190 Å thick. Of all the diodes made, the thinnest oxide was 100 Å, and no attempt was made to prepare one greater than about 1500 Å.

Any batch of diodes, prepared under apparently identical conditions, contains some which fit the simple form just described, whereas others display a large surface state density (characterized by large AC conductance and built in voltage). This is convenient because of the instability of switching devices (chapter 4) and allows detailed examination of the states observed in these devices. The capacitance of such a diode has been plotted as a function of bias and frequency in figure 2.5.2. The V_o in excess of 3 volts and the dispersion are indicative of a large surface state density. Devices with a lower trap density do exhibit some dispersion due to unfortunate values of oxide resistance and capacitance, but the variation is generally less than 10% in the range covered by figure 2.5.2. Equation 2.4.6 can be written in the form

$$\frac{G_p}{\omega} = \frac{C_s \omega \tau}{1 + \omega^2 \tau^2}. \qquad (2.5.1)$$

G_p/ω passes through a maximum when $\omega\tau = 1$, and the value of G_p/ω at the maximum is $C_s/2$. C_s can be directly related to the surface state density N_s by

$$N_s = C_s/e\,A \qquad (2.5.2)$$

where A is the device area. Figure 2.5.3 shows G_p/ω as a function of frequency

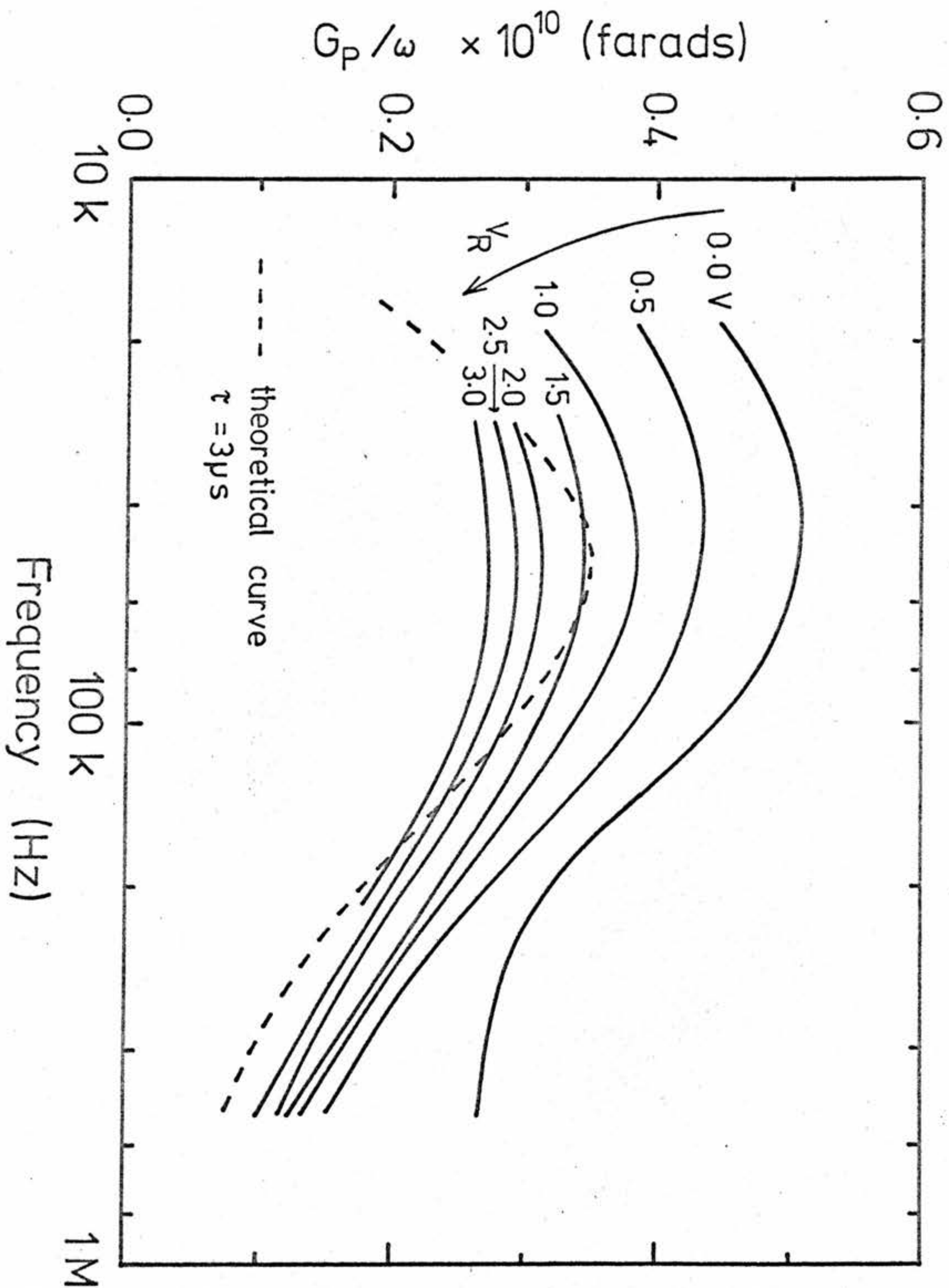

Figure 2.5.3. G_p/ω as a function of frequency and bias for the device of figure 2.5.2. The experimental curve is compared to the theoretical form predicted by Nicollian and Goetzberger.

and bias for the device of figure 2.5.2, and a theoretical curve obtained from equation 2.5.1 for $\tau = 3\ \mu S$. The value of C_s has been chosen arbitrarily to allow comparison of the theoretical and experimental curves. There is a good fit to the theoretical form for a surface state density around $10^{11}\ eV^{-1}\ cm^{-2}$. Thus, from the conductance of the junction we have sufficient parameters to allow us to correct the dispersion of figure 2.5.2 by substitution in equation 2.4.9. This correction has been applied and superimposed on the experimental C^{-2}-V plot. The spread in experimental values is now almost equal to that obtained from devices which do not show dispersion.

It is of interest to see how the result obtained for the insulator charge density in this diode, as calculated above, agrees with the value from COWLEY's[15] approach to the corrected C^{-2}-V plot. Having corrected the dispersion of the capacity results by using the conductance technique the C^{-2}-V plot now has the form of figure 2.5.1. That is, we can apply Cowley's method exactly as described in section 2.4. Unfortunately, to use 2.4.15 to find the surface state density requires a knowledge of the oxide thickness. The particular device under discussion has charge locked at the interface and it can not be switched into a state to which section 2.3 might apply. To obtain some estimate of the surface state density it is sufficient to use the oxide thickness of devices made in the same batch but with no trapped charge. This leads to a density of 4×10^{11} $eV^{-1}\ cm^{-2}$, in good agreement with the result obtained from the conductance method.

The examples discussed here indicate the use of the techniques developed in earlier sections, and show briefly how the data presented in later chapters has been obtained.

2.6 <u>I-V Characteristics.</u> The forward bias current-voltage characteristic of an ideal Schottky diode can be shown to have the form[11,12]

$$I = I_o(\exp \frac{eV}{kT} - 1) \qquad (2.6.1)$$

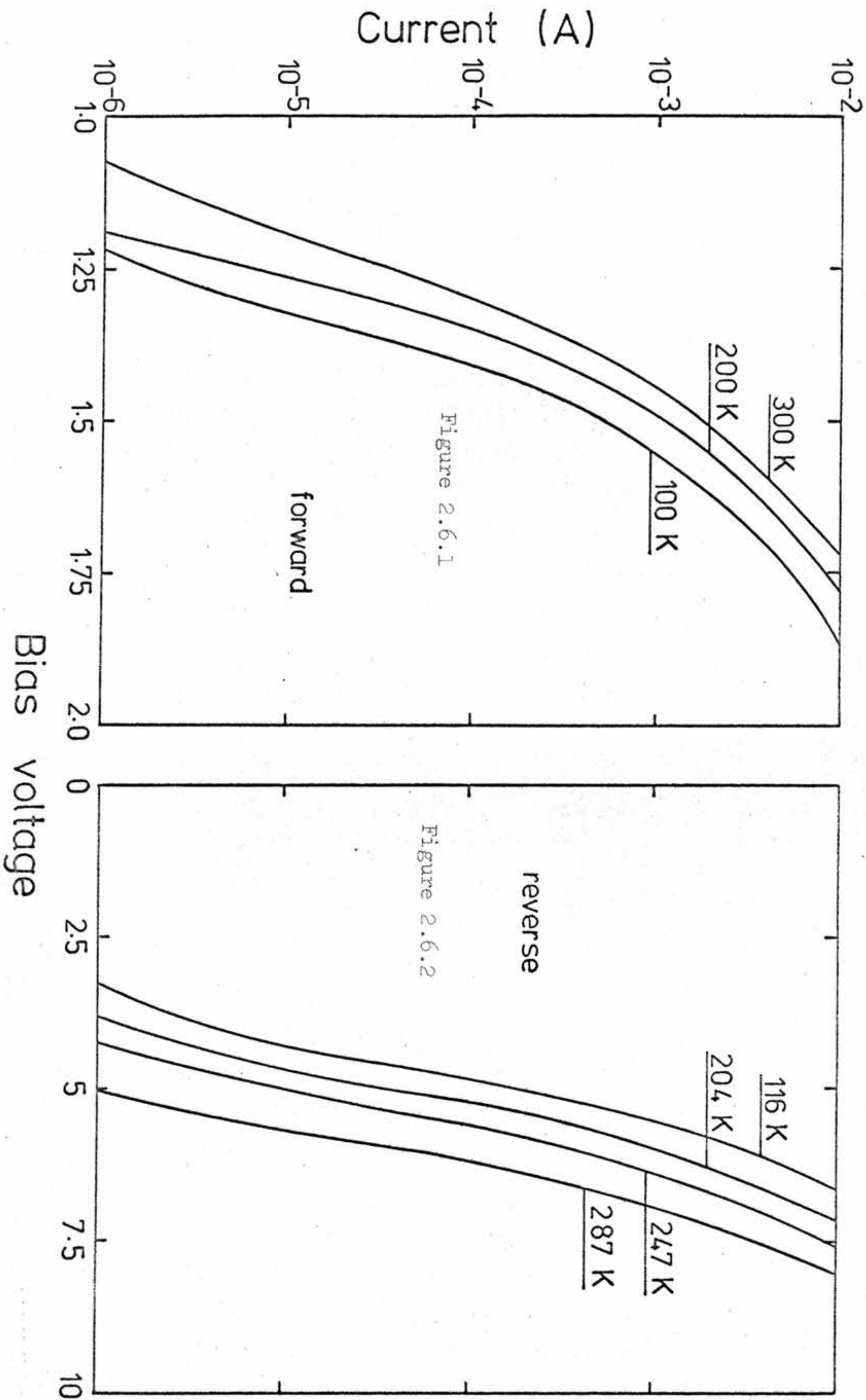

Figure 2.6.1. Temperature dependence of typical forward biassed characteristic.

Figure 2.6.2. Temperature dependence of typical reverse biassed characteristic.

where I_o is a constant. In practice, deviations from this form are common, and ATTALLA and SOSHEA[21] have shown that most of these can be fitted to a modification of equation 2.6.1. That is

$$I = I_o(\exp \frac{eV}{nkT} - 1) \quad (2.6.2)$$

where n is a dimensionless constant near unity. This parameter, commonly known as the 'n-value' of the diode, is used to quantify the deviation of a device's characteristic from that of an ideal diode. Even in the case of an M-I-S structure it has been shown that, for oxides <20 Å thick, n seldom rises beyond 1.5[22].

A typical forward bias I-V characteristic of the Au-ZnO-ZnSe structure is shown in figure 2.6.1. Although the exponential form is maintained, the 'n-value' is no longer a meaningful parameter since it appears to vary with temperature. In fact, as the temperature is increased the characteristic maintains its shape but shifts to lower voltages. This shift is typically 0.7 mV K^{-1} at constant current. In this respect the forward biassed characteristic is similar to that obtained in reverse bias. Figure 2.6.2 shows a set of such characteristics as a function of temperature, and we see the same general form, but with a thermal shift of near 6 mV K^{-1}. The rapid increase of current with applied bias, and the relative temperature insensitivity of the characteristics leads to the conclusion that both forward and reverse biassed currents are tunnelling initiated. In reverse bias the electrons tunnel from the metal to the conduction band of the semiconductor, but it is not clear where the process takes place in forward bias.

In addition to the tunnelling just discussed, there will be an effect due to the series resistance of both semiconductor and insulator. If we examine the characteristics shown in figures 2.6.3 and 4 we see that there is some variation with film thickness (as measured using the capacitance techniques). The slope of the semilogarithmic plot varies with oxide film thickness. This is not uncommon in other systems where the 'n-value' can be shown to be dependent on the insulating film[22]. There is also a series resistance apparent at high currents

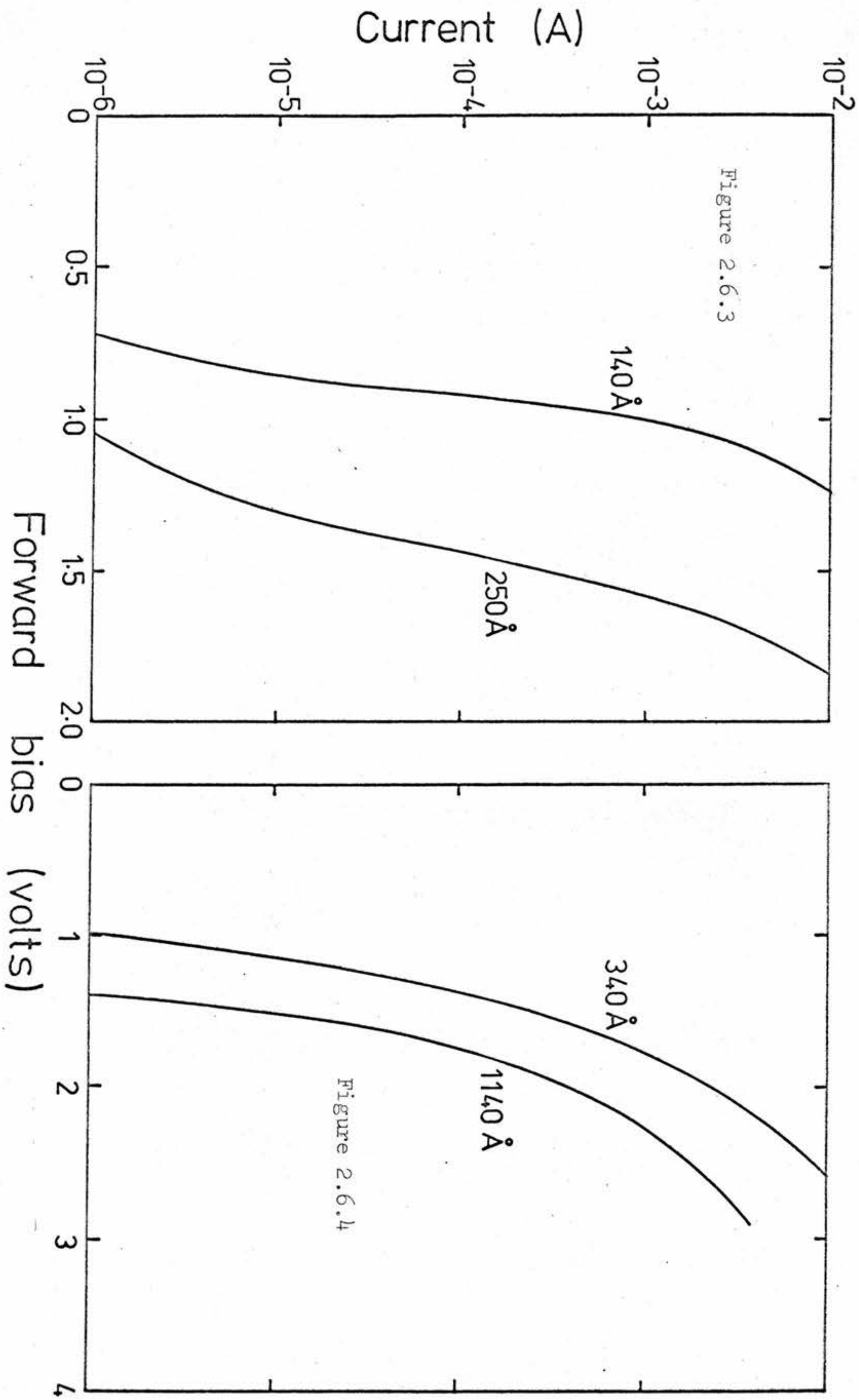

Figures 2.6.3 and 4. Forward biassed I-V characteristics for various oxide thicknesses calculated from capacitance results.

which would seem to be due to the insulator rather than the bulk semiconductor. This will be considered in greater detail later when the conduction mechanism within the insulator is discussed.

2.7 Discussion. In this chapter have been set out the theoretical considerations necessary for the separation of the depletion region capacitance from the value which is measured. This process also yields some useful parameters concerning the oxide layer.

The I-V characteristics shown in the preceeding section show that the oxide layer, even 1000 Å thick, has a resistance approaching only 200 Ω, a resistivity of 10^5 Ω cm. This is not normally the case with other M-I-S structures, but it makes little difference to the procedures involved. The calculated correction to the capacitance results takes care of the experimental dispersion to within the accuracy which the instruments can provide, and this alone would seem to confirm that the oxide conductance has produced no new problems.

The theory has been shown to give meaningful results when applied to the ZnO-ZnSe structure. In some parts this has been the only justification for pursuing a particular line of approach. However, in general, the argument is well understood, and the data provided by the results of this chapter will be invaluable in those which follow.

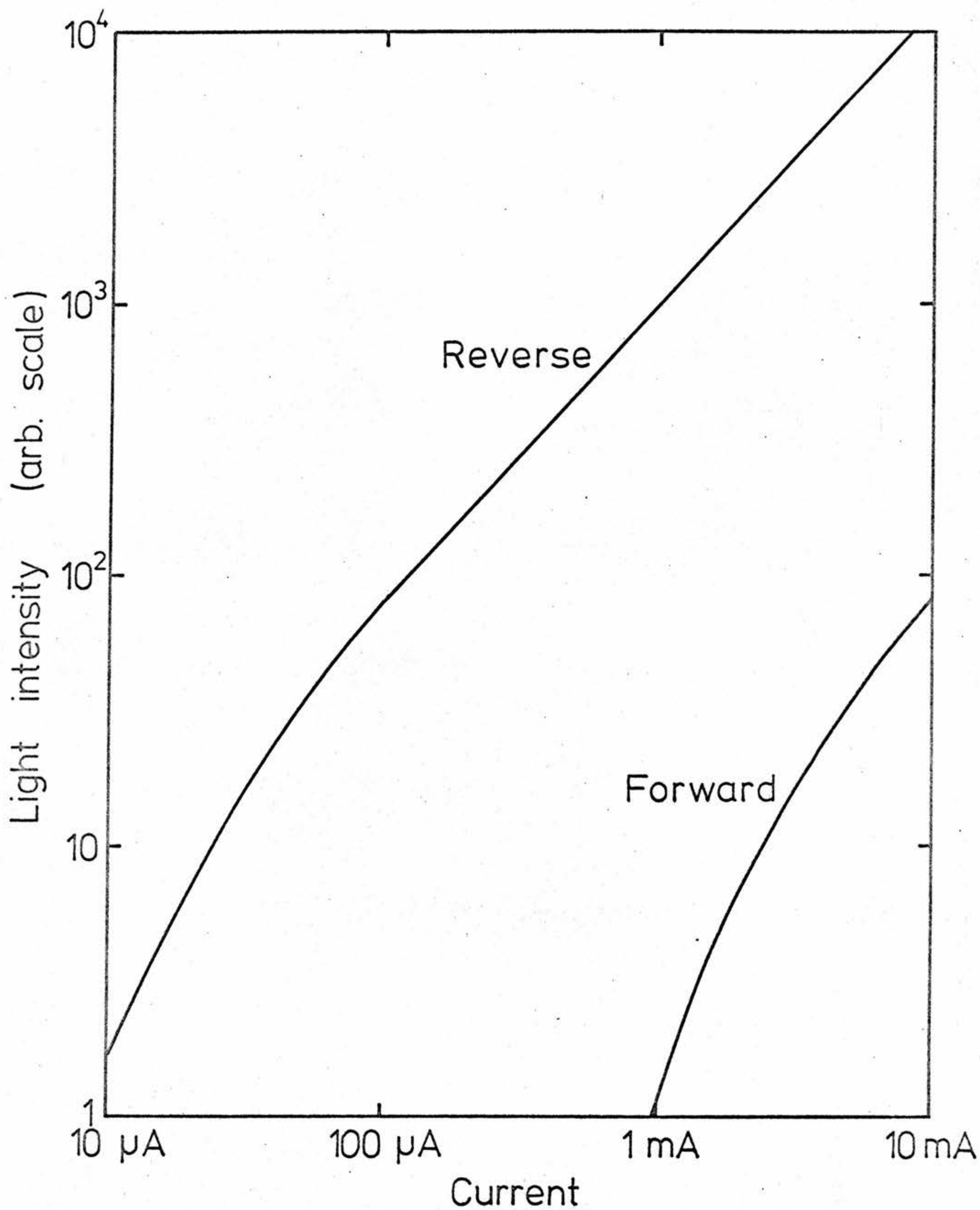

Figure 3.1.1. Comparison of the light intensity from a typical device under forward and reverse bias.

CHAPTER 3

LIGHT EMISSION FROM FORWARD BIASSED DIODES

3.1 Introduction. ZnSe diodes emit light when operated in the avalanche region of reverse bias[23]. The light output is better than that of currently available GaP_xAs_{1-x} diodes. The high operating voltage (typically 15 volts for 20 mA) gives the device an unfavourable power efficiency compared with competitive forward biassed devices and renders it slightly less attractive to the circuit designer. We have been able to obtain light in forward bias from an M-I-S structure using n-type ZnSe as the semiconductor[24]. The light output, which is considerably less than that obtained for the same current in reverse bias (figure 3.1.1), can reasonably be expected to improve with better device fabrication. Most of the physical principles involved in the operation of the device are now understood, and these will be described in this chapter.

For light to be emitted in reverse bias[23], electrons, having tunnelled from the metal to the semiconductor, are accelerated across the depletion region, gaining sufficient energy to impact excite the luminescent impurity atoms (chapter 5). The subsequent de-excitation causes the emission of a photon with energy equal to the excitation energy of the atom. In forward bias electrons can not achieve sufficient energy for this process to occur. Holes and electrons are injected into the depletion region and light is emitted as a result of their recombination. Hole injection into the semiconductor is not possible in an ideal Schottky diode but can occur in an M-I-S structure[25]. Other workers have observed forward biassed electroluminescence from this structure using CdS[26], ZnTe[27] or GaP[28] as the semiconductor.

3.2 Model for Light Emission. If gold is evaporated directly onto n-type ZnSe, the energy levels at the interface will be as in figure 3.2.1. The 1.4 eV barrier height is from MEAD[29]. As forward bias is applied the electron current over the potential barrier increases. However, since the density of holes which can be

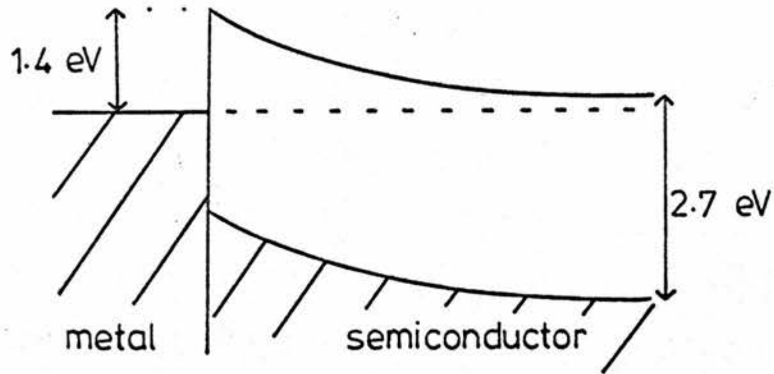

Figure 3.2.1. Energy levels at a Au-n-type ZnSe interface.

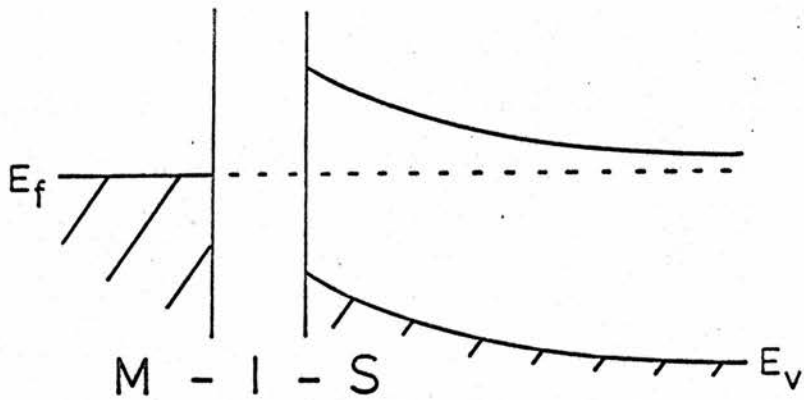

Figure 3.2.2. Energy levels at a metal-insulator-semiconductor junction without applied bias.

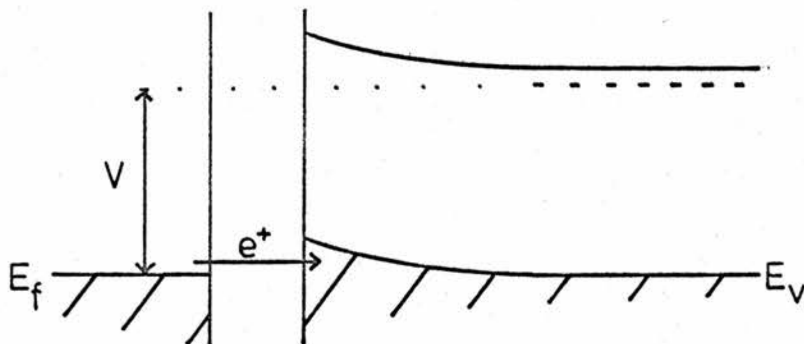

Figure 3.2.3. Energy levels at a M-I-S junction under an applied bias V. There can be injection of holes from the metal.

injected is very small at any reasonable temperature, the proportion of the total current which is being carried by holes, η_h, is also small. The hole current for all practical current levels is small and independent of bias.

In the presence of an insulating layer this situation no longer holds. The energy levels at the interface are not now pinned (figure 3.2.2), and as bias is applied to the device a voltage can be maintained across the insulator, allowing the semiconductor valence band to be raised towards the metal Fermi level. The potential barrier presented to holes is reduced but that which is presented to electrons is unaffected. Thus the hole injection efficiency is increased. As we approach the situation of figure 3.2.3 the density of holes which have an energy corresponding to the semiconductor valence band increases as $\exp((E_f - E_v)/kT)$. That is, the hole injection would increase as $\exp(V_{ox}/kT)$, where V_{ox} is the voltage dropped across the insulator. Once the valence band is more than a few kT above the Fermi level the number of holes available for injection will be roughly constant and will be reflected in the variation of η_h.

The conductivity of the insulating layer itself modifies the hole injection rate. In the case of the devices mentioned in section 3.1, the oxide is such a good insulator that holes can tunnel directly from metal to semiconductor. In the Au-ZnO-ZnSe structure the ZnO is a poor insulator. In order to maintain a voltage which is sufficient to allow aligning of the bands the insulator has to be too thick to be consistent with tunnelling. The same general principles still apply.

The number of electron-hole pairs which recombine to give useful light emission can be related to $\eta_r \eta_{ie}$, where η_r is the radiative recombination efficiency and η_{ie} is the ratio of internal to external efficiency. Generally the effects due to these are not easily separable. Thus the number of photons emitted for every charge carrier crossing the junction, ie the quantum efficiency η_q, is

$$\eta_q = \eta_h \eta_r \eta_{ie}. \qquad (3.2.1)$$

It is important to know the material and device parameters which affect η_q. In practice it is possible to devise experiments which show the factors governing either η_h or $\eta_r \eta_{ie}$ and these will be discussed in the following two sections.

3.3 Effect of Oxide Layer - Variation of η_h. Experiments reported in this section show how the interfacial oxide layer allows the energy band scheme of the M-I-S structure to be manipulated to permit the injection of holes as minority carriers. These experiments support the model for hole injection which was proposed in the last section. All light measurements were made using square wave drive of 1 kHz. The detector was an IP28 photomultiplier tube having S-5 response, and lock-in amplification was used. The entire system was calibrated by means of a standardized GaP (green) lamp supplied by Dr. D.R. Wight of SERL. The emission wavelength of this lamp is sufficiently near those in which we are interested to allow accurate correction for photomultiplier response.

As described in the previous section, an increase in forward bias will raise the semiconductor energy bands relative to the metal Fermi level. As the voltage dropped across the insulator is increased the hole injection rate rises rapidly as the potential barrier presented to holes is reduced. There is not a significant reduction in the barrier presented to electrons and the hole injection efficiency increases rapidly. Once the semiconductor valence band lies significantly above the metal Fermi level, η_h should become constant, as the density of holes above the metal Fermi level is no longer energy dependent. Figure 3.3.1 shows the variation of quantum efficiency of a typical device as bias is applied. The increase below 2 volts is so rapid that it can be assumed to be due almost entirely to the increase in hole injection efficiency, η_h. The recombination efficiency has been measured in this region and been found to increase by a factor of only 2[30]. Qualitatively, figure 3.3.1 shows the form expected for η_h, with a threshold at 1.4 volts. For a series of devices this threshold varied from 1.3 to 1.6 volts. (Some devices did not have such a rapid increase in η_q and the threshold was defined arbitrarily as the lowest detectable light level.) This indicates that at least 1.3 volts have to be dropped across the insulator before the energy bands at the interface have adjusted sufficiently to allow hole injection. Thus, at zero bias, the valence band of the semiconductor must lie

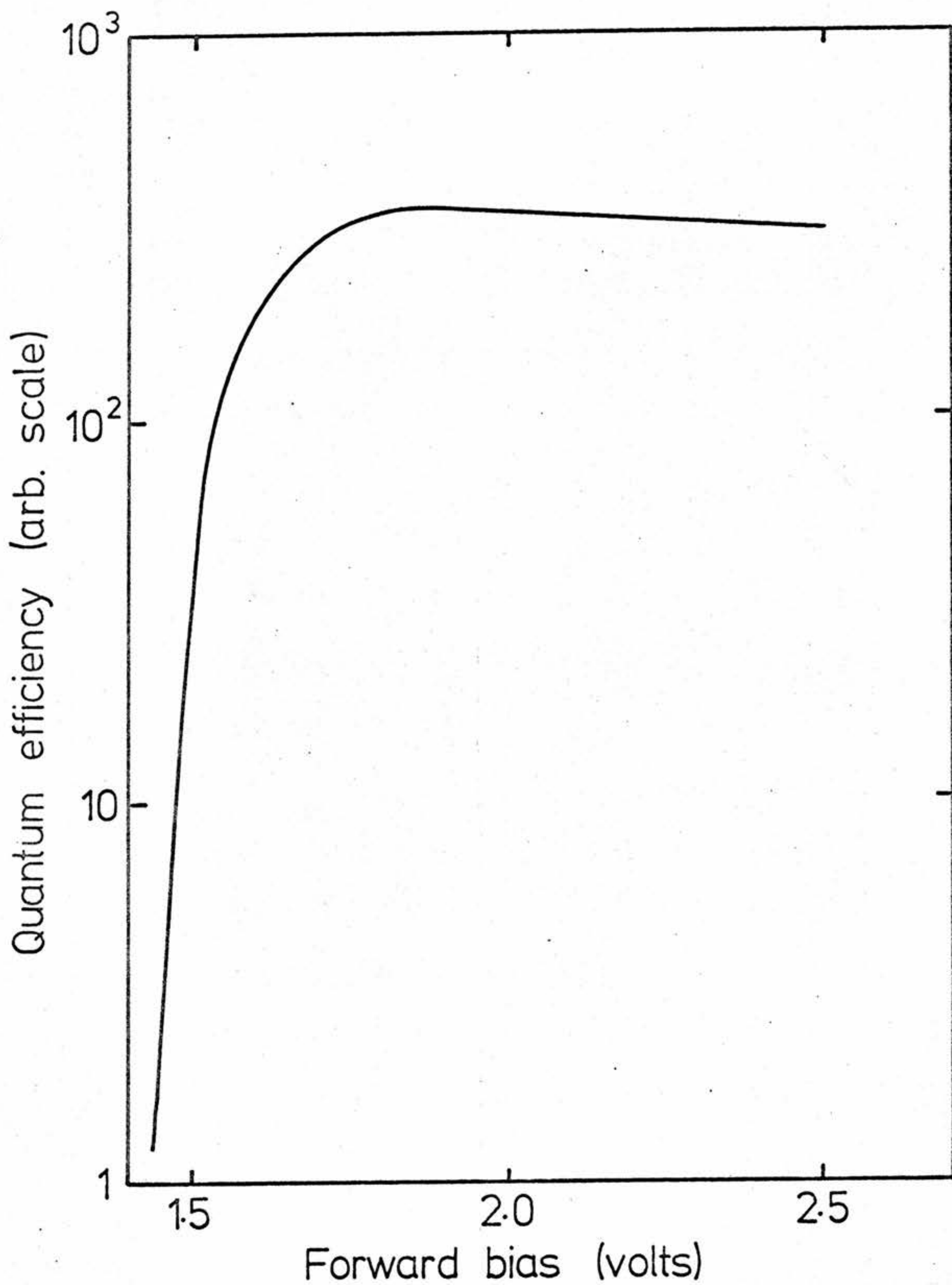

Figure 3.3.1. Variation of quantum efficiency with applied forward bias.

1.3 volts below the Fermi level. This is in reasonable agreement with the value of 1.4 eV obtained for the diffusion potential from photocurrent measurements[20], since the two must sum to 2.7 eV, the energy gap of the material.

From measurements of the quantum efficiency and the photoluminescent radiative recombination efficiency it is possible to estimate the maximum hole injection efficiency using form 3.2.1. This is near 10^{-5}.

Since the device performance is critically dependent on the voltage maintained across the oxide layer, at any particular current density the oxide thickness, and hence its resistance, can be expected to be just as important. Information on how the quantum efficiency varies with oxide thickness is difficult to obtain directly. In chapter 2 it was shown that there was some relationship, especially at high currents, between the voltage required to maintain that current and the film thickness obtained from capacitance measurements. This is not an easily quantifiable relationship, but figure 3.3.2 shows some results which seem to obey some empirical relationship. The results are probably confused by factors such as leakage currents, donor density and the conductivity of the insulator, over which we have little control. However, there does seem to be some relationship, and this has been arbitrarily assumed to be the least squares best fitting straight line. The quantum efficiency and bias voltage at a specific current can now be measured for a number of devices, and be related to the film thickness by the form obtained from figure 3.3.2. Such results are shown in figure 3.3.3. The results for all devices made on the same substrate have been normalized to a mean quantum efficiency obtained for all substrates. That is, the results have been corrected for variations in radiative recombination efficiency which may occur between dice. The largest correction applied, a factor near 2, is in agreement with the spread in results obtained for photoluminescence efficiency. These same measurements indicate a variation in $\eta_r \eta_{ie}$ of up to 50% depending on the crystal orientation in the junction.

The results shown in figure 3.3.3 agree with the conclusions reached in the

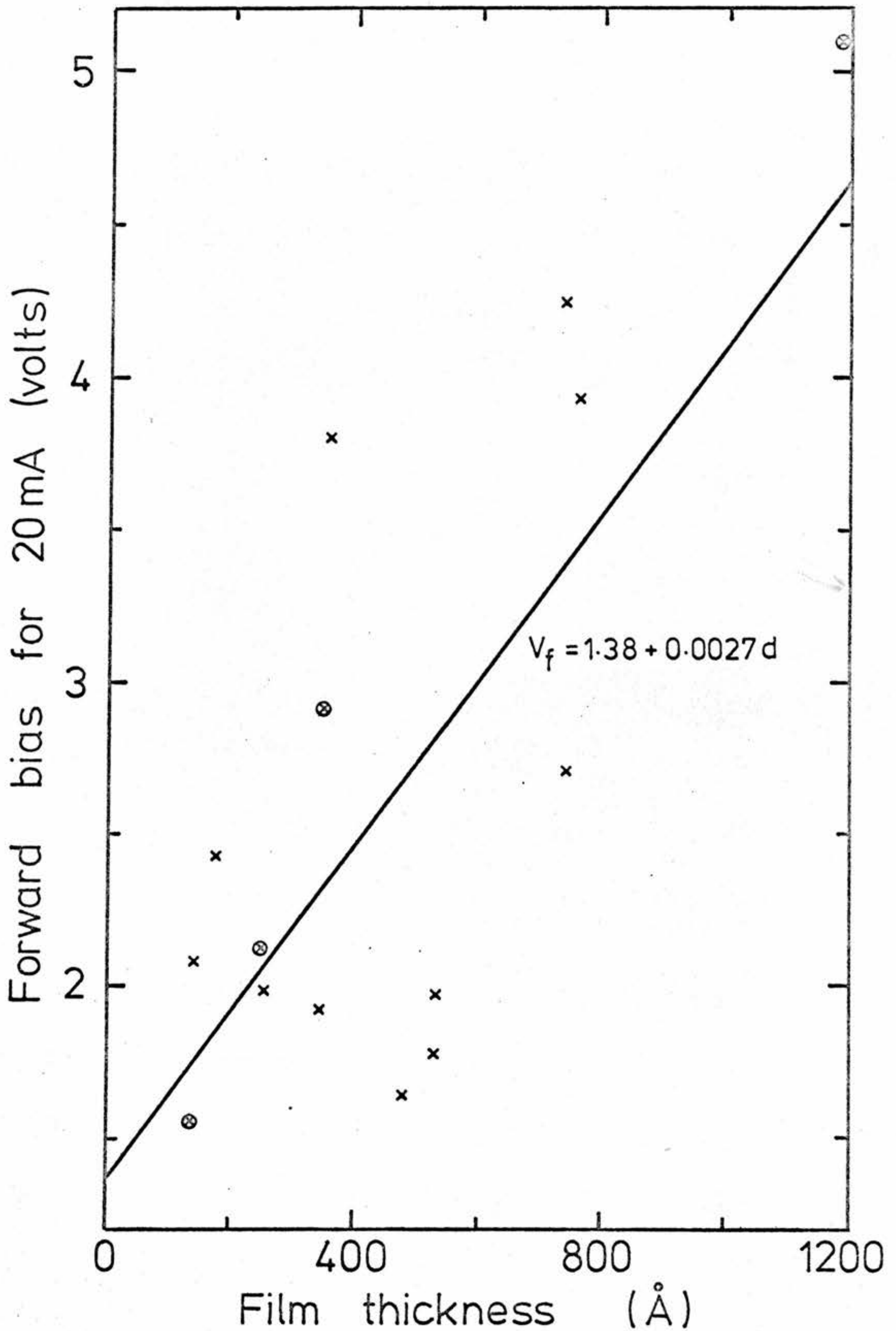

Figure 3.3.2. The film thickness obtained from capacitance results compared with the forward bias necessary to pass 20 mA. The best fitting straight line is drawn through the points. The circled points are the devices of figures 2.6.3 and 4.

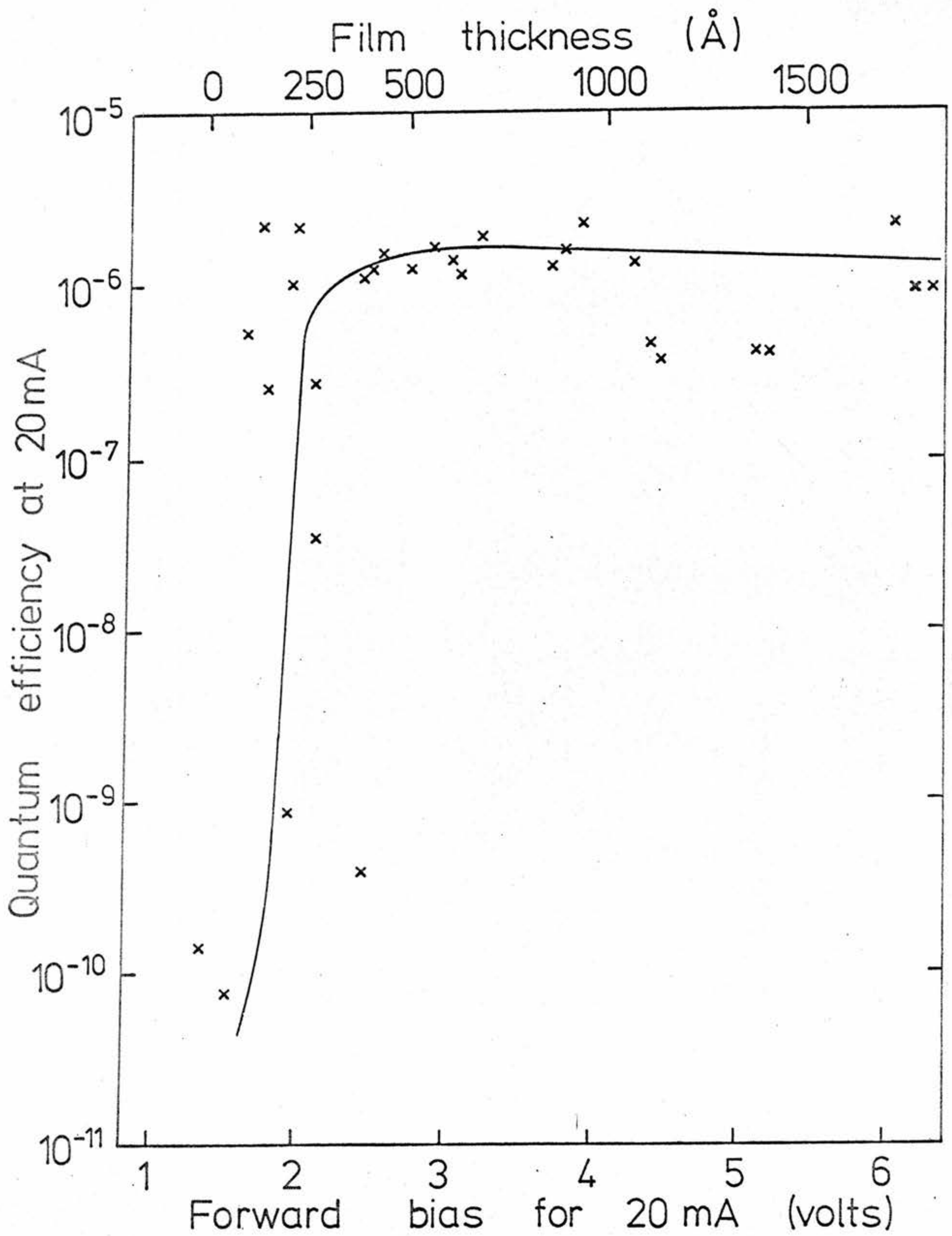

Figure 3.3.3. The quantum efficiency of several devices measured at 20 mA compared with the applied bias necessary to maintain that current. The film thickness has also been included using the best fitting line of figure 3.3.2.

last section. There is a threshold for the emission of light as the insulator becomes thick enough to sustain a sufficiently large voltage to align the energy bands at the interface. For a film greater than 300 Å in thickness the device requires more bias to drive the current through the insulator, but this does not enhance the hole injection. The peak quantum efficiency is near 1.5×10^{-6}.

One consideration which might explain the large spread in experimental observations reported in this section is the polycrystalline nature of the material which was used. In general, a device has one or two grain boundaries crossing the active region. Under reverse bias this does not present any problem; figure 3.3.4 shows light being emitted from a metal contact deposited across a grain boundary. (The picture quality is poor due to the imperfect crystal through which photograph has been taken. The camera is looking at the light emitting region below the metal contact.) Large applied biasses are required in the reverse direction making the extra volt drop across the insulator insignificant. This voltage drop cannot affect the potential barriers presented to the majority carriers. In forward bias, however, where the device is sensitive to film thickness, the varying speed with which an oxide can grow on faces of different crystalographic orientation can be very important. Figure 3.3.5 shows the device of figure 3.3.4 under forward bias. The oxide on one crystallite is considerably less than the 250 Å necessary for light emission. This variation in film thickness across the junction may represent a significant error in the calculated film thickness.

3.4 <u>Nature of the Emitted Light - Variation of η_r.</u> Before considering the nature of the light emitted specifically under forward bias, it is useful to review all the luminescent spectra obtained in ZnSe. Figure 3.4.1 shows spectra measured in this laboratory by K. Turvey and M.D. Ryall. In material which contains manganese as a luminescent centre, both forward biassed electroluminescence and photoluminescence give a broad peak near 2.0 eV. In reverse bias there is a much

Distribution of light over the junction

Figure 3.3.4 → reverse bias

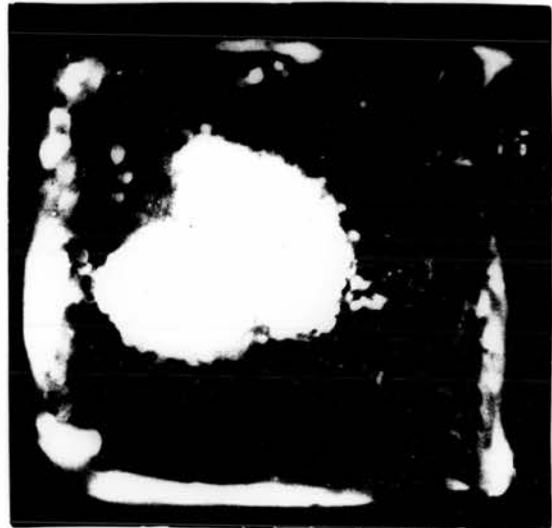

Figure 3.3.5 ↓ forward bias

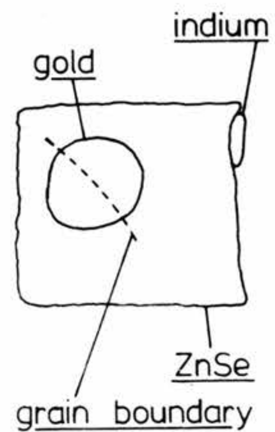

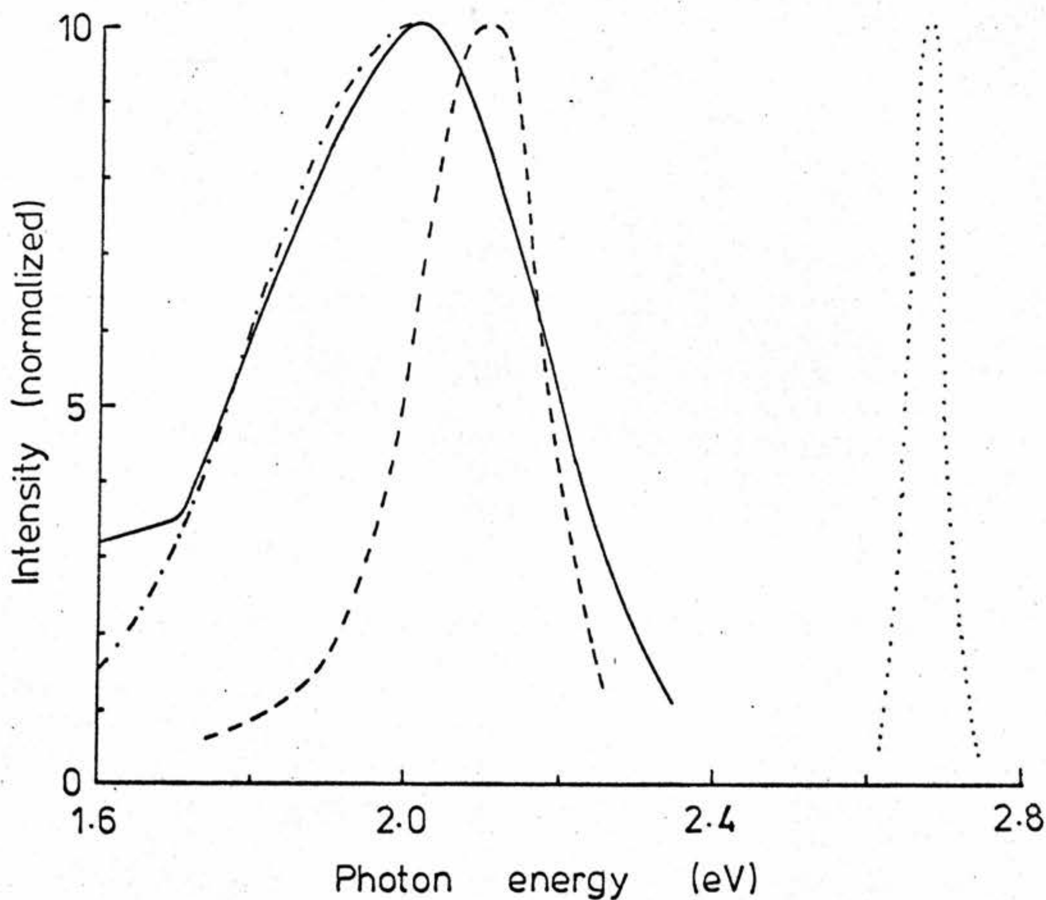

Figure 3.4.1. Photoluminescence (·—·—), forward (———) and reverse (- - -) biassed electroluminescence in ZnSe:Mn. Forward biassed blue emission (·········) from material containing no luminescent centre.

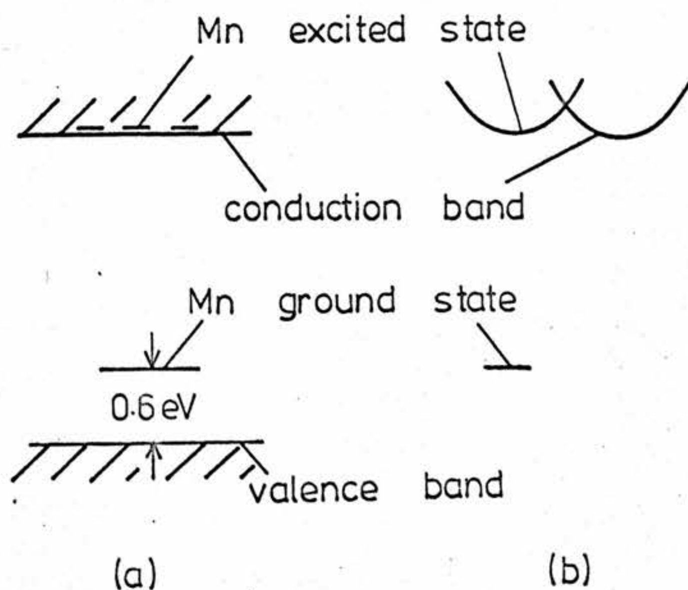

Figure 3.4.2. The manganese ground and first excited state on a) a conventional energy level diagram and b) a configuration co-ordinate diagram.

sharper line near 2.1 eV. The band gap of the material is 2.7 eV and the manganese ground state lies 0.6 eV above the valence band edge. The latter result has been obtained from photocapacitance measurements made by BRAUN et al[20] and later repeated in this laboratory. The first excited state of the manganese is thought to lie near the conduction band edge. If the energy levels are drawn on a configuration coordinate diagram (figure 3.4.2) it can be seen that the excitation of the manganese does not necessarily imply ionization. It is thought that in reverse bias electrons may achieve sufficiently high energies to cause excitation of the manganese. The subsequent de-excitation gives the 2.1 eV radiation shown in figure 3.4.1. A few carriers may be thermally stimulated into the conduction band and under suitable conditions these may be detected (see chapter 5). In both forward biassed electroluminescence and photoluminescence it is electrons associated with the conduction band minimum which contribute to the emission. This is thought to be the self activated emission and not related to the manganese impurity.

Spectra obtained from material containing copper as the luminescent centre do not have these different peak energies. Forward and reverse biassed electroluminescence are both thought to occur as a result of recombination through a defect complex near the conduction band edge. Both transitions have an energy near 1.9 eV, in agreement with the photoluminescence spectra. Material containing no intentional luminescent centres emits light of very near band gap energy when forward biassed (figure 3.4.1). This has a sharp peak at 2.675 ± 0.005 eV with a broad band of radiation at lower energies. Such devices age extremely rapidly, the blue band disappearing in a few minutes, probably as a result of the high currents ($\sim$ 10 A cm^{-2}) which are required for the emission to be visible. This transition is thought to be excitonic although no binding centre has yet been identified. The electroluminescence of reverse biassed lamps containing no intentional luminescent centre has been described elsewhere[31] and is quite different.

Since the forward biassed electroluminescence of ZnSe:Mn is so closely related to its photoluminescence, the processes might be expected to have other common properties. In particular, if an experiment could be devised which involved no temperature variation of the processes which create the electron-hole pairs, then the thermal quenching of both electroluminescence and photoluminescence should be that of the radiative recombination process which is common to both. Since the injection efficiency is governed by the tunnelling of holes into the semiconductor it should not show much variation with temperature. This will not be true when the device is operating in the threshold region discussed in the last section. In this region the hole injection process is limited by the density of holes which have suitable energy and this will be extremely temperature sensitive. Above threshold however, the temperature variation of η_q should be directly related to that of $\eta_r \eta_{ie}$ since the density of holes above the metal Fermi level will not be a function of temperature. Thus the thermal quenching of photoluminescence efficiency and the quantum efficiency of forward biassed electroluminescence should be similar.

Thermal quenching of radiative recombination in luminescent materials generally has a form

$$\eta_r = \frac{1}{1 + A\exp(-E_a/kT)}. \qquad (3.4.1)$$

APPERSON et al[32] have measured the photoluminescence efficiency of ZnSe:Mn and found that it fits the above form for an activation energy, E_a, of 0.6 eV. IIDA[33] obtained an activation energy equal to 0.35 eV in ZnSe without deliberately added impurities.

The forward biassed quantum efficiency of our devices also has this form. Figure 3.4.3 shows results for a series of current densities. The quantum efficiency varies slowly with current at constant temperature, indicating that the device is operating just above threshold. These results have been fitted to the form of equation 3.4.1 for an activation energy of 0.36 ± 0.10 eV. The deviation from the expected form at low currents is thought to be due to the temperature dependence of the hole injection process near threshold. This is

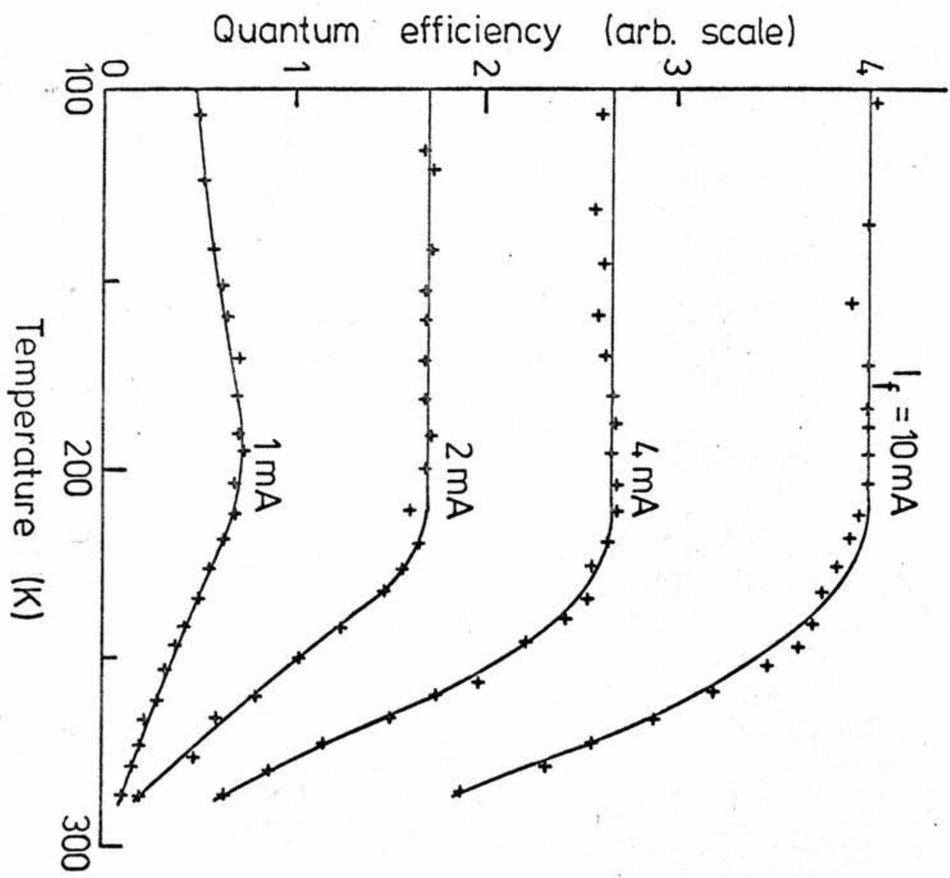

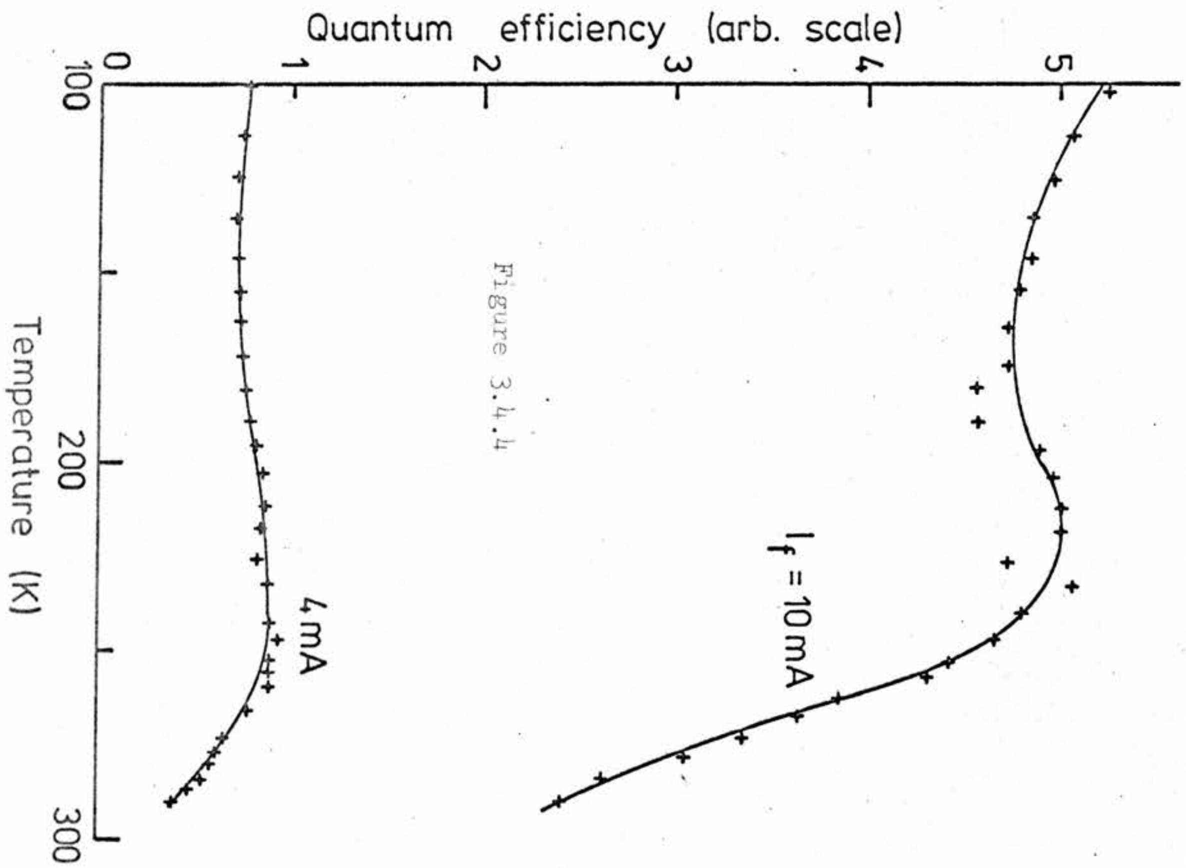

Figure 3.4.3. Quantum efficiency versus temperature above threshold.

Fihure 3.4.4. Quantum efficiency versus temperature near threshold.

seen more clearly in figure 3.4.4 which shows the same measurements performed on a device operating near threshold (as indicated by the rapid increase in quantum efficiency with current). This device has an activation energy near 0.34 eV.

Equation 3.4.1 suggests that at low temperatures η_r becomes constant. For the device of figure 3.4.3 the calculated radiative recombination efficiency at 300 K shows a steady increase with current as shown in the table. These values have been calculated assuming η_r to be 100% at low temperatures. The same super-linear trend has been observed in measurements of photoluminescence efficiency as the exciting intensity is increased[30].

I (mA)	η_r (%)
1	4.8
2	7.4
4	14.9
10	26.7

3.5 Discussion. The results contained in this chapter indicate that a M-I-S structure on ZnSe can give light emission in forward bias. The device in its present form is not sufficiently efficient to be of commercial value, but the experiments can indicate how η_q might be increased.

Improvement of the quantum efficiency of the device can be approached from two directions. The simplest might be to change the semiconductor. As the last section has shown, the radiative recombination rate is primarily a material property, and in ZnSe:Mn is only of the order of a few per cent. An immediate improvement might occur by using ZnS, which can have radiative recombination efficiencies approaching 100% at room temperature. There seems no reason why the same method of oxide deposition by etching should not work on this material.

A long term solution might be to try and improve the hole injection

efficiency. It is not clear what the limiting process is, but it would seem to lie in the conduction mechanism through the insulator. Other materials have provided much higher injection rates and it seems likely that this can be improved in our devices either by changing the insulator, or just by altering its method of preparation.

These devices are probably simpler to fabricate than most other M-I-S structures which have been used in this application. The ZnO has a small conductivity which means that a slightly thicker oxide is required than is normal in other devices. However, in a device which has to rely on holes tunnelling through the insulator, there is an upper limit to the oxide thickness. The conductivity of the ZnO eliminates this problem. A device with a thick oxide merely requires more applied voltage. Hence there is less control needed over the oxide thickness during manufacture.

The efficiency obtained in the Au-ZnO-ZnSe structure is compared with other materials in the following table.

Semiconductor	Insulator	Efficiency		Reference
		77 K	300 K	
ZnSe	ZnO	10^{-5} 20 mA	10^{-6} 20 mA	This work
GaP	SiO_2		3×10^{-5} 10 mA	28
ZnTe	Insulating ZnTe	green 10^{-3} red 4×10^{-3}	2×10^{-4} 3×10^{-3}	27

CHAPTER 4

MEMORY AND SWITCHING

4.1 Introduction. An unexpected advantage of the M-I-S structure on ZnSe, apart from the hole injection already discussed, is that such a device can be made to exhibit two independent rectifying characteristics[34]. By application of suitable voltage and current pulses either of these states can be selected. This is not the first observation of switching and there is already a great deal of research endeavour directed at producing a switching device.

A vast range of materials has been observed to exhibit the required bistable properties and almost as many physical mechanisms have been proposed to explain their operation. Among the first in the field were chalcogenide glass[35,36] and thin film[37-40] devices, and recently switching phenomena have been observed in p-n junctions, heterojunctions, point contact rectifiers[41] and M-I-S devices[42]. Of most relevance to the devices reported in this work are the ZnSe-Ge heterojunctions developed by HOVEL et al[43,44] at IBM. Of our devices, not all those prepared as in chapter 2 exhibit switching and memory properties, whereas all will emit forward bias light if the insulating layer is more than 200 Å thick. Switching diodes generally occur for films of 750 Å or thicker and the device yield is low.

In this chapter the device will be considered first from the circuit designer's viewpoint, that is, typical characteristics will be presented. Additional results which help lead to a possible mechanism will then be discussed.

Observations on our particular system are not easy. Reproducibility is a major problem, particularly of the oxide thickness and conductivity. There have been results obtained in particular diodes which are not generally applicable but which have some significance if they can be related to the overall scheme. These will be noted as they occur.

Lastly, possible mechanisms for the device behaviour will be discussed. The switch will be shown to be due to a change in conductivity of the oxide film, and

a model will be postulated which is consistent with this picture.

4.2 Device Characteristics. The devices have two distinct states, each with its own rectifying characteristic as shown in figure 4.2.1. The high conductivity state COD is the more ideal of the two. That is, it is the characteristic one obtains from a device which does not exhibit switching and also the state in which diodes end up after many switchings. This state can be traced and retained until the current at point D is exceeded, corresponding to a current density of approximately 10 A cm^{-2}. The device then undergoes a transition to the low conductivity state AOB and this too can be retained until the voltage at point B is exceeded. This threshold value can vary considerably from device to device, and in any particular diode can vary from 2 volts when new to perhaps 15 volts after many operations. The device then reverts to its original state and the cycle is complete. The high conductivity state will in future often be referred to as the high state, and similarily for the low conductivity state. Figure 4.2.2 shows the forward characteristics on a semilogarithmic scale, demonstrating that the current differential for some bias below threshold can exceed two orders of magnitude. The low state of the device has been maintained, without the need for a retaining bias, for periods in excess of 5000 hours.

The preceeding chapter showed how the inclusion of the insulating layer in the Schottky diode allowed light to be emitted in both bias states. The fact that the diode exhibits switching properties does not alter this. Light is emitted under all bias and conductivity conditions. In fact the quantum efficiency of the device at a given current is found to be unaffected by the conductivity state, as will be shown in section 4.3. That is, the intensity of the emitted light is dependent only on the magnitude of the driving current, not on the device state.

The variation of the high state I-V characteristic with temperature has already been described (section 2.6). Figure 4.2.3 shows both states as a function of temperature. This clearly shows a difference between the two conduction mechanisms.

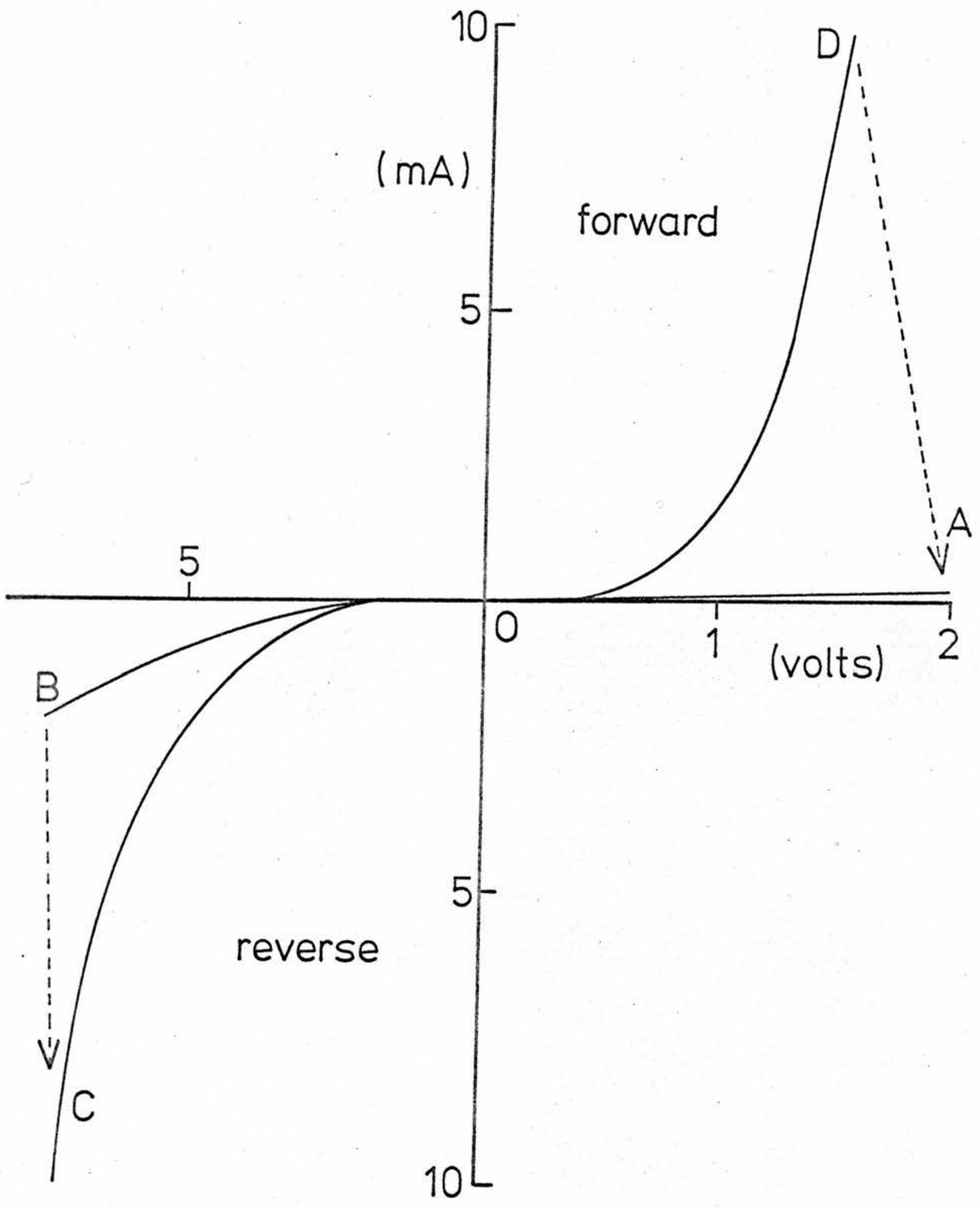

Figure 4.2.1. DC characteristic showing the two switched states in a typical diode. Note the different voltage scales.

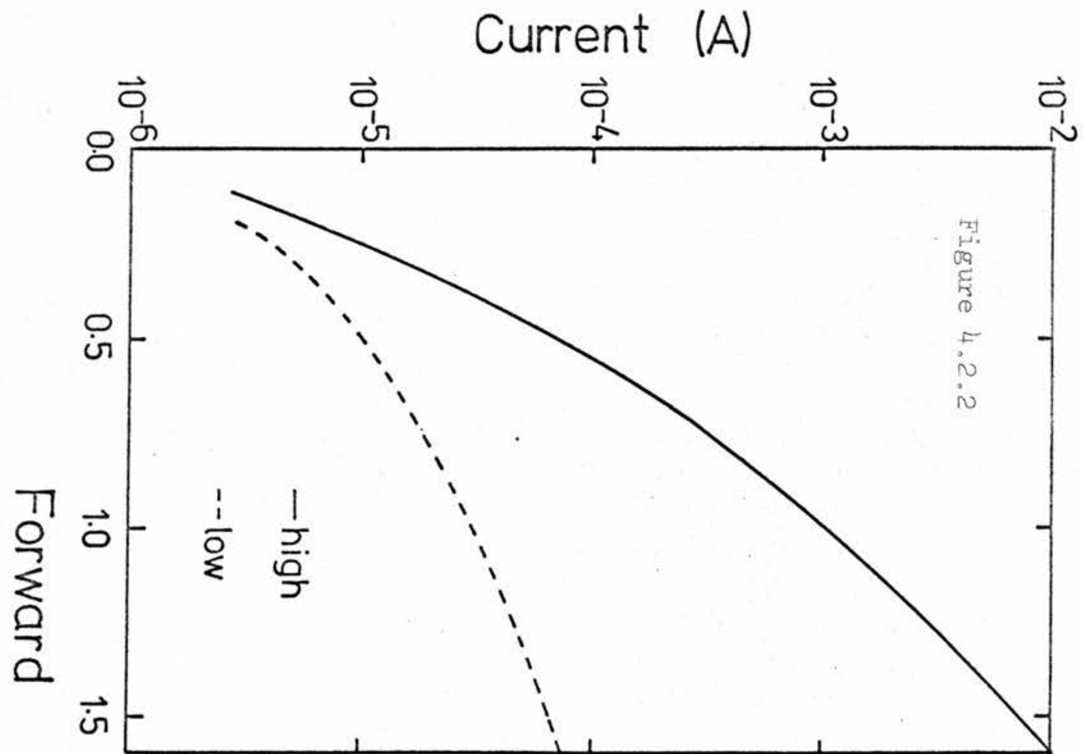

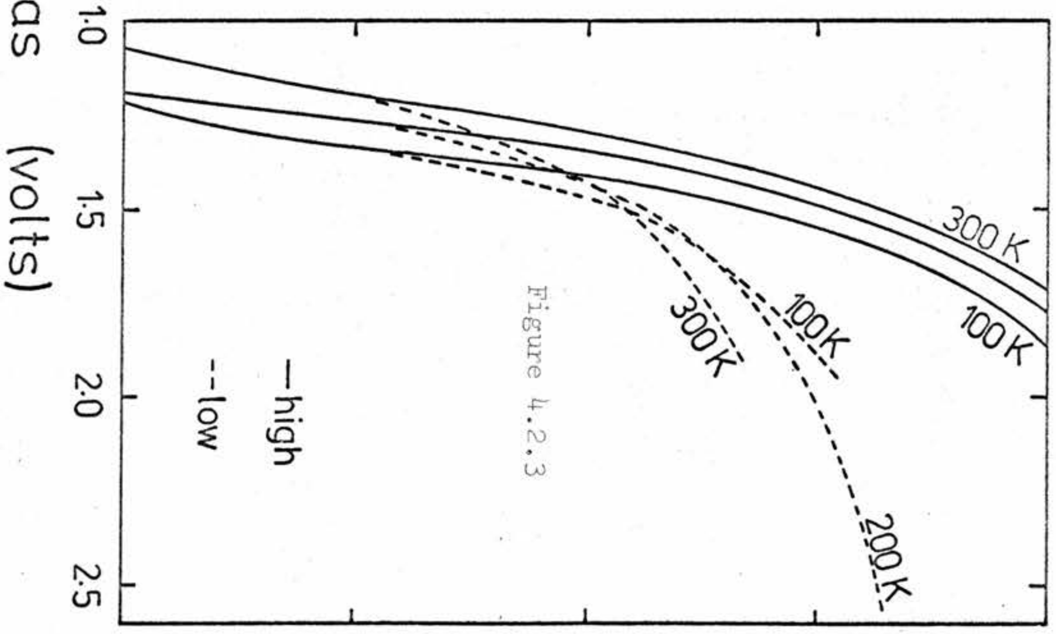

Figure 4.2.2. The forward characteristics of figure 4.2.1 shown on a semilogarithmic scale.

Figure 4.2.3. Typical temperature variation of the forward biassed characteristic.

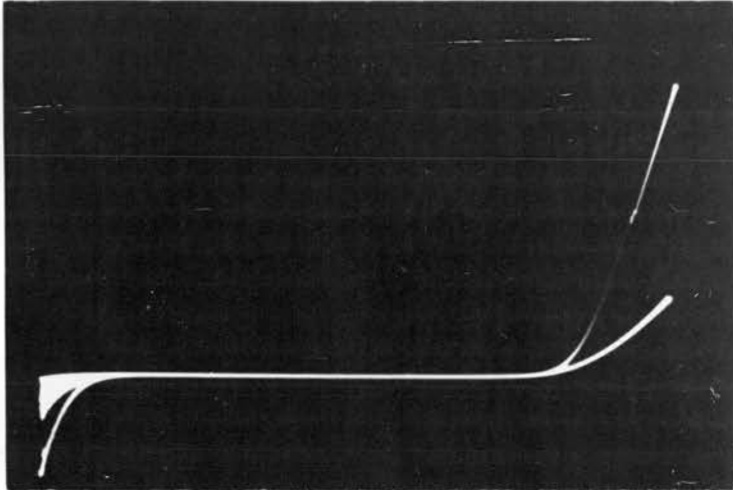

Figure 4.2.4 Typical curve tracer characteristic showing switched states.

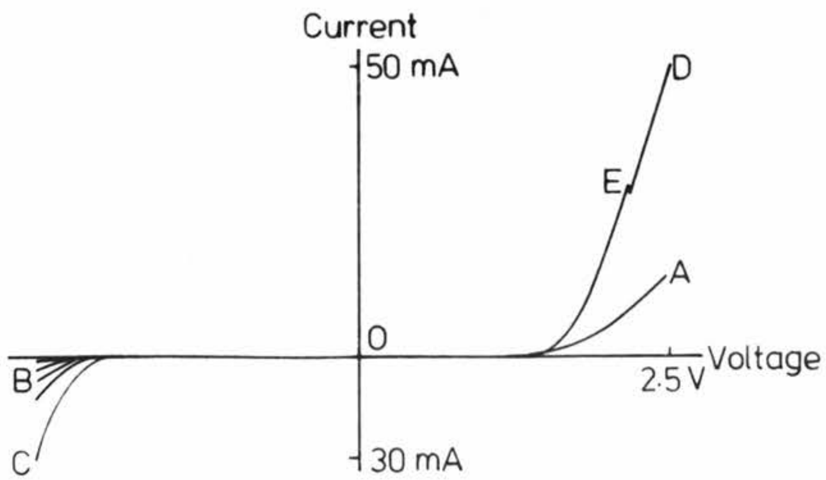

The AC operation of the device is not well understood, and the devices have never been run repetitively round the switching cycle other than by multiple measurement of the DC characteristics. The reason for this can be seen in figure 4.2.4. This is an oscilloscope photograph obtained from a characteristic curve tracer designed and built in this laboratory. In this instrument the maximum forward and reverse bias voltages are always represented by equal displacements on the oscilloscope. As the maximum bias applied to the device is varied the maximum x-displacement on the oscilloscope remains constant, now being calibrated in terms of the new bias. Thus, in figure 4.2.4, characteristic AOB represents the low conductivity state with maximum applied biasses of 2.5 and 13 volts in the forward and reverse directions respectively. The maximum reverse bias has been slowly increased (hence the blurring due to the 50 Hz sweep) to 15 volts when the device has undergone a transition to the high conductivity state COD. The point E is of interest. It appears to be a partial switch from the high state and the device will only switch completely if it is maintained in this region for a time long enough to initiate the transition. The device in figure 4.2.4 is running under a 50 Hz sinusoidal bias, and will switch only erratically when the peak of the sine wave is maintained in the switching region. The period for which this condition is satisfied can reasonably be expected to be of the order of 1 mS. It would seem that our device, in common with the glass switches, has a considerable delay time before a transition will take place. Certainly the actual transition time is very much shorter than this, but is of lesser device significance since the time which is important is that for which a bias must be maintained before the switch is complete.

The irreproducibility of the switching point has also hampered the measurement of the transition time, as has the extremely fast ageing of the devices. It was at first thought that the two states of the device moved towards each other after many cycles. More specifically, it was thought that the low state moved towards the high. This was because devices which could no longer be made to switch still

exhibited the small deviation in characteristic labelled E in figure 4.2.4, and this was thought to be a switch between two very close conductivity states. The same figure shows that this is not in fact true. In this case, both conductivity states and the 'partial switch' exist in the same device, and it now appears that ageing of a device is made apparent by the increasing difficulty with which it can be switched from the high to the low state, neither of which alter appreciably. The method of ageing is not understood, but with use the switching thresholds move to higher currents and voltages. The increased power dissipation probably causes the process to be accelerated.

4.3 Experimental Results. In certain respects the Au-ZnO-ZnSe structure is better defined, and therefore more amenable to measurement, than some other systems in which switching has been observed. A common conclusion of work done on these other systems is that the device operation is, in some way, controlled by the presence of some unknown traps in the energy gap of the semiconductor. In the ZnSe which we have used there is a high concentration of deep impurities of which the position and occupancy can be measured by suitable experiments. The second advantage of the ZnSe based device is that it emits light, and measurements of the variation of this emission can give information about energy levels at the interface.

Changes in the number of luminescent centres which are ionized can be seen in capacitance results. Chapter 2 described how the slope of the C^{-2}-V plot could be related to the density of ionized impurities in the depletion region, and as figure 4.3.1 shows, this density alters as the device changes state. These measurements were obtained at 100 kHz and show the high state giving a result closer to that expected for an ideal diode, the low state having a higher extrapolated voltage. The change in occupancy of the luminescent centres during switching indicates that the transition is not merely an oxide effect, but does depend on the deep centres. Such large changes in junction capacity are not

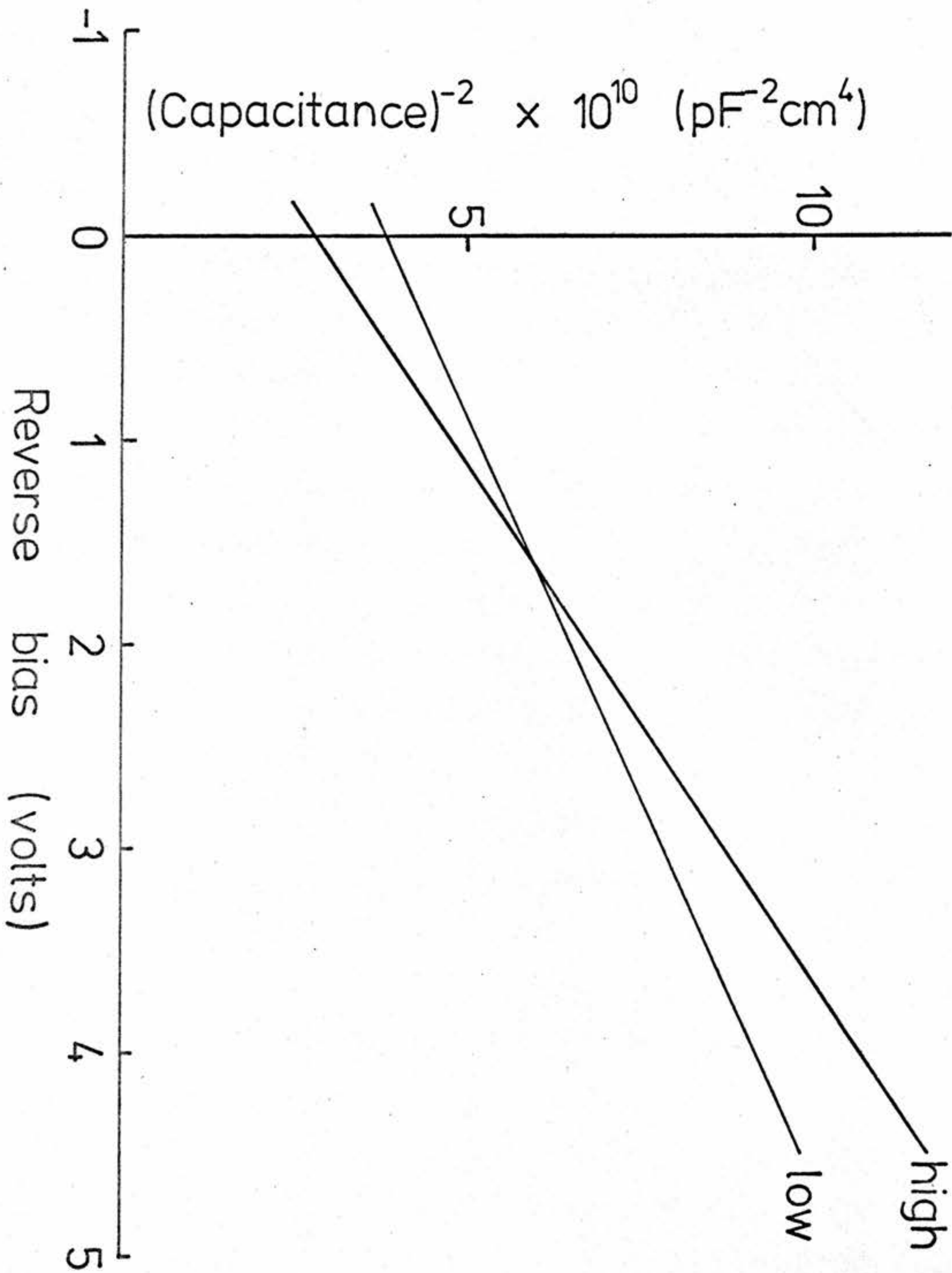

Figure 4.3.1. C^{-2}-V plot for the switched states showing a larger ionized imurity concentration in the low state.

observed in all devices. Chapter 2 described how an AC conductance could arise due to the finite response time of the charge centres. This conductance generally shows a greater variation between states than does the capacitance, and is a useful way of determining the state of charge of the interfacial layer.

In chapter 2 it was noted that of several devices made under apparently identical conditions some could have charge locked at the interface, whereas others had none. This can now be seen to be the low and high states respectively of a switching diode which cannot be made to change state. To demonstrate this effect the I-V and C^{-2}-V characteristics of two such devices are shown in figures 4.3.2 and 3. These are remarkably similar to the results contained in figures 4.2.2 and 4.3.1.

The light emission which was described in the preceeding chapter was discussed only in terms of what we now see to be the high state. In fact it is obvious that the same processes must be present in both states if the nature of the light is unaltered. That is, for light emission we still require a process of hole injection and subsequent electron-hole recombination. Figure 4.3.4 shows the quantum efficiency of a device as a function of current for both its conductivity states. It is seen that η_q is dependent only on the current, not the state of the device. Similarily figure 4.3.5 shows that the light emission has the same threshold voltage regardless of state.

There are two other observations, one qualitative and the other only relevant to a few devices, which will have some influence on the discussion in the following section. The first is that when the light being emitted by the junction is examined under a microscope it does not appear to come from a few discrete points, but be distributed more or less uniformly over the whole active area. This is common to all devices. Secondly, there have been devices which exhibited peculiar light sensitive properties. In particular, a device has been switched between states by leaving it in daylight or darkness, just as efficiently as by the application of bias. Figure 4.3.6 shows an example of this. Here the high

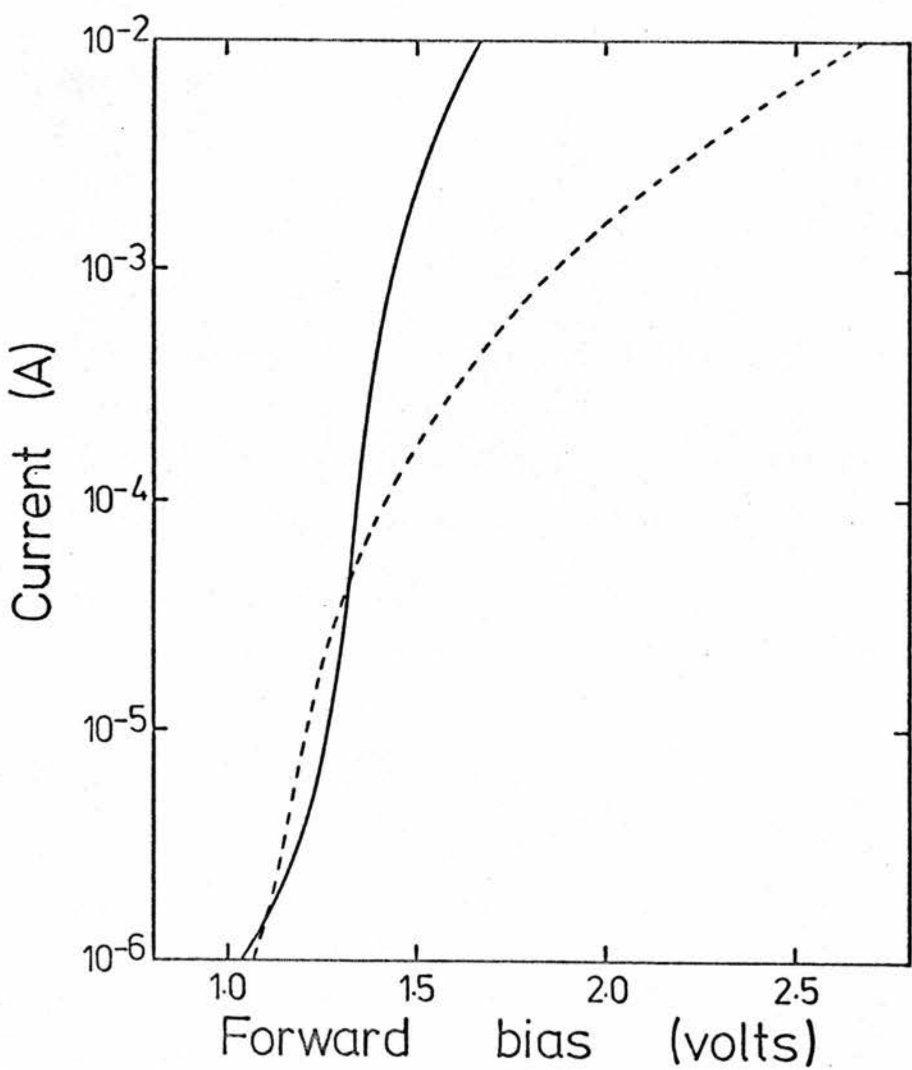

Figure 4.3.2 I-V characteristics of two devices showing what appear to be two permanent high and low states.

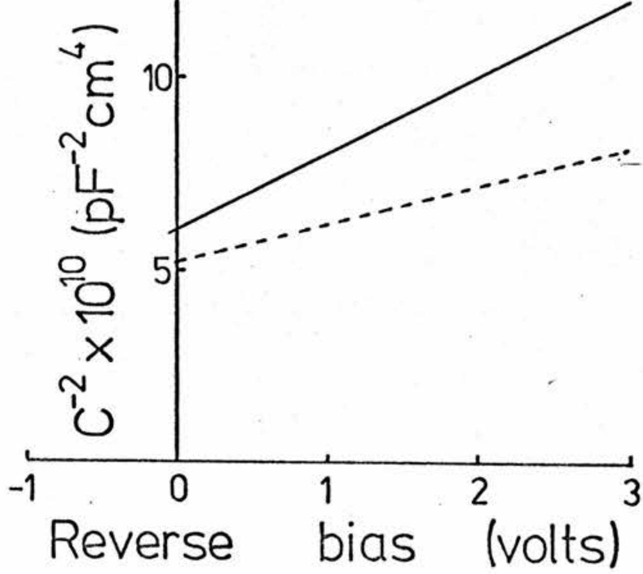

Figure 4.3.3 C^{-2}-V plot for the devices of figure 4.3.2. The device (- - -) has a large stored charge indicated by the junction conductance.

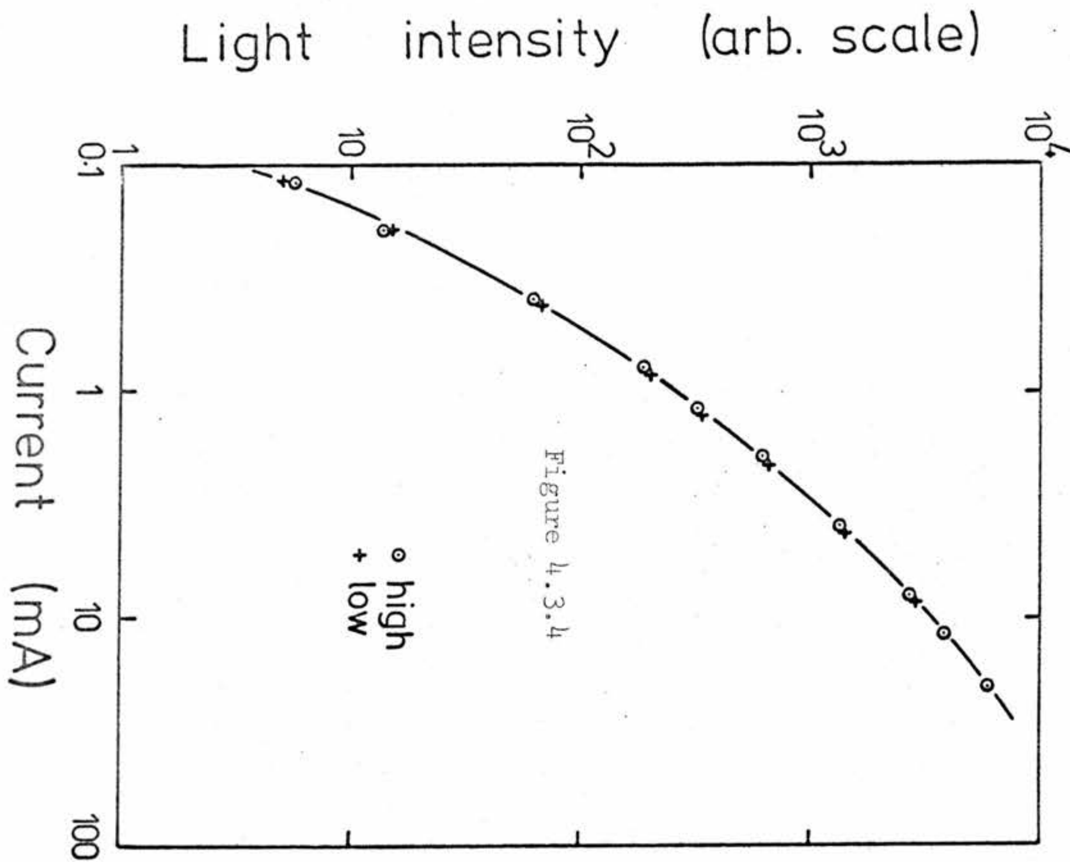

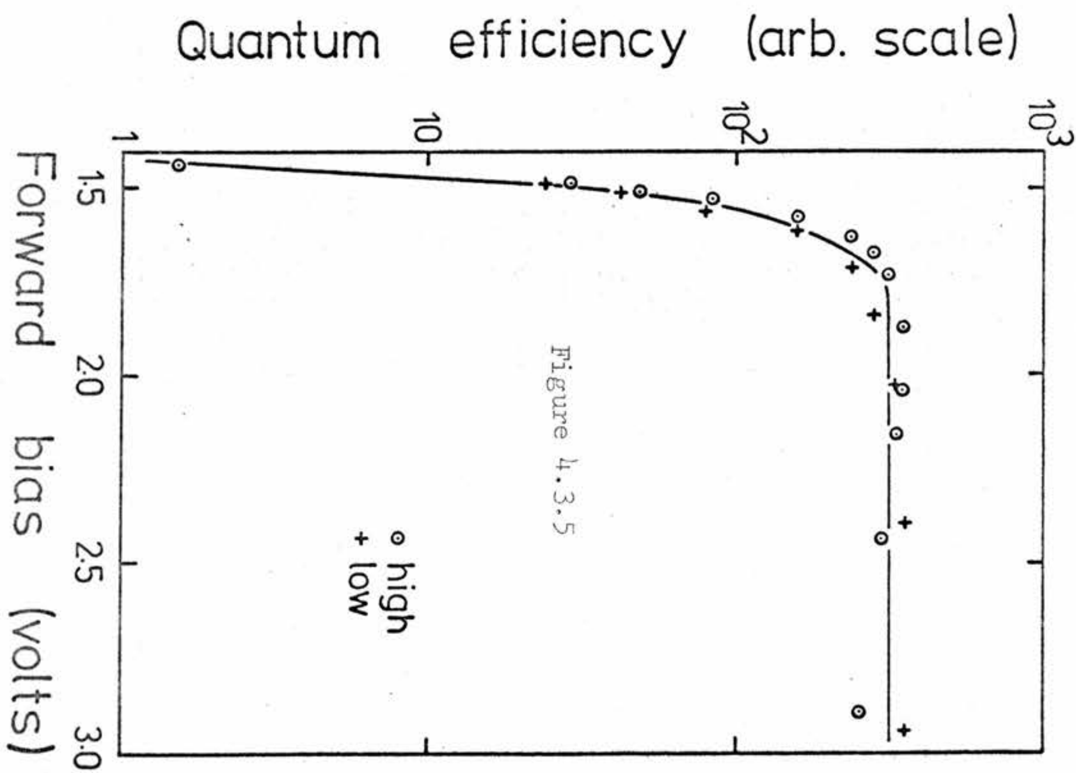

Figure 4.3.4. Variation of light output with current in both states.

Figure 4.3.5. Variation of quantum efficiency with bias for the device of Figure 4.3.4. The threshold voltage is independent of state.

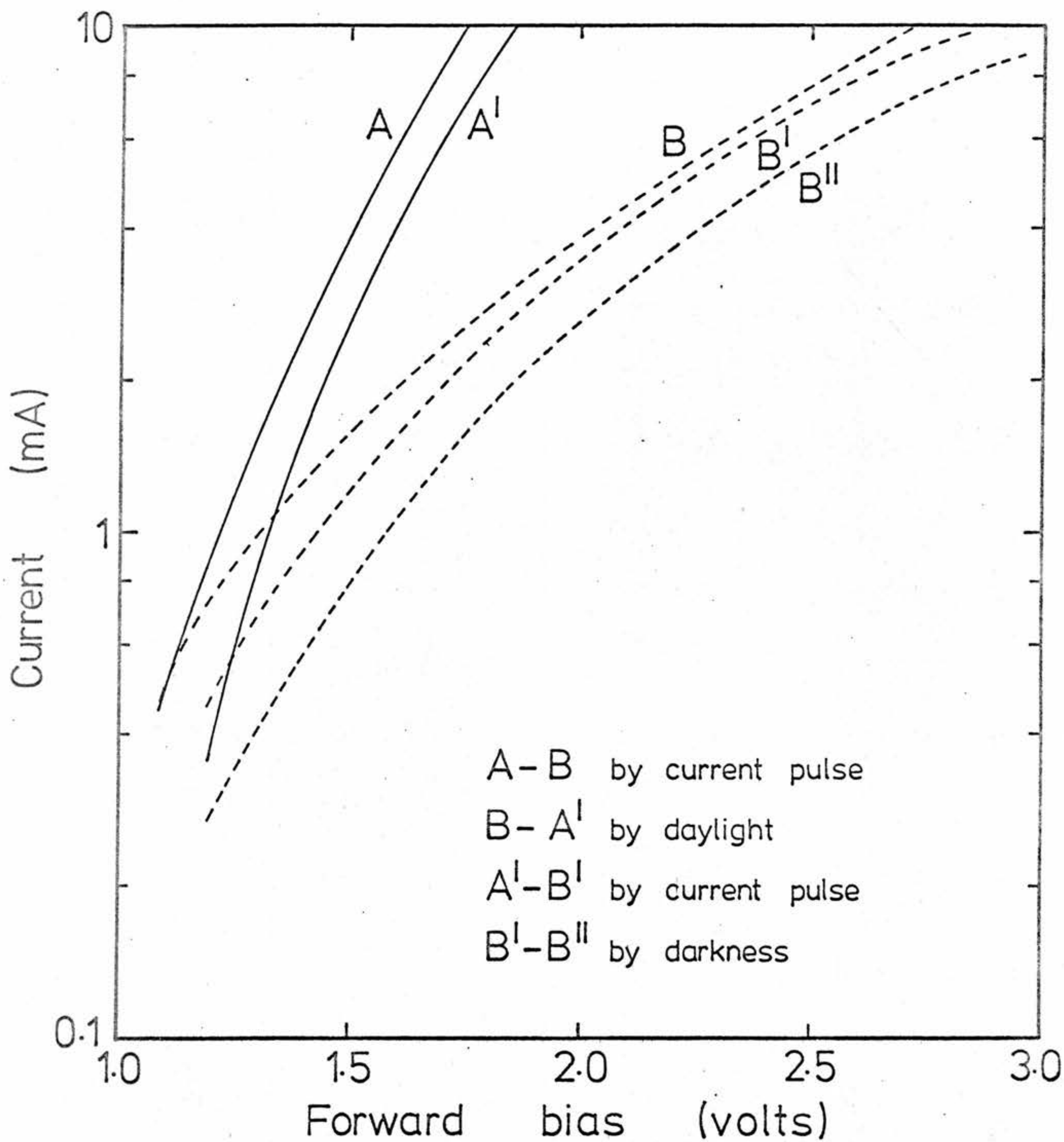

Figure 4.3.6. Switching achieved by application of light.

state A has been switched to the low state B in the conventional manner by means of a current pulse. State B has then been restored to high state A' by exposure to daylight for several hours, whereas leaving the device in darkness while in its low state makes little difference. Unfortunately this particular device locked in the high state before it was possible to measure the spectral dependence of the effect and subsequent measurements on other devices have been inconclusive. It seems likely that the diode of figure 4.3.6 was in an extremely unstable condition and that more conventional devices would require considerably more intense radiation to produce the same effect.

4.4 Switching Mechanism. It is possible to envisage several processes which might take place in an M-I-S structure and which could conceivably lead to a change in device conductivity. This section will examine some of the more obvious of these in terms of results which have already been described. The switching problem can best be approached from three viewpoints. These are that the bistability might be due to

a) a change in conductivity of the depletion region

b) a change in conductivity of the insulator

c) a change in barrier heights at the interface.

Consider first the effect of the switch on the semiconductor depletion region. The luminous quantum efficiency in both conductivity states is the same at a given current density. Since the light is produced due to some recombination in the depletion region, it would appear that the voltage configuration in the semiconductor is dependent only on current, not on state. Charge is however moved from the deep traps in the semiconductor during switching. Coincident with this change in charge density there is an increase in the high frequency parallel loss component of the capacity measurements. This can be attributed to charge being swept back and forth across the semiconductor-insulator interface between the deep traps and some, as yet unidentified, charge centres in the insulator.

It is conceivable that a transfer of charge could cause a change in energy levels at the interface. A small change in barrier height could easily cause a large variation in device conductivity. In the preceeding chapter a model for light emission was proposed which predicted a threshold voltage for this emission. This threshold is the voltage necessary to align the metal Fermi level and ZnSe valence band and is a measure of the energy separation of these levels. However measurements indicate that this threshold is independent of the device state, suggesting that there is no adjustment of energy levels during switching.

Since the volt drop across the semiconductor seems to be independent of state, and there is no change in barrier heights at the interface during switching, the change in conductivity of the device must be due to a change in the conduction process in the insulator. To be more precise, for a given current density the extra voltage required in the low conductivity state must all be dropped across the insulator. This does not mean that we have a simple oxide switch. The deep impurities in the semiconductor take part in, and indeed seem to be necessary for, the switching process. Switching has not been observed in devices without intentional deep impurities even though examination of the blue emission from such material requires the devices to be run at currents considerably in excess of those normally required for switching.

Filamentary conduction has often been proposed[45,46] as a mechanism for switching. Indeed HOVEL et al[44] indicate that they think this might be an explanation of the behaviour of their ZnSe-Ge heterojunctions. This process requires conduction along a filament which is physically different from the host material. Some process such as Joule heating can cause this filament to rupture with a correspondingly rapid change in device conductivity. This does not seem to be a likely process in the ZnO-ZnSe system despite Hovel's suggestion. There are two reasons for this. Firstly, light is emitted over the entire junction area. Since this corresponds to the regions of the junction through which current is flowing, conduction can not be said to be through a few discrete points.

Secondly, the device has been made to change state by the application of light. The only conceivable process by which light could change the conductivity of ZnO using a filamentary model is in direct contradiction of the observed results. In this model the high state would consist of zinc filaments running through the oxide. Application of light would convert these to ZnO causing the device to go to its low state. The observed transition is from low to high when illuminated.

The results described previously, and the discussion in this section, lead to a proposed model of switching as follows. During switching, charge is transferred between the deep centres in the semiconductor and trapping sites in the insulator. By some method, which will be discussed in the next section, this charge can alter the conductivity of the insulator, and would appear to have an indefinite storage time under zero bias. This model satisfactorily describes the experimental observations which have been reported in this chapter.

4.5 Charge Transport in Insulators. By examination of the I-V characteristics of the switch we shall seek in this section to establish a possible mechanism for the current flow in the insulator. This does not in any way add to the switching mechanism which has already been discussed, but shows that there might be a conductivity process which is consistent with the conclusions of the last section.

DEARNALEY, STONEHAM and MORGAN(47) have reviewed the charge transport mechanisms which may operate in insulators. These will be mentioned briefly here in order to see how they relate to the ZnO film.

a) Schottky emission of electrons over a potential barrier is a process which may account for carrier injection into the insulator. There may exist similar barriers inside the material, and the field assisted thermal excitation of carriers over these barriers is the basis of the POOLE-FRENKEL(48) current, J_{pf}

$$J_{pf} = (\text{const.})\, V \exp - \left\{ \frac{V_b}{kT} - (\text{const.}) \frac{V^{1/2}}{kT} \right\} \qquad (4.5.1)$$

where V_b is the barrier height.

b) In a disordered material it is possible that the electron states can become localized[49]. Thermally assisted transport of electrons between these states gives rise to hopping conduction. This may take two forms

$$J_h = (\text{const.})\ V \exp\left\{-\frac{V_h}{kT}\right\} \qquad \text{(ref. 50)}\ (4.5.2)$$

$$J_h = (\text{const.})\ V \exp\left\{-\frac{(\text{const.})}{k\ T^{1/4}}\right\} \qquad \text{(ref. 51)}\ (4.5.3)$$

where V_h is the effective activation energy. MOTT has shown[52] that these two results can be achieved from the same general approach using two different sets of simplifying assumptions. The dividing line between the two is rather fine, depending on the spacing of the localized centres, and no attempt has been made to distinguish between them in the ZnO in our devices.

c) At low current densities one expects the insulator to be ohmic. However, as the current is increased so that the carrier density becomes comparable with the trap density there exists in the solid the direct analogue of a space charge in a vacuum tube[53]. The current now rises more rapidly with increasing bias than Ohmic behaviour would predict. The space charge limited current has the form

$$J_{sc} = (\text{const.})\ \mu\ \frac{V^2}{d^3} \qquad (4.5.4)$$

where μ is the electron mobility and d the film thickness. The constant factor is dependent on the density and nature of the impurities in the insulator.

In order to discuss these mechanisms more fully it is necessary to define certain parameters related to the I-V characteristics found in the ZnSe switch. Chapter 2 has indicated that the slope of the forward biassed current-voltage characteristic was dependent on the oxide thickness. The change in slope of the semilogarithmic plot as the insulator thickens has been noted previously in other materials[16]. Figures 2.6.3 and 4 indicate that at high current densities there becomes apparent a resistance in series with the junction, ie that of the insulator. Figure 4.5.1 shows a simplified I-V curve. The variation of V_H

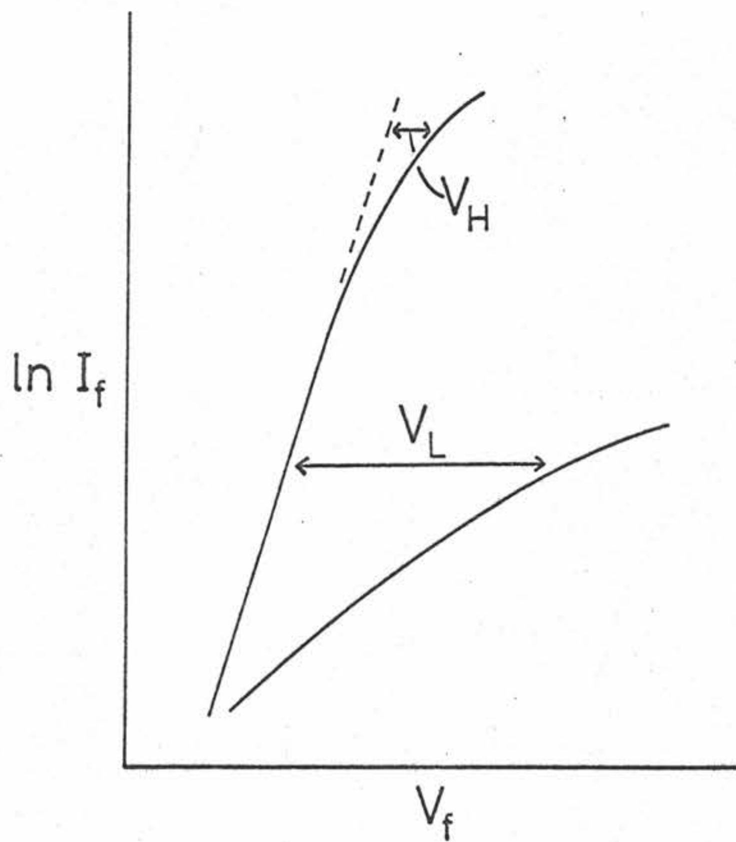

Figure 4.5.1. Schematic representation of the switched states defining the terms V_H and V_L which are used in the text.

with current gives the I-V characteristic of the insulator in its high conductivity state. This is shown for several devices in figure 4.5.2. Similarily, I vs V_L will give that of the low state. The variation of V_H and V_L with current, as a function of temperature, is shown in figure 4.5.3.

On the basis of this last figure two of the conduction mechanisms can be discarded. These are the Poole-Frenkel and hopping mechanisms. The latter provides a characteristic which will always move in the same direction as the temperature is varied, whereas figure 4.5.3 shows a different variation in each state. If the constant in the exponential term of the Poole-Frenkel form varied sufficiently between the two states the thermal shift of the I-V characteristics could be different in these two states. However the form of the ln I-ln V plot would not agree with that of figure 4.5.3.

Figure 4.5.3 shows characteristics which seem to lie somewhere between ohmic and space charge limited. The error bars on the extreme characteristics indicate that in this particular experiment it is not possible to distinguish clearly between the two conditions although the trend is obvious. In the variation of ohmic or space charge limited currents there are, as a rule, two competing processes, and it is not difficult to envisage a set of conditions which could satisfy the experimental form. For instance, if in the high state the temperature dependence of the conductivity is governed by an ionized trap density, then this would have a exp(-(const.)/kT) form. If during the switch the occupancy of the activating centre is altered in such a way to make the current mobility dependent, then this could have a $T^{-3/2}$ form which would mean a different temperature variation in the two states. This would satisfy the results contained in figure 4.5.3 if only qualitatively.

It is no more obvious now what the exact nature of the switch might be. There is no conclusive evidence as to which conduction mechanism pertains to the ZnO-ZnSe structure, but experiments have ruled out certain processes.

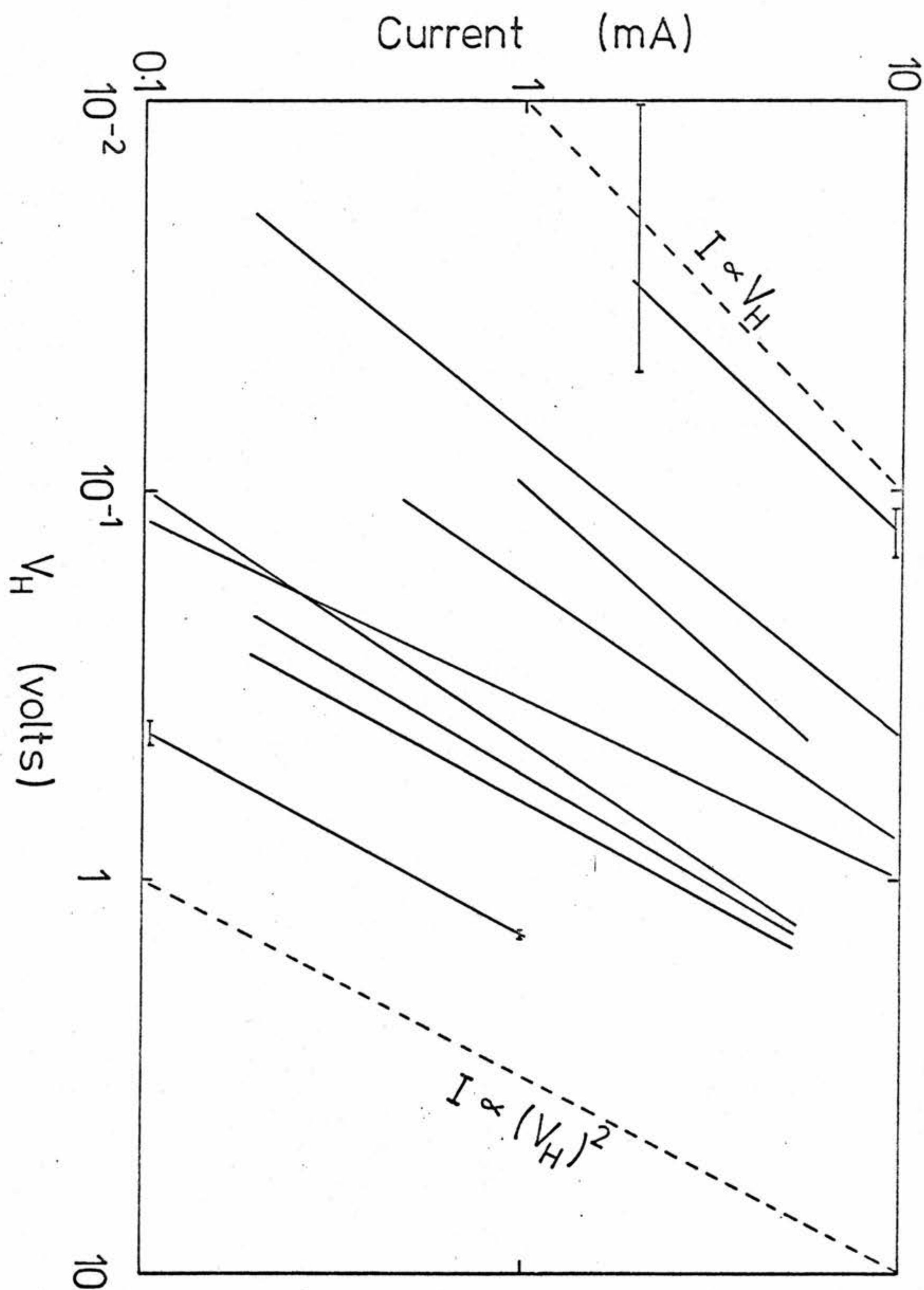

Figure 4.5.2. The variation of V_H with current for several devices. The lines shown (- - -) represent the ohmic and space charge limited limits. For clarity the error bars are only shown on the two extreme characteristics.

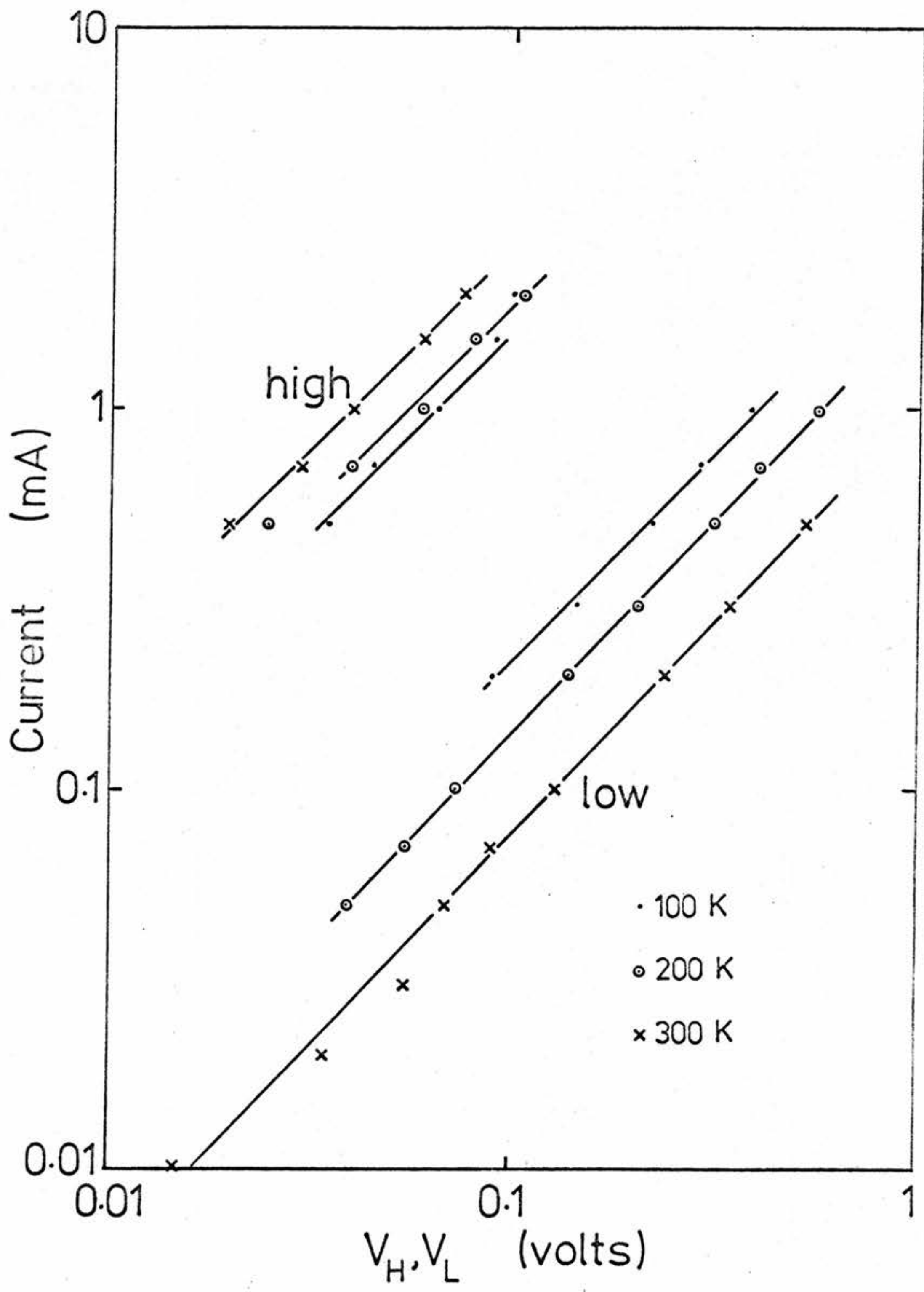

Figure 4.5.3. Variation of V_H and V_L with current and temperature. The I-V characteristic has the same form in both cases, but the temperature variation is different.

4.6 Discussion. A device has been described which displays all the required characteristics of a solid state memory and switching element. The fact that the device is, additionally, electroluminescent is important to the potential of the device, and possible applications will be discussed in the concluding chapter.

In the search for a model which will describe the switching action there are three major device properties which have to be considered. Firstly, the increase in ionized impurity concentration coupled with an increase in AC conductivity as the device switches into the low state indicates that the action is not merely that of an oxide switch, and that there are charge centres in the insulator. Secondly, the emission of light in forward bias suggests that neither the barrier heights at the interface, nor the volt drop across the semiconductor, change substantially during switching, and leads to the conclusion that the switch is due to a change in conductivity of the insulator. This conductivity is further analysed using the third device parameter, the thermal variation of the I-V characteristics. Although the model is not conclusive in all respects, it suggests potential mechanisms wherever possible as well as eliminating some processes to which other workers have often resorted in the past.

The method of preparing the insulator in our structure is not ideal nor indeed is the nature of the insulator understood. However it seems likely that a well defined M-I-S structure should be more readily understood than a heterojunction such as Hovel has developed.

CHAPTER 5

IMPACT IONIZATION

5.1 Introduction. In a reverse biassed Schottky diode the electric field may be in excess of 5×10^5 V cm^{-1}. In a field of this order electrons are no longer in thermal equilibrium with the host lattice. This means that electrons are gaining energy from the field faster than they can lose it by interaction with accoustical or optical phonons. Eventually the electron will gain sufficient energy for an additional relaxation process, that of pair production or impact ionization of a deep centre. As the name implies, pair production requires the energetic electron to give up a sufficient proportion of its energy to raise a valence electron to the conduction band, with the simultaneous creation of a hole. During impact ionization of an impurity the incident electron removes an electron from an atom with an energy level in the energy gap of the semiconductor and raises it to the conduction band. Observations of the light emission from ZnSe containing luminescent centres indicate that a photon is emitted as a result of a conduction electron's recombination with the centre(23). Impact ionization is one method whereby that electron may be removed to allow the process to continue. Verification that impact ionization of luminescent centres does occur was one of the reasons for undertaking this work.

Pair production in ZnSe is an interesting process since the band structure of the material can be expected to play an important part. This is because, with an energy gap of 2.7 eV, electrons are required to attain energies between 3 and 4 eV before they can excite other carriers across the gap. Thus they have to be accelerated considerably further from the band edge than for the same process to occur in say silicon or germanium, and the band structure can be expected to be quite important. There has been a great deal of theoretical work directed at the problem of avalanche breakdown (References 54 and 55 give good reviews) which has been subsequently applied to Si and Ge(56,57). This same theory has been applied to band to band ionization in ZnSe(58) and found to give satisfactory results which are in fair agreement with those obtained for other materials.

Impact ionization has also been observed in material containing luminescent centres[59]. Because no theory existed which predicted how the carriers multiply as a result of these ionizations while crossing the depletion region, we have developed a simple model which predicts the form of the observed multiplication and also fits qualitatively the variation of emitted light with bias.

5.2 Theoretical Considerations - Band to Band Transitions. The process of avalanche breakdown in a semiconductor is a solid state analogue of the Townsend breakdown in gases. This implies that there will be a multiplication of carriers as they cross the junction depletion region. McKAY[60] and MILLER[57] have described this multiplication in terms of the impact ionization rates associated with both electrons and holes. Their theoretical approach will be described briefly here.

By definition $\alpha_i(E)$ is the number of electron-hole pairs produced in unit distance by an electron travelling in the direction of the electric field E. There is a corresponding function, $\beta_i(E)$, which describes hole multiplication (McKay's original theory assumed equal electron and hole ionization; Miller expanded this to allow different rates for the two carriers.) Consider an element of the depletion region (figure 5.2.1) extending from x to x + dx. Let the number of electrons

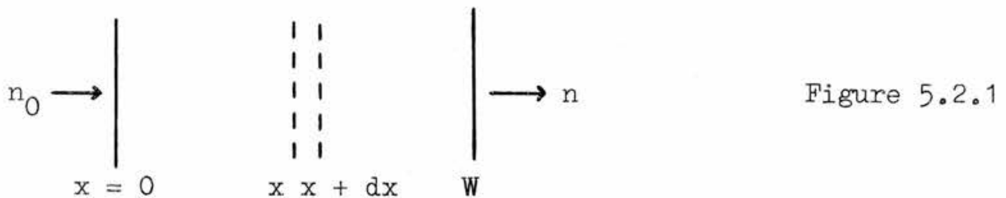

Figure 5.2.1

entering the junction be n_0 and the number leaving be n. The number produced between 0 and x is n_1 and between x and W is n_2. Since after every pair-producing collision an electron moves toward W and a hole toward 0, the total number of electrons produced between x and x + dx is

$$dn_1 = (n_0 + n_1)\,\alpha_i dx + n_2\,\beta_i dx \qquad (5.2.1)$$

For a junction where the current is initiated by electrons equation 5.2.1 can be

integrated with the limits $n_1 = 0$ at $x = 0$ and $n_2 = 0$ at $x = W$ to give

$$1 - \frac{1}{M} = \int_0^W \alpha_i \exp(-\int_0^x (\alpha_i - \beta_i)dx')dx \qquad (5.2.2)$$

where

$$M = \frac{n_0 + n_1 + n_2}{n_0} = \frac{n}{n_0} \qquad (5.2.3)$$

is the multiplication factor for electrons crossing the junction.

To evaluate the ionization rate in ZnSe we have measured the multiplication as a function of electric field. A constant number of electron-hole pairs are created in the depletion region by radiation of energy just greater than the band gap, and the current initiated by these carriers is measured as the field is varied. The ratio of the photocurrent at high fields to that at low fields, ie before multiplication begins, is the multiplication ratio. Experimentally, the multiplication ratio is the same whether the exciting radiation is blue (near band gap) or ultra violet (much greater than band gap). Since the absorption depth for ultra violet light is of the order of a tenth of the depletion layer width, whereas that for blue light is appreciably greater, the distribution with distance of photo produced holes and electrons is quite different for the two sources of radiation. The identity of the multiplication ratios therefore requires that, within the accuracy of the experiments, α_i and β_i are equal. Equation 5.2.2 now becomes

$$1 - \frac{1}{M} = \int_0^W \alpha \, dx. \qquad (5.2.4)$$

The form of α has to be known before this integral can be evaluated. The two principal calculations of the variation of α with field were performed by WOLFF[8] and SHOCKLEY[9]. Wolff solved the Boltzmann equation for high field strengths assuming that the electrons gain more energy from the field between collisions than they lose in the subsequent emission of an optical phonon. That is, they reach the ionization energy step by step. His simplified expansion of the distribution function in terms of spherical harmonics is quasi-Maxwellian below the threshold for impact ionization, resulting in a form for the ionization coefficient

$$\alpha(E) = \alpha_o \exp(-\frac{E_o^2}{E^2}) \qquad (5.2.5)$$

where α_o is a constant and E_o is the impact ionization parameter. Shockley assumed that the electrons which attain sufficient energy to cause ionization are those which escape the collisions which randomize the motion. Thus the distribution function for those electrons is a spike in the direction of the applied field. By considering only these electrons the solution has a form

$$\alpha(E) = \alpha_o \exp(-\frac{b}{E}) \qquad (5.2.6)$$

where b is the impact ionization parameter. The values of α_o in 5.2.5 and 6 are not necessarily equal.

By choosing an admixture of spiked and spherically symmetric distribution functions BARAFF(10) showed that the two results are limiting cases of the same general solution and has calculated α in terms of E_i, the energy required for ionization, and λ, the mean free path for optical phonon scattering. The essential difference between the two approximations lies in the relationship of mean electron energy to ionization energy. If the mean energy is less than the threshold energy α has the E^{-1} form, and the E^{-2} form holds when the mean energy is greater than that required for ionization. In the case of band to band transitions it is not clear what the ionization energy should be. From a consideration of the momentum and energy changes during the production of an electron-hole pair (in the case of parabolic energy bands, and for particles of equal mass) one can show that $E_i = \frac{3}{2} E_g$, where E_g is the band gap. SHOCKLEY(9) suggests that this may be reduced to E_g by phonon cooperation. Indeed it is apparent that E_i can be reasonably expected to assume any value greater than E_g. Thus in the case of band to band excitation the threshold for ionization is well above the thermal energy of the lattice and equation 5.2.6 can be expected to be valid.

Using 5.2.6, 5.2.4 can be reduced to

$$1 - \frac{1}{M} = \alpha(E_m)W_{eff} \qquad (5.2.7)$$

where E_m is the maximum electric field and is equal to twice the average field in a Schottky junction, while W_{eff} is an effective depletion layer width defined by this expression. MOLL(11) has tabulated values of W_{eff} as a function of E_m for various values of the parameter b.

5.3 Experimental Results - Band to Band Transitions. The multiplication factor is the ratio of the photocurrent at high fields to the photocurrent at low fields, that is, before ionization begins.

The photocurrent was initiated by a constant number of electron-hole pairs created in the depletion region by light of energy near the band gap of ZnSe. This was obtained from a tungsten filament lamp and a Wratten 47B filter. The light was chopped at frequencies between 600 Hz and 1 kHz and phase sensitive techniques were used to amplify the signal. A block diagram of the apparatus is shown in figure 5.3.1. Anti-vibration mountings on the chopping wheel and motor helped limit the acoustic pick-up by the electronics. Careful focussing of the incident light ensured a near square light pulse. Figure 5.3.2 shows typical photocurrent pulses obtained using the apparatus of figure 5.3.1 with the PSD replaced by a Boxcar detector.

In this particular series of experiments devices were made with an electrolyte solution as the rectifying contact. The sample was sealed into the base of a small glass pot containing a 1M solution of HCl. The normal indium dots made the ohmic connection and a copper wire formed the counter electrode in the electrolyte. This particular structure was used to allow a repetition of work already carried out by WILLIAMS[61, 62] and the results were then related to measurements on the metal-semiconductor system. The electrolyte solution also forms a Schottky barrier at the interface, and the junction capacitance obeys the C^{-2}-V law. The main problem with the structure is the ease with which the interface can be damaged. As soon as any appreciable current is drawn electrolysis very rapidly leaves a deposit on the crystal surface[62]. This restriction on the maximum current severely hampers the measurement of the multiplication since the region where M is increasing most rapidly corresponds to fairly high current densities. The metal-semiconductor structure does not suffer from this problem. Figures 5.3.3 and 4 show typical plots of photocurrent as a function of reverse bias for an electrolyte and metal contact respectively. With the metal contact much higher

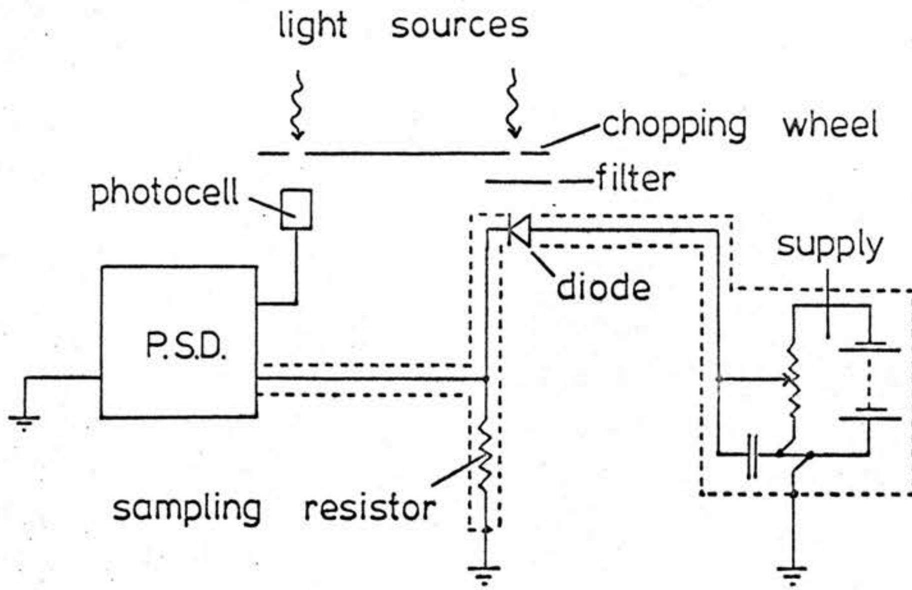

Figure 5.3.1. Apparatus for measuring the multiplication factor.

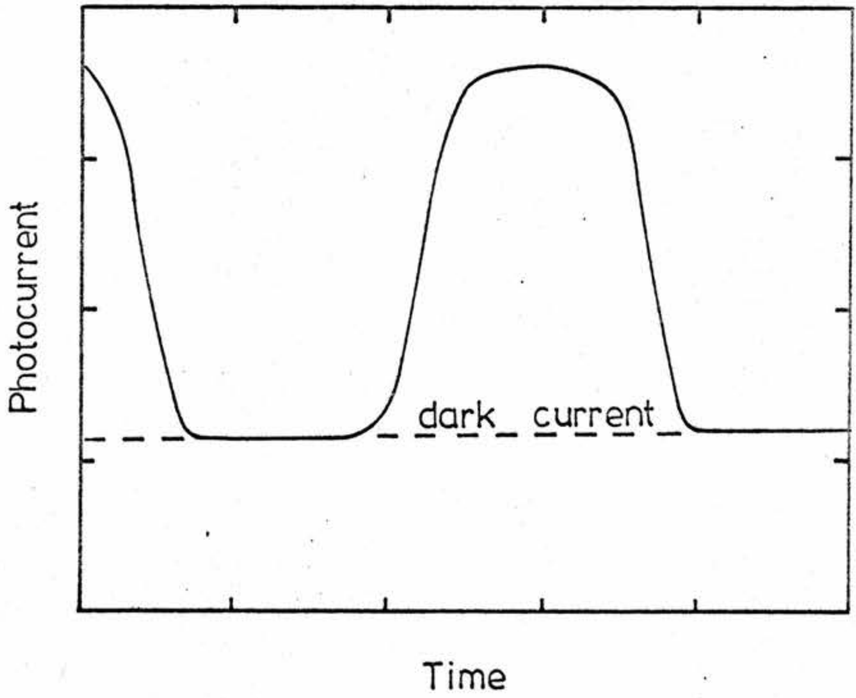

Figure 5.3.2. Photocurrent detected by above apparatus. Measured by replacing PSD by a Boxcar detector.

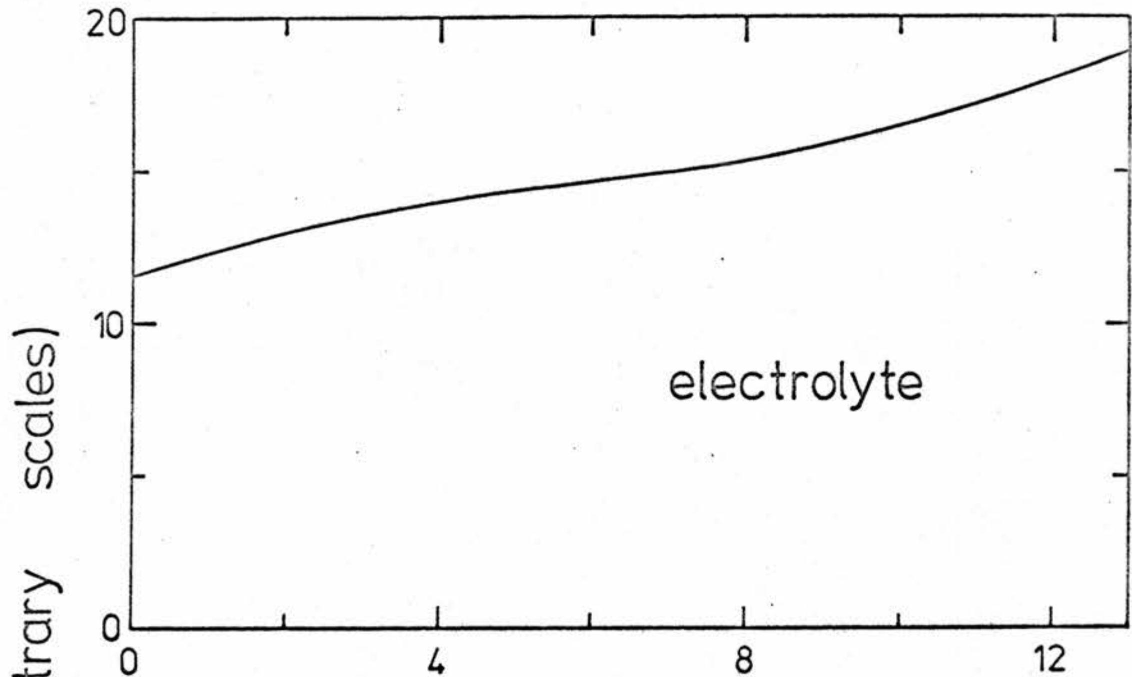

Figure 5.3.3. Photocurrent as a function of bias for a diode containing no luminescent centres.

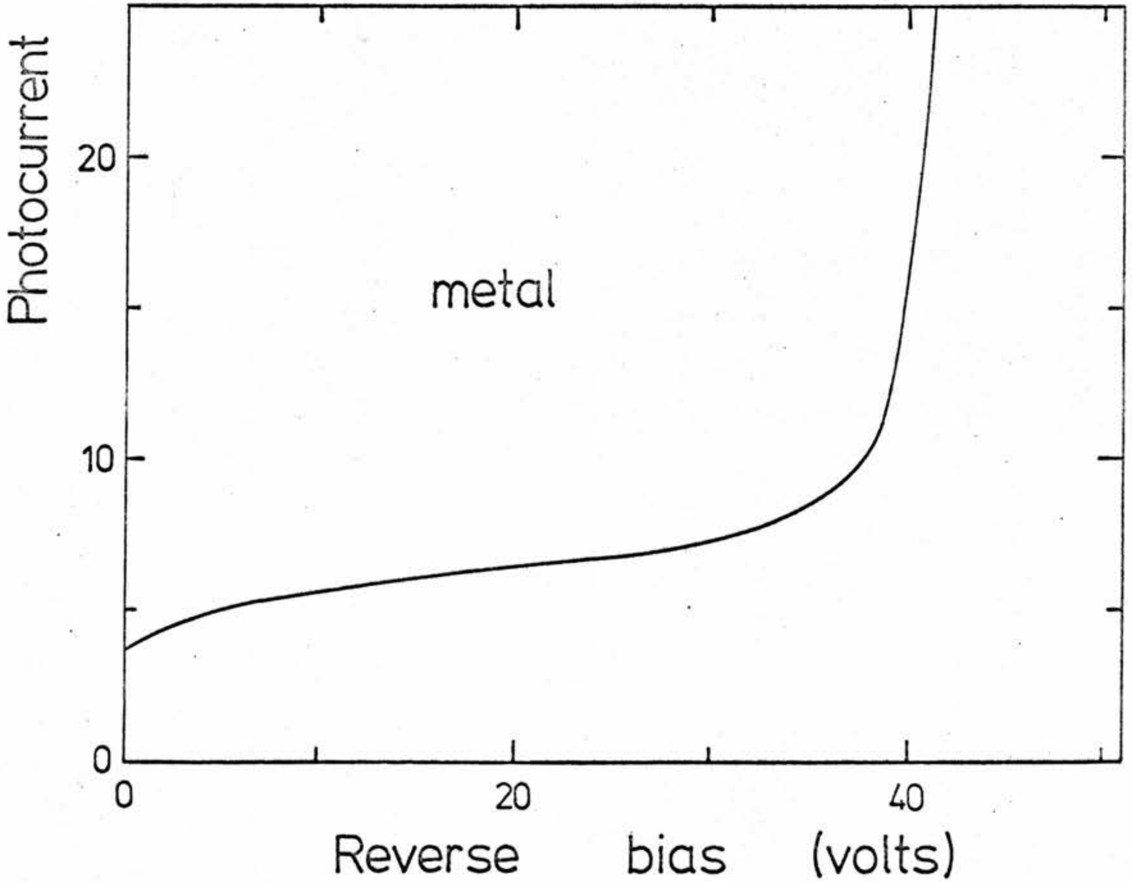

Figure 5.3.4. Photocurrent as a function of bias for a diode containing no luminescent centres.

multiplications can be observed.

Both these results show an initial rise in photocurrent which is not due to ionization. It has been observed previously in GaP[63] but is not usually seen in measurements made on Si or Ge. The photocurrent, I_p, is due to carriers generated within the depletion region and reaching the junction by diffusion. Thus I_p will depend on the depletion layer width, W, and the carrier diffusion length, L_d, as follows

$$I_p \sim (W + L_d). \qquad (5.3.1)$$

If L_d is small the photocurrent will exhibit the initial behaviour observed in figures 5.3.3 and 4 as the depletion region is widened by the applied bias. This is, in fact, a useful technique for measuring short diffusion lengths. When a correction has been applied, the rise in photocurrent at higher biasses gives the multiplication.

The impact ionization coefficient has been calculated from the multiplication using an iterative procedure to solve equation 5.2.6. Having measured M, an approximate value of α is obtained using $W = W_{eff}$ as a trial solution. Substitution into 5.2.6 gives a value of b which is then used to obtain a better estimate of W_{eff}, and the process repeated (Reference 11, ch 11). In practice only one iteration was required in view of the spread in experimental data. The results for several devices are shown in figure 5.3.5. They fit the form of the impact ionization coefficient

$$\alpha = \alpha_o \exp(-\frac{b}{E}). \qquad (5.3.2)$$

For these devices W_{eff} lies between 0.05 W and 0.2 W. These results have been fitted to the theory of BARAFF[10]. (A numerical form developed by CROWELL and SZE[64] can be used to reproduce Baraff's curves.) Figure 5.3.6 shows some of Baraff's curves of $\ln \alpha\lambda$ vs $E_i/E\lambda$ as a function of E_r/E_i. Here λ is the mean free path for optical phonon scattering. In section 5.2 we discussed the expected value of the ionization energy. Figure 5.3.6 shows the results of sample B fitted to Baraff's curves for E_i between 2.6 and 3.9 eV. The results lie in the region of the curves where form 5.3.2 applies. Within the accuracy of the experiment we

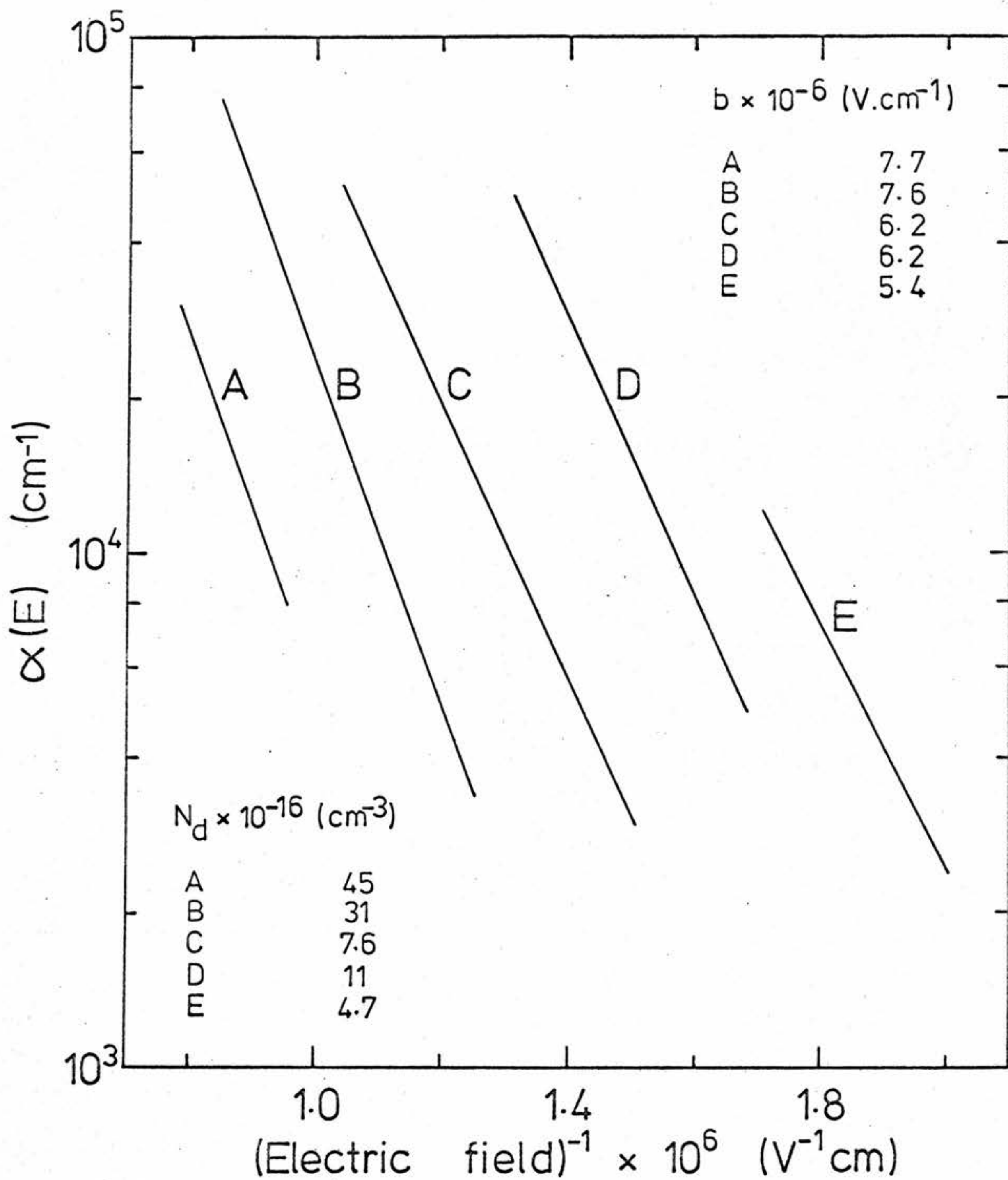

Figure 5.3.5. Ionization coefficient for diodes containing no luminescent centre. A, B and E have electrolyte contacts and C and D have metal contacts. All except D are polycrystalline.

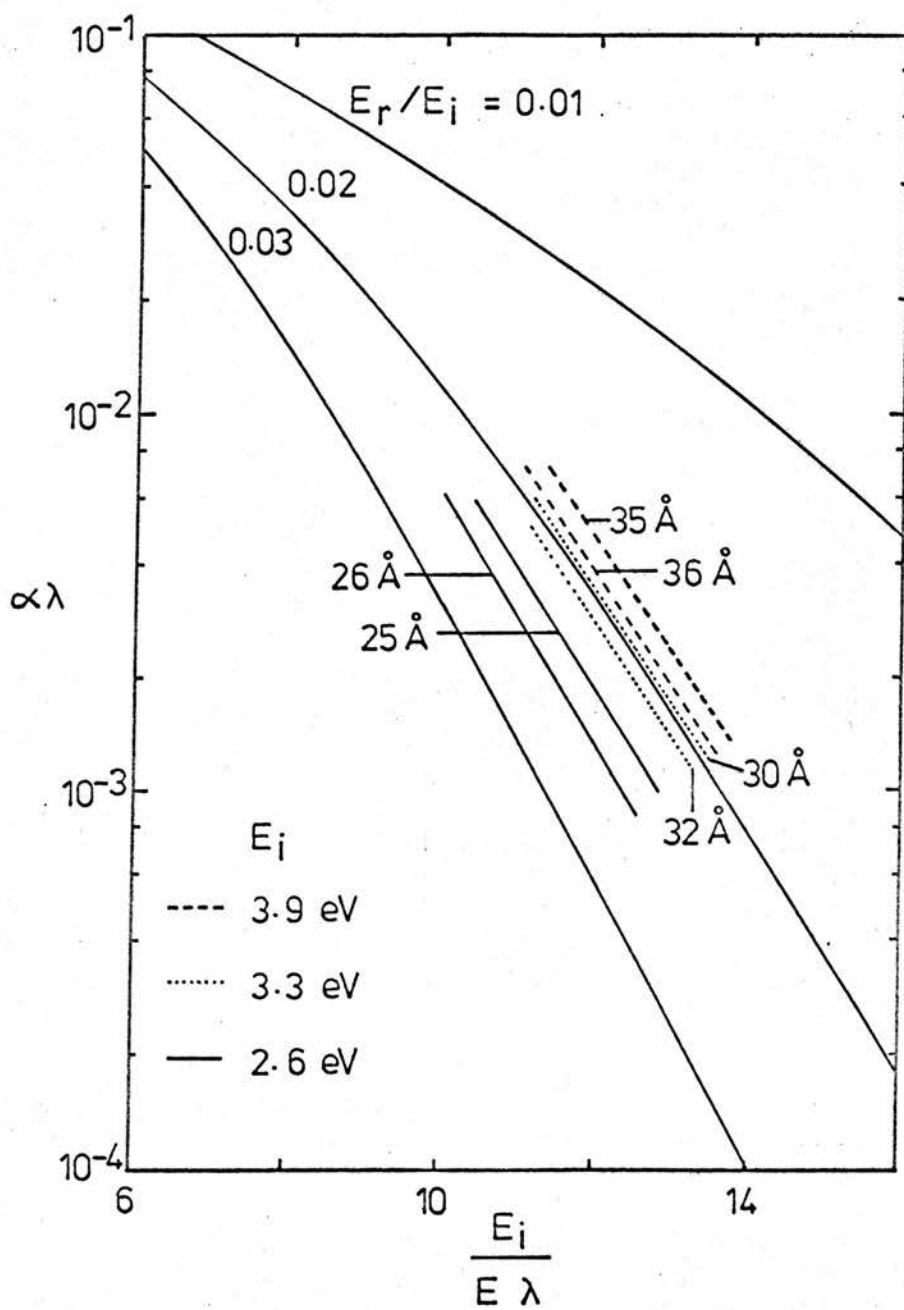

Figure 5.3.6. Fit to Baraff's curves of the results from sample B of figure 5.3.5, using E_i and λ as the adjustable parameters. Note that E is an electric field whereas E_r and E_i are energies.

have a good fit to the theory for values of λ between 25 and 36 Å depending on the ionization energy used. Alternatively, using one particular value of E_i the results from several samples can be fitted to one of Baraff's curves by considering λ to be the adjustable parameter. For $E_i = 3.3$ eV the samples have values of λ varying from 24 to 52 Å. Some of these are shown in figure 5.3.7 for the theoretical curve corresponding to $E_r/E_i = 0.02$.

5.4 Discussion - Band to Band Transitions. Although the results of the preceding section are of the expected form, they are unusual in that the value of the impact ionization parameter, b, varies from sample to sample. It is suggested that this is due to the effect of the band structure at energies far from the band gap.

Consideration of the band structure of ZnSe, as shown in figure 5.6.1[65,66], indicates that for an electron to achieve energies consistent with ionization it must be accelerated up the conduction band and scattered to the next highest band in the vicinity of X. (In section 5.2 it was noted that the ionization energy lay between E_g and $\frac{3}{2}E_g$.) As the electrons travel up the conduction band they will spend some time trapped in the impurity level associated with the minima at X before scattering and continuing to higher energies. As far as Baraff's theory is concerned, the trapping of the carriers is analagous to a decrease in the mean time between optical phonon scattering events. Thus the parameter λ of that theory should decrease as the concentration of ionized impurities increases. This has been observed qualitatively as shown in figure 5.4.2.

5.5 Conclusions - Band to Band Transitions. Measurements of the band to band impact ionization parameter have been made which are in reasonable agreement with the existing theories. However they differ substantially from those obtained by WILLIAMS[61,62]. Our values do seem to fit the theory of Baraff whereas Williams' do not for any reasonable value of λ. Moreover our results seem to be consistent with those obtained by other workers in other materials. We have shown that there

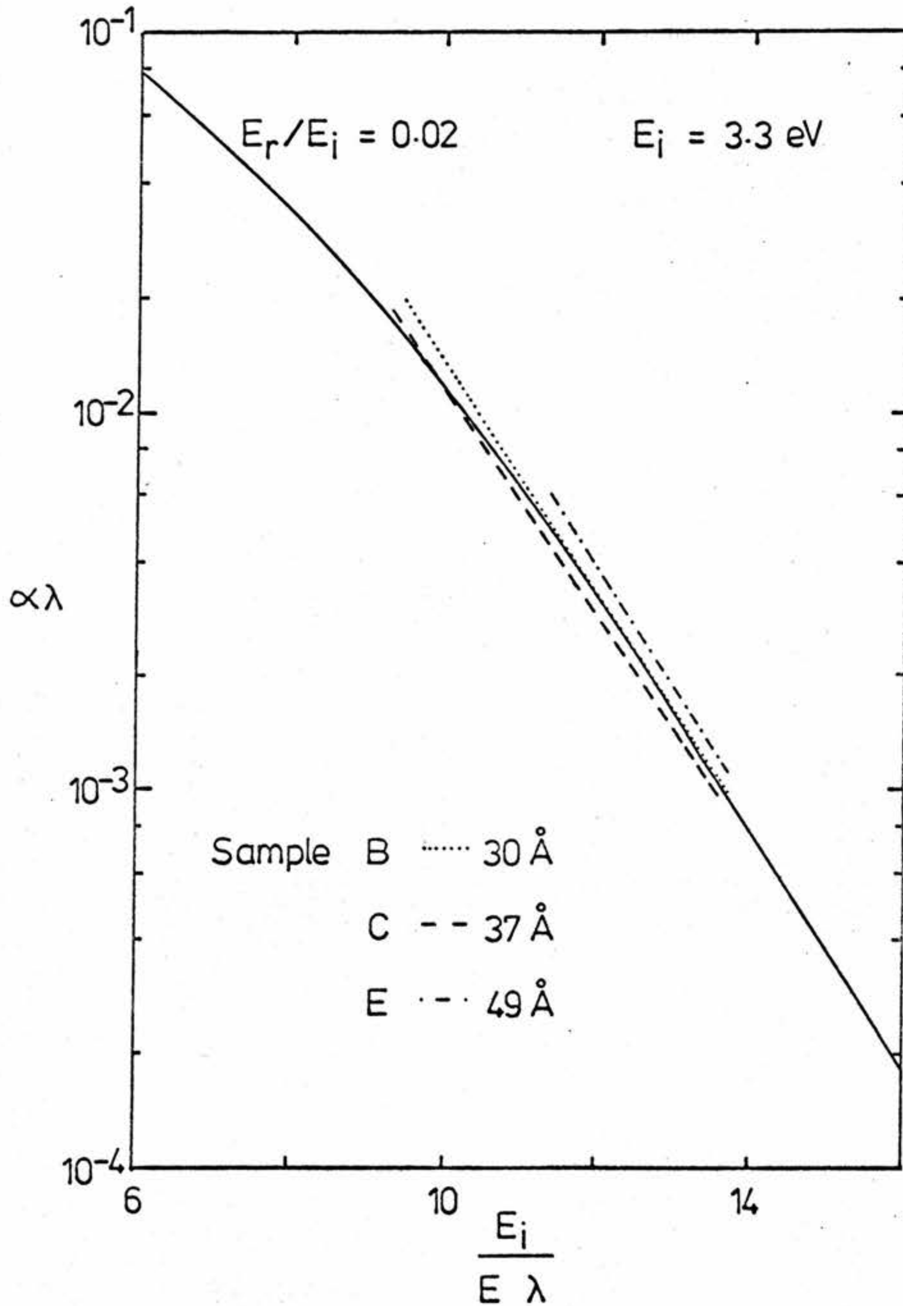

Figure 5.3.7. Fit to Baraff's theory for E_i = 3.3 eV and E_r/E_i = 0.02. Here λ is the adjustable parameter. Note that E is an electric field whereas E_r and E_i are energies.

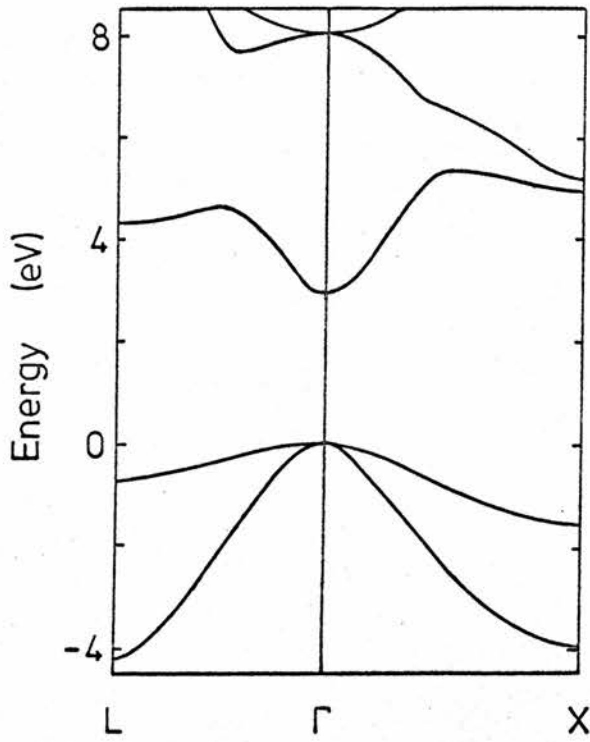

Figure 5.4.1. Band structure of zinc selenide.

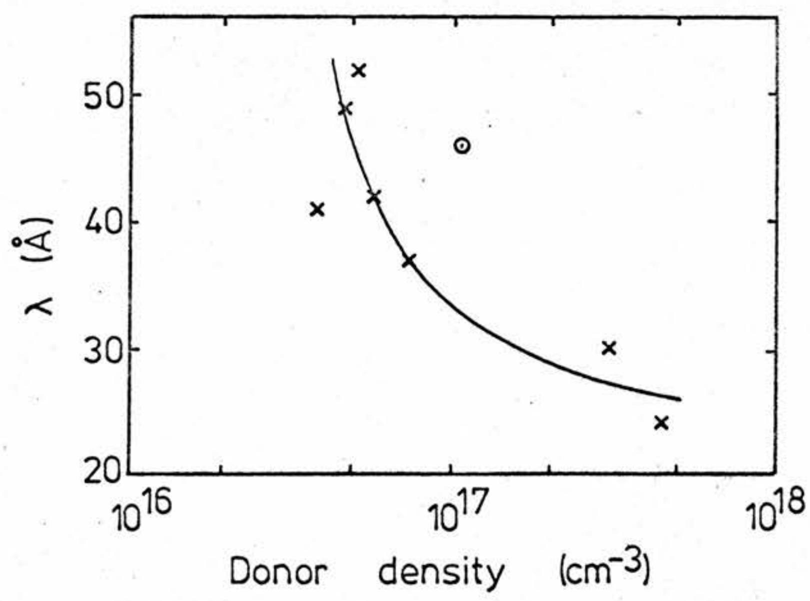

Figure 5.4.2. Variation of the parameter λ of Baraff's theory with donor density. The circled point is a monocrystalline sample.

exists a qualitative relationship between the impact ionization parameter and the energy gap of the material. The average coefficient obtained for the devices in figure 5.3.5 is shown in figure 5.5.1 compared with those obtained[67] in Si, Ge, GaAs and GaP. Where these other results have not been exactly of the form shown in equation 5.2.5 they have been approximated to this form over the region of interest. Williams' results give b around 3×10^6 V cm^{-1} which does not fit the qualitative form of figure 5.5.1.

5.6 Theoretical Considerations - Luminescent Centres. In the absence of a theory which could predict the multiplication which would result from the impact ionization of deep impurities, we have developed a theoretical form which related the impact ionization coefficient, α, to the multiplication. It is in good agreement with experiment.

As in section 5.2, multiplication is assumed to take place in a region of the depletion region of thickness W_{eff} in which the field is constant and equal to the

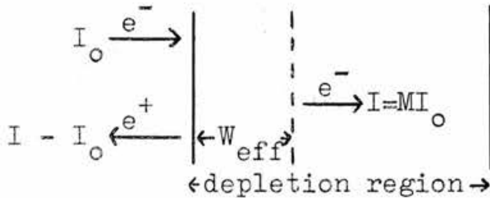

Figure 5.6.1

maximum field (figure 5.6.1). We postulate four principal processes of electron-hole generation and recombination associated with the impurities. These are shown in figure 5.6.2. The impurity concentration is N_t per unit volume, of

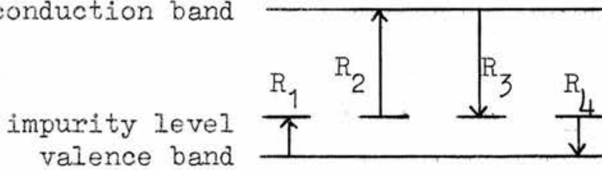

Figure 5.6.2

which $(N_t - n_t)$ are ionized. We have considered the case where ionization is due only to electrons. By definition R_1 is the density of electrons raised from the valence band to a trap in unit time. Thus

$$R_1 = n\,\sigma_1\,v_n \qquad (5.6.1)$$

where σ_1 is an impact ionization cross section, and n the density of free electrons

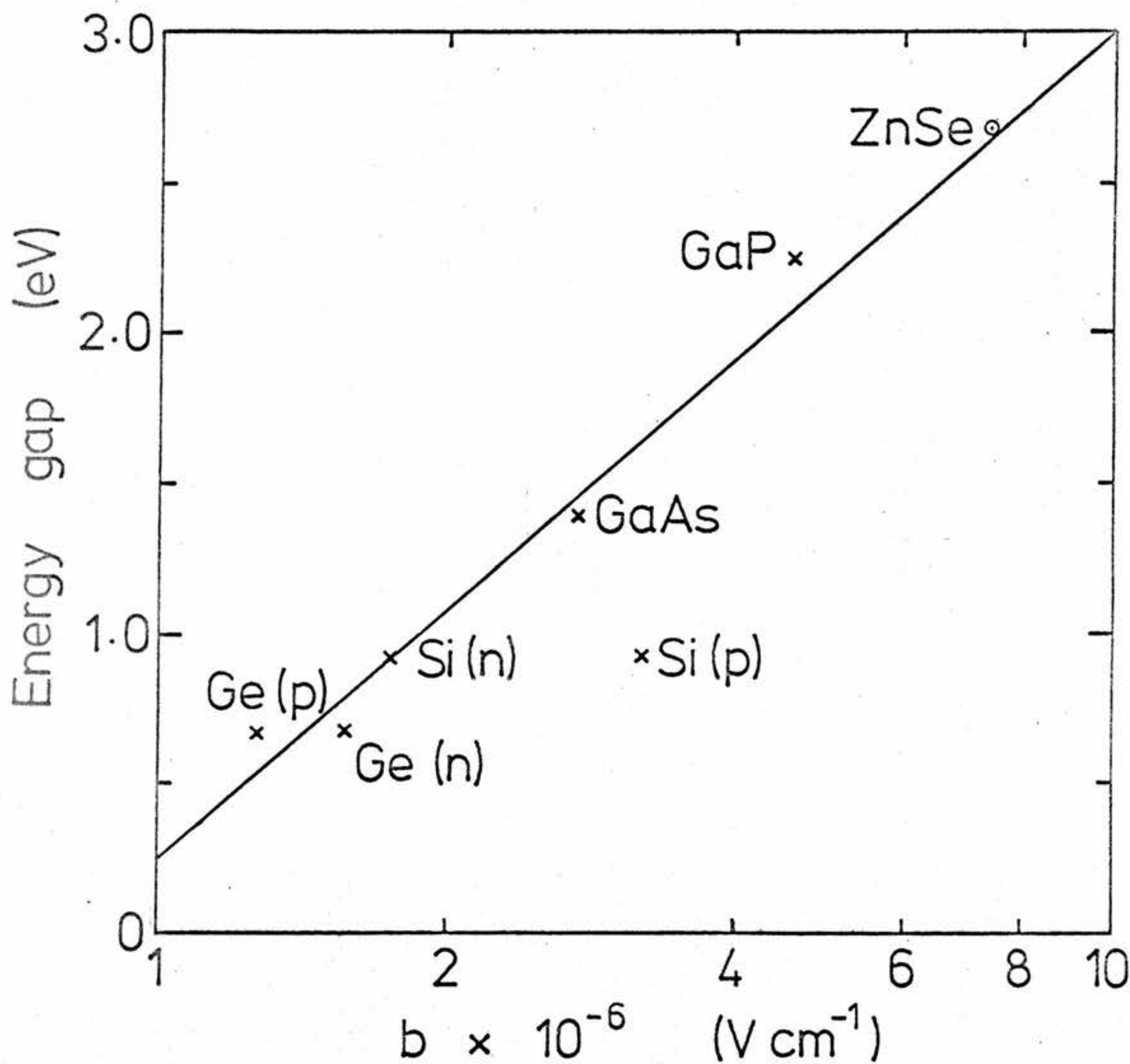

Figure 5.5.1. The impact ionization parameter for various semiconductors. The values for materials other than ZnSe were taken from reference 67.

with drift velocity v_n. There are similar relationships for R_{2-4}.

In the steady state the number of electrons moving onto traps must equal the number being removed. Thus

$$n\, v_n(\sigma_1 + \sigma_3)(N_t - n_t) = (n\, v_n\, \sigma_2 + p\, v_p\, \sigma_4)n_t. \tag{5.6.2}$$

However current continuity requires that

$$I = I_n + I_p$$
$$= n\, e\, v_n + p\, e\, v_p \tag{5.6.3}$$

where I, the total current, has electron and hole components I_n and I_p respectively. Now equation 5.6.2 can be rewritten such that

$$n_t = N_t \frac{\sigma_1 + \sigma_3}{(\sigma_1 + \sigma_2 + \sigma_3 - \sigma_4) + \sigma_4\, I/I_n}. \tag{5.6.4}$$

The rate of flow of electrons from the valence to the conduction band due to the ionization processes involving the traps is

$$\frac{\partial n}{\partial t} = n\, v_n\, \sigma_1(N_t - n_t) - p\, v_p\, \sigma_4\, n_t. \tag{5.6.5}$$

Since the electron flow can be described by

$$\frac{\partial}{\partial x}(n\, v_n) = \frac{\partial n}{\partial t} \tag{5.6.6}$$

we can write (assuming constant electron velocity)

$$\frac{\partial n}{\partial x} = n\, N_t \left\{ \frac{\sigma_1\, \sigma_2 + \sigma_3\, \sigma_4 - \sigma_3\, \sigma_4\, I/I_n}{(\sigma_1 + \sigma_2 + \sigma_3 - \sigma_4) + \sigma_4\, I/I_n} \right\}. \tag{5.6.7}$$

Integrating this with the limits $n = \frac{I_o}{e\, v_n}$ at $x = 0$ and $n = \frac{I}{e\, v_n}$ at $x = W_{eff}$, we can obtain the form

$$\ln M = N_t\, W_{eff}\, \sigma_1 \frac{(\sigma_2 + \sigma_a)}{(\sigma_2 + \sigma_b)} +$$
$$\left\{1 + \frac{\sigma_1}{\sigma_3} \frac{(\sigma_2 + \sigma_a)}{(\sigma_2 + \sigma_b)}\right\} \ln\left(1 - (M - 1) \frac{\sigma_3\, \sigma_4}{\sigma_1\, \sigma_2}\right) \tag{5.6.8}$$

where $M = I/I_o$, $\sigma_a = \sigma_3\, \sigma_4/\sigma_1$ and $\sigma_b = \sigma_1 + \sigma_3 - \sigma_4$.

This expression can be simplified considerably. First, σ_1 and σ_2 have to be related to the impact ionization coefficients for the processes, α_1 and α_2. An electron travelling a distance l in the material will ionize $\alpha_i l$ atoms, where

i = 1 or 2. By definition of the cross section the number ionized must equal $\sigma_i l N_t$. Thus

$$\sigma_i = \frac{\alpha_i}{N_t} . \quad (5.6.9)$$

Let us consider the case of manganese as the luminescent centre. As discussed in section 3.4, not all the electrons raised from the luminescent centre will enter the conduction band. Some process is required to remove them from the excited state. The proportion which do become free has been assumed to be field independent and is included in the form of α_2.

Regardless of the form we choose for α, σ will saturate at high fields; the magnitude of the field required for saturation being roughly proportional to the ionization energy. So at fields which are of interest when considering the ionization of the deep centre, σ will already have saturated, and in fact we assume that σ_2 is the only field dependent cross section. In the case of a manganese centre, light emission results from the de-excitation of the trap, so we can say that $\sigma_3 > \sigma_1$ or σ_4 since both the latter represent capture by a neutral centre. The impact ionization cross section, σ_2, must be smaller than σ_3 at low fields, however, as the field is increased σ_2 must exceed σ_3. This is apparent from the fact that there is an observable multiplication. If σ_2 remained smaller than σ_3 then electrons removed from the trap would all recombine before they left the depletion region.

Applying these conditions equation 5.6.8 can be reduced to

$$M = \exp\left\{ N_t W_{eff} \frac{\sigma_1 \sigma_2}{\sigma_2 + \sigma_3} \right\}. \quad (5.6.10)$$

When $\sigma_2 < \sigma_3$ the multiplication will increase with σ_2. At higher fields σ_2 becomes greater than σ_3 and the multiplication will saturate. This is by contrast to the multiplication due to pair production across the energy gap. Section 5.2 showed that once band to band ionization took place the multiplication tended to infinity very rapidly. This makes more obvious the differences in the two systems. In band to band ionization every time an electron is created a hole

passes back through the depletion region and may produce another electron, so that it is possible for the process to run away. This is not the case when an electron ionizes a luminescent centre to produce only one additional electron.

Since the model describes the state of charge of the luminescent centres, it should be capable of predicting how the intensity of the emitted light varies with applied field. If we write the number of electrons capable of emitting photons as

$$n_1 = n\, v_n\, \sigma_3(N_t - n_t) \tag{5.6.11}$$

then essentially the same calculation as gave the multiplication shows that

$$L \propto I(1 - \frac{1}{M}) \tag{5.6.12}$$

where L is the luminous intensity. This result is a convenient check on the model and its assumptions, because equation 5.6.12 is readily obtained from very simple considerations. Since the light emission is roughly proportional to the number of ionizing events in the depletion region, then

$$\begin{aligned} L &\propto (I - I_o) \\ &\propto I(1 - \frac{1}{M}). \end{aligned} \tag{5.6.13}$$

The discussion so far has not considered any recombination of electron-hole pairs which might not be radiative. We will show that the inclusion of such a process, under certain conditions, does not alter the conclusion reached in equation 5.6.10. The simplest case to consider is that shown in figure 5.6.3.

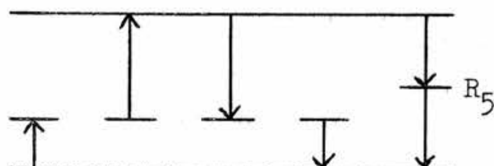

Figure 5.6.3

A process R_5 has been included which in its simplest form can be written as

$$R_5 = n\, v_n\, \sigma_5. \tag{5.6.14}$$

Equation 5.6.2 now contains an additional term and thereafter the calculation proceeds much as before until 5.6.8 is reached. This now contains terms which involve σ_5 and there is an additional assumption required. That is, σ_5 should be greater than any other cross section. This is not unreasonable since we know the radiative recombination efficiency to be low at room temperature.

The net result of the calculation is that the magnitude of the multiplication is reduced by a factor corresponding to σ_5 and to the density of the non-radiative recombination centres. This means that the form of the multiplication is unaffected by the presence of such a centre, and, in the absence of other data, its effect can not be quantified.

The above discussion concerns only the simple form of R_5 shown in 5.6.14, and the validity of such a form has to be considered. SHOCKLEY and READ[18] have shown that for recombination through a single centre, the recombination rate can be written as

$$\frac{\delta n}{\delta t} = - \frac{n\,p - n_i^2}{(n + n_1)\tau_{po} - (p + p_1)\tau_{no}} \qquad (5.6.15)$$

where n and p are the densities of electrons and holes available for capture, n_i is the intrinsic hole density, n_1 and p_1 are the electron and hole densities which would exist if the Fermi level were at the trap level, and τ_{po} and τ_{no} are the mean times for hole and electron capture. In an order of magnitude calculation, assume the carriers to have equal drift velocities and that $p \sim n$. Then, for a current density of 1 A m^{-2}, it can be shown that equation 5.6.15 reduces to a form containing either p or n (5.6.14) when the recombination centre is more than 0.5 eV from a band edge. Outside those limits 5.6 15 reduces to a quadratic form, containing both n and p, which is difficult to solve algebraically.

5.7 <u>Experimental Results - Luminescent Centres.</u> The procedure for measuring multiplication due to luminescent centres is exactly as described in section 5.3. In the present case however electrolytic contacts were not used.

Throughout the remainder of this chapter the electric field used in calculations is the maximum field encountered in the junction. This is for consistency with the preceding work on material with no luminescent centre. In the present case however there is no theory to define the effective depletion layer width (section 5.2).

The multiplication curves for typical manganese doped diodes are shown in

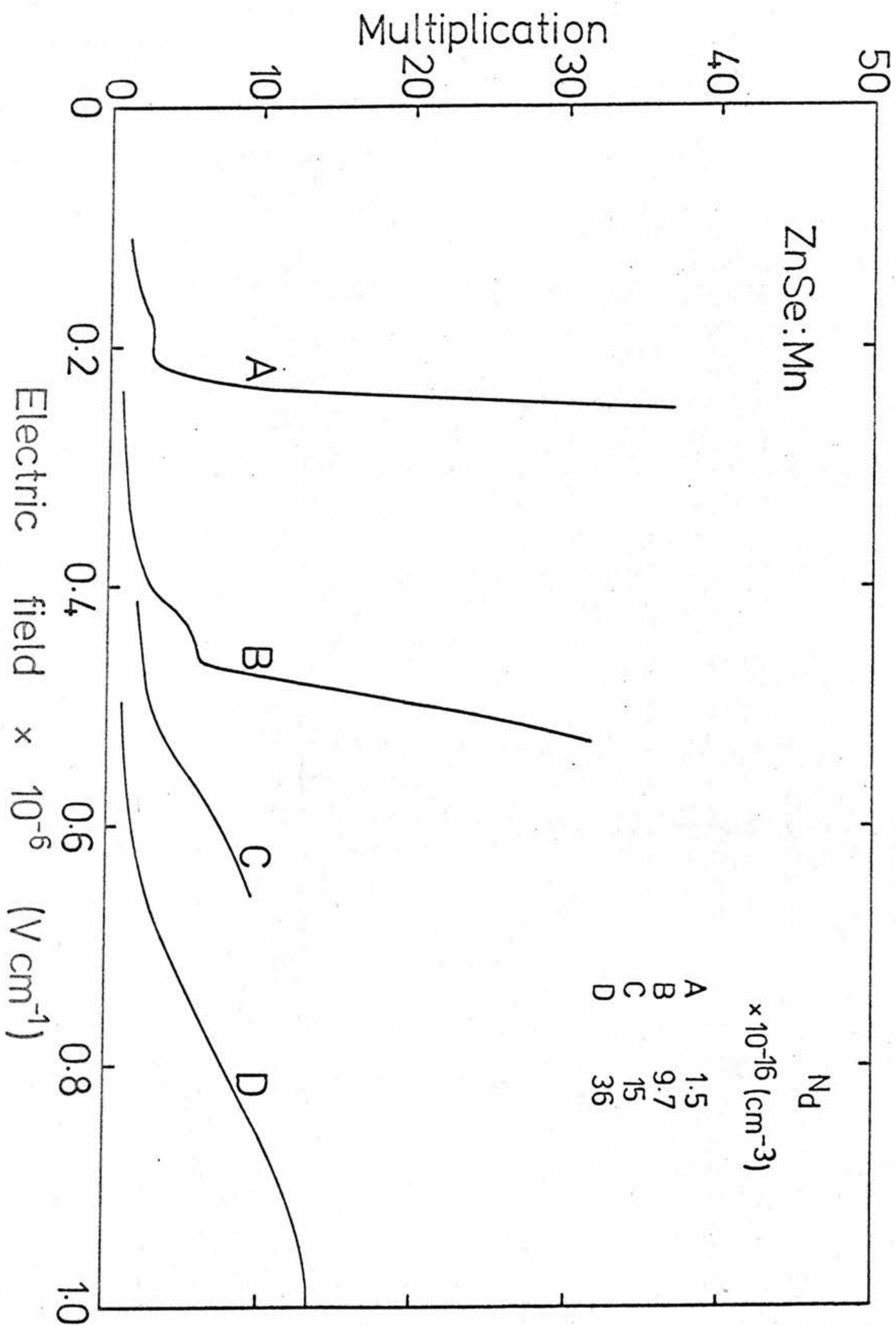

Figure 5.7.1. Multiplication curves for manganese doped diodes of several donor densities.

figure 5.7.1. They are characterized by a rapid rise at high fields with a smaller multiplication superimposed at some lower field. The multiplication changes with donor density exactly as it did in the case of band to band ionization. In material which contains copper as the luminescent centre the multiplication exhibits only the high field increase with no component at lower fields. A series of results at various donor densities is shown in figure 5.7.2.

The rapid increase in the multiplication at high fields is due to the band to band ionization. This is demonstrated by the similarity of the results obtained for the same donor density in material containing either copper, manganese or no luminescent centre.

We postulate that the additional multiplication obtained at lower fields in manganese doped material is due to impact ionization of the manganese. As described earlier, electrons are raised to the first excited state of the manganese by impact. However some of these electrons may reach the conduction band. It is these electrons which are detected as the photocurrent. If there was no ionization of the manganese excited state we would see no multiplication due to the centre. One of the experiments which helps confirm this theory is the variation of emitted light with bias. If the luminescent centre was indeed being excited, the subsequent de-excitation might be expected to cause the emission of a photon. Thus the threshold for light emission should coincide with the threshold for excitation and subsequent ionization of the centre. Figure 5.7.3 shows the variation of light with field for sample B of figure 5.7.1. The threshold for light emission is in agreement with the onset of ionization.

In section 5.6 it was shown that the multiplication should have the form

$$M = \exp\left\{ N_t \, W_{eff} \, \frac{\sigma_1 \, \sigma_2}{\sigma_2 + \sigma_3} \right\} \qquad (5.7.1)$$

where $$\sigma_i = \alpha_i / N_t . \qquad (5.7.2)$$

It is not obvious in the case of impact ionization of the luminescent centre what form α should take. All the experimental results were fitted to both forms

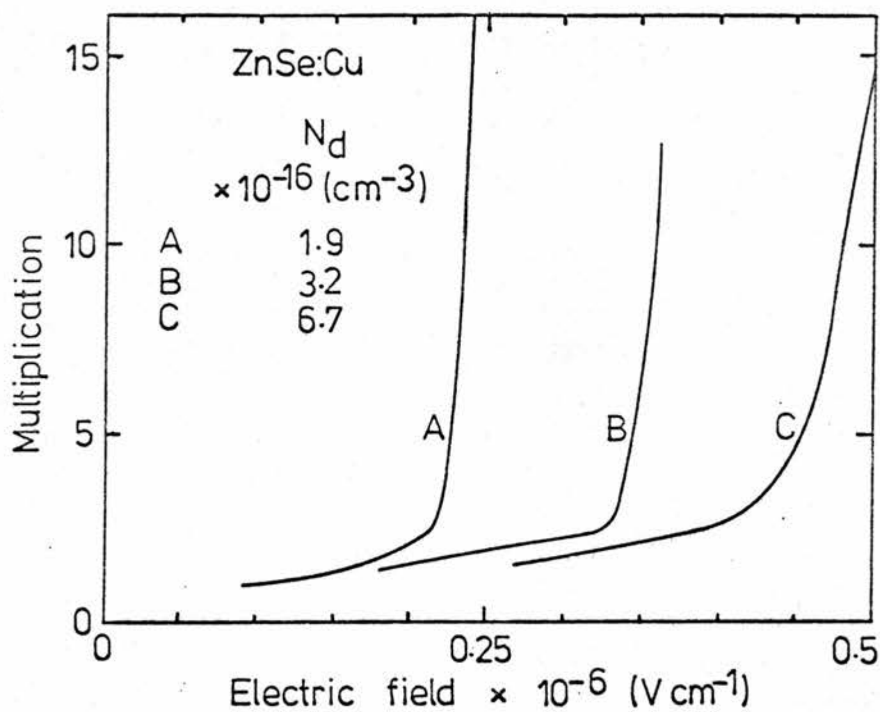

Figure 5.7.2. Multiplication curves for copper doped diodes of several donor densities.

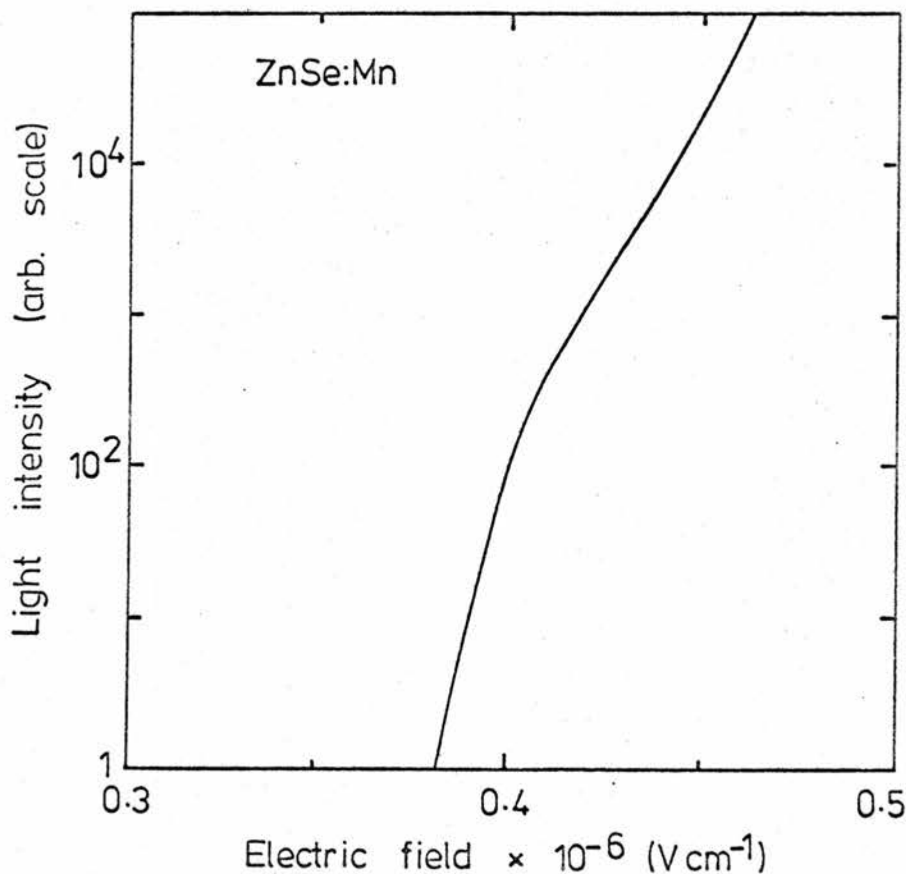

Figure 5.7.3. Variation of light with electric field for sample B of figure 5.7.1.

of the impact ionization coefficient, that is, $\ln \alpha \propto -\frac{E_o^2}{E^2}$ and $\ln \alpha \propto -\frac{b}{E}$. The fitting of the experimental results to expression 5.7.1 was done by computer. After the results had been corrected for the initial widening of the depletion region (section 5.3) the difference between the experimental and theoretical forms was minimized with respect to four variables using a variant of an IBM scientific subroutine. The four variables A, B, C, D are defined as follows

$$M = A \exp\left\{ B\, Q(E)/(1 + Q(E))\right\} \qquad (5.7.3)$$

$$Q(E) = C \exp(-D/E) \qquad (5.7.4)$$

or

$$Q(E) = C \exp(-D/E^2). \qquad (5.7.5)$$

Here A should be near unity if the initial rise has been correctly extracted, $B = W_{eff}\,\alpha_{10}$, $C = \alpha_{20}/\alpha_{30}$ and D equals either b or E_o^2 depending on the form of α. α_{i0} is the constant term in the expression for α_i.

It seems that the results for this material are probably in the transition region between the two forms of the impact ionization coefficient. Figures 5.7.4 and 5 show the fit obtained, using both forms of α, to results from two samples with different donor densities. Although it is by no means conclusive, it seems that at the lower field the better fit is that of 5.7.4, whereas at higher fields it is that of 5.7.5. Using either form there seems to be a good fit to the theory of section 5.6.

Although many samples exhibited the behaviour shown in figure 5.7.1, there were relatively few which could give quantitative data with any precision. The multiplication due to band to band ionization and the depletion region widening effect tended to swamp the multiplication due to the centre, and reliable extraction of the latter depended on how well the other two were characterized. In practice the widening effect was the limiting factor. If the initial rise was separable from the luminescent centre ionization it was fitted to the form of equations 5.7.3 and 5. This was not because it could be predicted to have this form, but because some approximate numerical representation had to be obtained. This was only possible for three samples - samples B, C and D of figure 5.7.1.

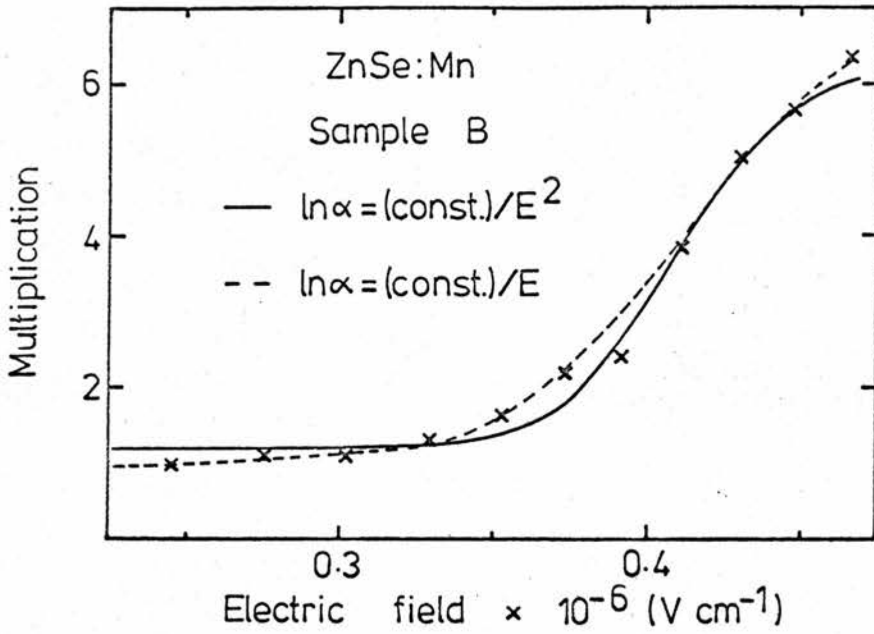

Figure 5.7.4. Best computer fits to the experimental points using both forms of the ionization coefficient.

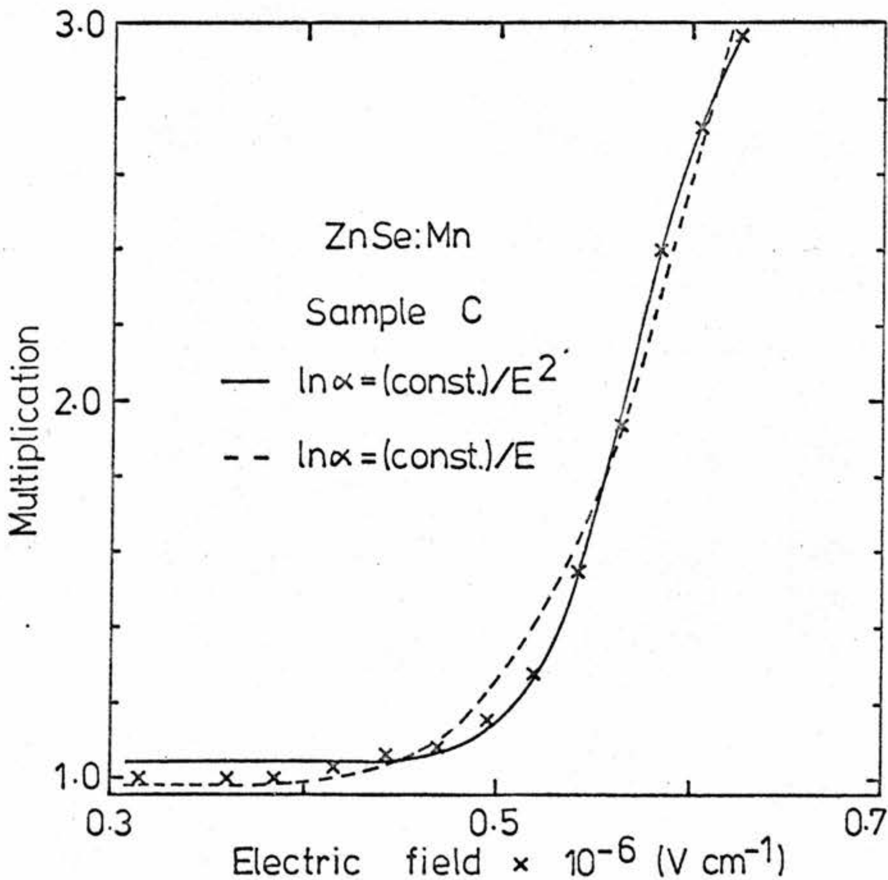

Figure 5.7.5. Best computer fits to the experimental points using both forms of the ionization coefficient.

The results of the fit of the corrected results to equations 5.7.3,4 and 5 are shown below. Underlining indicates the better fit.

Sample	Values of the constants					N_d
	A	B	C	b $\times 10^{-6}$ V cm^{-1}	E_o $\times 10^{-6}$ V cm^{-1}	cm^{-3}
A	1.05 1.21	2.08 1.72	1.1×10^5 1.8×10^4	<u>4.55</u>	1.24	9.7×10^{16}
B	1.00 1.06	1.49 1.09	4.2×10^5 3.0×10^5	7.44	<u>1.98</u>	1.5×10^{17}
C	1.13 1.30	2.64 2.52	9.8×10^3 2.0×10^2	6.54	<u>1.66</u>	3.6×10^{17}

In the case of copper as the luminescent centre, there is no noticeable multiplication due to its ionization. However if the light emission is measured as a function of field there is a threshold which corresponds to the ionization of the centre. Figure 5.7.6 shows a multiplication curve with the light emission superimposed. The light was measured using a photomultiplier with an extended S-20 response for greater sensitivity. It can be seen that there are now two thresholds. At low fields there is an increase in emission as the copper is ionized, and at higher fields the increase in the number of electron-hole pairs due to band to band excitation also causes an increase in intensity. Previous authors have postulated both of these processes as being responsible for the emission; in our work the two are clearly distinguished.

The experiments have shown that impact excitation of both copper and manganese luminescent impurities takes place in ZnSe, and that the subsequent de-excitation causes light to be emitted.

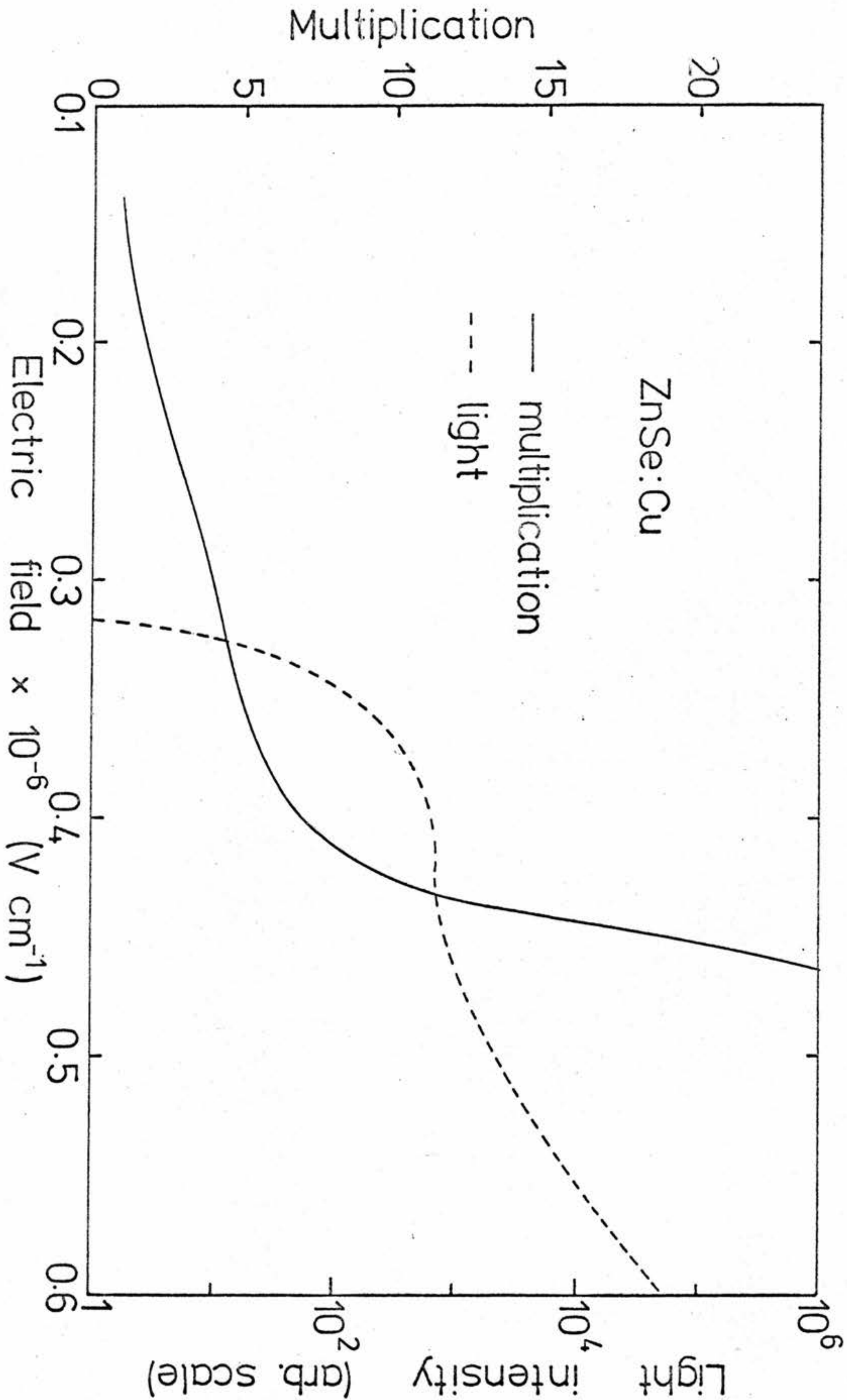

Figure 5.7.6. Variation of light and multiplication with field for a copper doped diode. Note that the light scale is logarithmic.

5.8 Discussion - Luminescent Centres. In previous sections there has been some discussion concerning the form of the ionization coefficient. In section 5.3 the results of band to band ionization were fitted to Baraff's theory, and they occurred very near the transition between the two forms of α. It seems likely that a similar situation exists in the case of the manganese ionization, and within the accuracy of the experiments the two forms can not be positively distinguished. Thus, depending on the form which is applicable, the impact ionization parameter for manganese in ZnSe is either

$$b = 6 \times 10^6 \text{ V cm}^{-1}$$

or

$$E_o = 1.5 \times 10^6 \text{ V cm}^{-1}.$$

We have shown elsewhere(23) that the emitted light intensity is related to the ionization parameter, and this approach gives a quadratic form for $\ln \alpha$ as a function of field. The value obtained is $E_o = 6 \times 10^5$ V cm^{-1}. However this was calculated using the average electric field in the junction which is half the maximum value used here. The values are thus in excellent agreement.

There should be no variation of the ionization parameter with donor density in the case of the luminescent centre as there was for band to band multiplication. This is because the ionization energy required is only 2.1 eV, in the case of manganese, and for electrons to achieve energies of this order they need not go through the subsidiary minimum in the conduction band at X (section 5.4).

5.9 Conclusions - Luminescent Centres. The most obvious conclusion from the experiments which have just been described is that measurements of any significance on this system are difficult. The most unsatisfactory factor of all is that it is fairly clear why the measurements are so imprecise, but not at all clear how they may be improved.

There are two reasons why the multiplication due to the luminescent centre should be so small. The first is that only a small number of impact excited electrons are ionized. Secondly the impact ionization is operating in direct

competition with the non-radiative transitions which tend to reduce M. For example, sample A in figure 5.7.1 contains approximately 1% manganese yet gives a small multiplication due to the centre. It is possible that in adding the luminescent centre to the material we also add some other complex which assists the non-radiative processes.

Material containing copper may suffer from similar problems, but the major one would seem to be the limit to the copper concentration which is set by the donor density.

Although the results for only three devices are quoted in section 5.7, they represent the only significant results from measurements made on several tens of devices. Without a clearer understanding of the complexes responsible for the non-radiative processes, multiplication measurements will remain uncertain.

CHAPTER 6

CONCLUSIONS

6.1 Device Applications. When trying to market a device in direct competition with another which is already well established there are two criteria for success. The new device must do the same job more cheaply, or else it must cost no more but do the same job plus something extra. In this respect ZnSe is rather anomalous. Its greatest single advantage over the GaP_xAs_{1-x} with which it is in competition is its comparative cheapness, apparently satisfying the first of our criteria. And yet, when predicting how ZnSe is likely to fare in this confrontation it seems unlikely that it will take over in existing applications of the gallium compounds. The reason is that in most applications in which one finds, for example, GaP_xAs_{1-x} the material cost is only a small part of the total production cost. This is especially true in the case of solid state indicator lamps. In the case of alphanumeric displays however, we can resort to the second of our two criteria for commercial success. That is, for the same cost ZnSe can produce a display which is more attractive to the customer than the GaP_xAs_{1-x} equivalent. Using ZnSe an alphanumeric display as large as 2-3 cm can be prepared before the material cost becomes prohibitive. Thus, in many applications where a character less than 1 cm in height is unacceptable ZnSe should find a market.

To visualise the possible impact of a ZnSe electroluminescent device with memory, it is necessary to understand the techniques used to prepare character displays. Producing any alphanumeric character can require as many as 35 light emitting elements. One can either do all the decoding of the incoming binary information and then make connection to each lamp individually or, more usually, include the decoder in the encapsulation of the display. This means fewer external connections to the display. The decoder sequentially scans the elements of the array, applying a current pulse to those which are required to be illuminated. This means that each element has to be driven hard to ensure that

the mean illumination is satisfactory, which may mean current pulses approaching 1 A. A large scale array of perhaps 1000 elements would require such large currents as to be impractical and the designer is now looking for an electro-luminescent device with some additional property which can help surmount this problem.

A satisfactory approach would be to incorporate a memory element into the light emitting device so that these could be run at moderate currents for the whole of the scanning cycle, and industry is currently very active in this field. The combined lamp and memory unit would have a characteristic very similar to that obtained in the forward biassed ZnSe switch. That is, there must be two conductivity states sufficiently different for the emitted light to appear to be either on or off with the same applied bias. On the first of the multiplexing cycles, as this sequential scanning is known, a current or voltage pulse is applied to place the device in the required state. Since there is a constant DC bias applied to the device, it now remains illuminated or otherwise until it is updated on the next cycle.

Current attempts to construct a device with the necessary properties are aimed at matching a GaP_xAs_{1-x} diode to a chalcogenide glass switch, but there is the problem of characteristic incompatability which is hindering their development. The ZnSe switch would be an ideal device for the application.

So it would seem that ZnSe Schottky diodes have properties which could make them successful in the fast expanding displays market. This is, of course, looking to the future optimistically. There is still a lot of device development to be done, and in the next section we shall discuss the likelihood of the potential described in this section ever being realised.

6.2 Future Research. The preceeding discussion assumed that the ZnSe devices described in this work could be made as efficient and reliable as their competitors. The present device does not meet this requirement and this

concluding section would hope to suggest what lines of future research are required to ensure that it does satisfy these in the near future.

Reverse biassed electroluminescence is already sufficiently efficient to compare favourably with the luminescence obtained from the best GaP_xAs_{1-x}, and sample ZnSe lamps are now being marketed. However with their rather high operating voltage they are incapable of being driven directly by conventional TTL, and require additional driving stages. Although this is not of sufficient importance as to render the device unmarketable, it is a significant disadvantage. This is less of a problem in arrays where each chip needs a decoder which can include the driver stage. However it would be more satisfactory if the same light output could be achieved in forward bias.

As we have described in chapter 3, light can be emitted in forward bias by a M-I-S structure on ZnSe. The mechanisms described in that chapter indicate which material and device properties are important in obtaining useful light emission, and it seems likely that better oxide control, plus perhaps a switch to ZnS:Mn, could provide the extra efficiency.

When discussing the switch very similar conclusions are reached. In a primitive form the device has worked satisfactorily. However not enough is known about the oxide to allow the mechanisms to be understood as fully as is necessary. In view of the potential of the switch in large scale arrays it is important that these problems are solved.

The nature of the insulating layer is one factor which will have to be examined very carefully if the M-I-S structure is ever to be prepared in a controlled manner. Reverse biassed electroluminescence, which does not rely on oxide behaviour, is now well understood because there is a great deal of information available about the ZnSe. In particular, the material has a well characterized impurity level which controls the luminescent transitions. The impact ionization measurements have given a great deal of information about the processes which occur in the depletion region, and we could say that reverse

biassed electroluminescence is well understood directly as a result of knowledge of the starting material.

When talking of devices which rely on particular properties of the insulator however, we are frequently reduced to hypothesis. There are still too many unknown parameters, and one of the major lines of future research must be to obtain an oxide free ZnSe surface with a subsequent deposition of a well characterized oxide such as silicon monoxide.

From the purely physical point of view, improvements in the quality of the ZnSe could probably make possible more meaningful impact ionization measurements. The technique could also be extended to other impurities. Very little is known about the blue excitonic transition observed in forward bias. As this is visible at room temperature it could prove useful in defining variations of the energy gap with temperature.

As with most research, for every problem the work has solved, several more have been created. This is perhaps a criterion of success. Had it solved every problem it could not have been realistic. One can only hope that one day a few more of the problems will be solved.

REFERENCES

1. H.J. ROUND, Electl. Wld., 19, 309 (1907).
2. O.V. LOSSEV, Phil. Mag., 6, 1024-44 (1928).
3. G. DESTRIAU, J. Chim. Phys., 33, 587-625 (1936).
4. K. LEHOVEC, C.A. ACCARDO and E. JAMGOCHIAN, Phys. Rev., 83, 603-7 (1951).
5. G.A. WOLFF, R.A. HERBERT and J.D. BRODER, Phys. Rev., 100, 1144-5 (1955).
6. J. STARKIEWICZ and J.W. ALLEN, J. Phys. Chem. Solids, 23, 881-4 (1962).
7. A.G. FISCHER, Radiation Recombination in Semiconductors, p. 259, Dunod, Paris (1964).
8. P.A. WOLFF, Phys. Rev., 95, 1415-20 (1954).
9. W. SHOCKLEY, S. Stat. Electron., 2, 35-67 (1961).
10. G.A. BARAFF, Phys. Rev., 128, 2507-17 (1962).
11. J.L. MOLL, Physics of Semiconductors, McGraw-Hill, New York (1964).
12. H.K. HENISCH, Rectifying Semiconductor Contacts, Clarendon Press, Oxford (1957).
13. R.K. SWANK, M. AVEN and J.Z. DEVINE, J. App. Phys., 40, 89-97 (1969).
14. A.M. GOODMAN, J. App. Phys., 34, 329-38 (1963).
15. A.M. COWLEY, J. App. Phys., 37, 3024-32 (1966).
16. H.C. CARD and E.H. RHODERICK, J. Phys. D, 4, 1589-601 (1971).
17. E.H. NICOLLIAN and A. GOETZBERGER, BSTJ, 46, 1055-133 (1967).
18. W. SHOCKLEY and W.T. READ, Phys. Rev. 87, 835-42 (1952).
19. A.R. HUTSON, Phys. Rev., 108, 222-30 (1957).
20. S. BRAUN, H.G. GRIMMEIS and J.W. ALLEN, to be published.
21. M.M. ATALLA and R.W. SOSHEA, Scientific Report No 1, Contract No AF 19(628)-1637, Hewlett-Packard Associates (1962).
22. H.C. CARD and E.H. RHODERICK, J. Phys. D, 4, 1602-11 (1971).
23. J.W. ALLEN, A.W. LIVINGSTONE and K. TURVEY, S. Stat. Electron., to be published.
24. A.W. LIVINGSTONE, K. TURVEY and J.W. ALLEN, to be published.

25. A.G. FISCHER and H.I. MOSS, J. App. Phys., 34, 2112-3 (1963).

26. R.C. JACLEVIC, D.K. DONALD, J. LAMBE and W.C. VASSELL, App. Phys. Lett., 2, 7-9 (1963).

27. J.P. DONNELLY, A.G. FOYT, W.T. LINDLEY and G.W. ISELER, S. Stat. Electron., 13, 755-8 (1970).

28. H.C. CARD and B.L. SMITH, J. App. Phys., 42, 5863-5 (1971).

29. C.A. MEAD, Phys. Lett., 18, 218 (1965).

30. D.R. WIGHT, private communication.

31. K. TURVEY and J.W. ALLEN, to be published.

32. J. APPERSON, Y. VOROBIOV and G.F.J. GARLICK, Brit. J. App. Phys., 18, 389-99 (1967).

33. S. IIDA, J. Phys. Soc. Jap., 25, 177-84 (1968).

34. A.W. LIVINGSTONE and J.W. ALLEN, App. Phys. Lett., 20, 207-8 (1972).

35. S.R. OVSHINSKY, Phys. Rev. Lett., 21, 1450-3 (1968).

36. A.D. PEARSON, IBM J. Res. Develop., 13, 510-4 (1969).

37. H. OKUSHI, M. SAITO, M. KIKUCHI and A. MATSUDA, Sol. Stat. Comm., 9, 991-4 (1971).

38. R.R. SUTHERLAND, J. Phys. D, 4, 468-79 (1971).

39. J.G. SIMMONS and R.R. VERDERBER, Proc. Roy. Soc., 301, 77-102 (1967).

40. A. CUSDIN and J.C. ANDERSON, J. Phys. D, 3, 1776-81 (1970).

41. M. KIKUCHI, M. SAITO, H. OKUSHI and A. MATSUDA, Sol. Stat. Comm., 9, 705-7 (1971).

42. T.L. TANSLEY and J.E. RALPH, J. Phys. D, 3, 807-11 (1970).

43. H.J. HOVEL, App. Phys. Lett., 17, 141-3 (1970).

44. H.J. HOVEL and J.J. URGELL, J. App. Phys., 42, 5076-83 (1971).

45. G. DEARNALEY, Phys. Lett., 25A, 760-1 (1967).

46. J.F. GIBBONS and W.E. BEADLE, Sol. Stat. Electron., 7, 785-97 (1964).

47. G. DEARNALEY, A.M. STONEHAM and D.V. MORGAN, Rep. Prog. Phys., 33, 1129-91 (1970).

48. A. JONSCHER, Thin Solid Films, 1, 213-34 (1967).

49. N.F. MOTT and E.A. DAVIS, Electronic Processes in Non-crystalline Materials, Clarendon Press, Oxford (1971).

50. A. MILLER and E. ABRAHAMS, Phys. Rev., 120, 745-55 (1960).

51. N.F. MOTT, Non-crystalline Solids, 1, 1-17 (1968).

52. N.F. MOTT, Phil. Mag., 19, 835-52 (1969).

53. A. ROSE, Phys. Rev., 97, 1538-44 (1955).

54. A.G. CHYNOWETH, "Charge Multiplication Phenomena", Semiconductors and Semimetals, 4, 263-325, Academic Press, New York (1968).

55. W. MONCH, Phys. Stat. Sol., 36, 9-48 (1969).

56. C.A. LEE, R.A. LOGAN, R.L. BATDORF, J.J. KLEIMACK and W. WIEGMANN, Phys. Rev., 134, A761-73 (1964).

57. S.L. MILLER, Phys. Rev., 99, 1234-41 (1955).

58. A.W. LIVINGSTONE and J.W. ALLEN, J. Phys. C, 3, 2468-73 (1970).

59. A.W. LIVINGSTONE and J.W. ALLEN, to be published.

60. K.G. McKAY, Phys. Rev., 94, 877-84 (1953).

61. R. WILLIAMS, Phys. Lett., 25A, 445-6 (1967).

62. R. WILLIAMS, J. Electrochem. Soc., 114, 1173-9 (1967).

63. R.A. LOGAN and A.G. CHYNOWETH, J. App. Phys., 33, 1649-54 (1962).

64. C.R. CROWELL and S.M. SZE, App. Phys. Lett., 9, 242-4 (1966).

65. J.P. WALTER and M.L.COHEN, Phys. Rev., 183, 763-72 (1969).

66. D.J. STUKEL, R.N. EUWEMA and T.C. COLLINS, Phys. Rev., 179, 740-51 (1969).

67. S.M. SZE and G. GIBBONS, App. Phys. Lett., 8, 111-3 (1966).